AD NUMBER: AD0059715

LIMITATION CHANGES

TO:

Approved for public release; distribution is unlimited.

FROM:

Distribution authorized to U.S. Gov't. agencies and their contractors; Administrative/Operational Use; 1 Mar 1955. Other requests shall be referred to the Office of Naval Research, Washington, DC 20350

AUTHORITY

ONR ltr dtd 9 Nov 1977

FC

THE AEROTHERMOPRESSOR—
A DEVICE FOR IMPROVING THE PERFORMANCE OF A GAS TURBINE POWER PLANT

by

Ascher H. Shapiro

Kenneth R. Wadleigh

Bruce D. Gavril

Arthur A. Fowle

57715

AEROTHERMOPRESSOR PROJECT

Report Submitted Under

Office of Naval Research Contract N5ori-07878

M.I.T. Division of Industrial Cooperation, DIC 5-6985,

March, 1955

Department of Mechanical Engineering, Gas Turbine Laboratory

MASSACHUSETTS INSTITUTE OF TECHNOLOGY, CAMBRIDGE, MASSACHUSETTS

1. SUMMARY

Theoretical and experimental investigations of a novel gas dynamics device having no moving parts yet performing the function of a compressor, are described. This device, called the "Aerothermopressor", exploits the possibility of raising the total pressure of a high speed gas stream through cooling of the gas. When placed at the exhaust of a gas turbine, the Aerothermopressor will reduce the exhaust pressure, thereby improving both fuel economy and power capacity per unit of air flow. Basic elements of the apparatus comprise a nozzle which accelerates hot gas into an evaporation section; a water injection system which delivers finely-atomized water into the high-speed stream; an evaporation section in which the gas is cooled and most of the water evaporated; and, finally, a diffuser in which the gas stream is decelerated and the static pressure increased.

Although the Aerothermopressor is simple in structural arrangement, the physical processes occurring within it are exceedingly complex in their details. The simultaneous effects on the gas stream of droplet drag, evaporative cooling, area variation and wall friction lead to many regimes of operation, including the hitherto unknown passage from subsonic to supersonic speeds in a constant-area duct. Theoretical calculations of a one-dimensional nature, involving for the gas stream the equations of continuity, momentum, and energy, and for the liquid droplet cloud the equations of motion, heat transfer, and mass transfer, have been carried out on a high-speed, electronic digital computer. The theory reproduces all the behavior

patterns of experimental units and is in generally good quantitative agreement with the experimental data.

The results of experiments on a small-scale, constant-area unit of 2.13 inches diameter are presented and compared with theoretical calculations. The experiments and theory both show that a net stagnation rise is possible only with gas flows greater than about 2 lb/sec; below this value the detrimental effects of wall friction completely absorb the gains due to cooling. In the range of 25 lb/sec. a net stagnation pressure rise of about 10% seems assured, while 20% seems possible.

Early tests on a recently-completed medium-scale unit of 25 lb/sec capacity have already demonstrated a net over-all rise in stagnation pressure.

2. NOMENCLATURE

A	cross-sectional area of duct
c	speed of sound in gas phase
c_p	specific heat at constant pressure of gas phase
$c_{p\ell}$	specific heat of water in droplet
$\bar{c}_{p12}$	mean value of c_p between 1 and 2
C_D	drag coefficient of droplet
d	volume-surface mean droplet diameter
d_o	value of d immediately after atomization
d_{oj}	value of d_o given by Nukiyama and Tanasawa formula (ref. 4)
D	duct diameter
$\mathcal{D}$	diffusivity of water vapor into air
E	$dp_o/p_o M^2$
f	skin-friction coefficient of pipe

G	see Eq. 8b
h_a	specific enthalpy of air
h_ℓ	specific enthalpy of liquid water in droplet
h_v	specific enthalpy of water vapor
h_D	film coefficient of mass transfer (Eq. C-2)
h_T	film coefficient of heat transfer (Eq. C-5a)
h_o	stagnation enthalpy of gas phase
h_{oa}	stagnation enthalpy of air
h_{ov}	stagnation enthalpy of water vapor
k	ratio of specific heats for gas phase
L	length of evaporation section
$\mathcal{L}$	latent heat of water vapor at temperature T_ℓ
M	Mach Number of gas phase, V/c
Nu_D	Nusselt Number for mass transfer, $h_D d/\mathcal{D}$
Nu_T	Nusselt Number for heat transfer, $h_T d/k$
p	static pressure of gas phase
p_o	stagnation pressure of gas phase
P_o	stagnation pressure of mixture (Eq. A-15)
Pr	Prandtl Number, $c_p \mu/k$
Q	heat added per unit mass of gas
R	gas constant of gas phase
R_a	gas constant of air
R_v	gas constant of water vapor
$\overline{R}$	universal gas constant
Rey	relative Reynolds Number of droplet, $(\rho d \lvert V - V_\ell \rvert)/\mu$
Sc	Schmidt Number, $\mu/\rho\mathcal{D}$
t	time

T	absolute temperature of gas phase
T_ℓ	temperature of droplet
T_o	stagnation temperature of gas phase
V	gas velocity
V_ℓ	droplet velocity
w	mass rate of gas flow
w_a	mass rate of air flow
w_ℓ	mass rate of water flow
$w_{\ell o}$	mass rate of water injected
W	molecular weight of gas phase
W_a	molecular weight of air
W_v	molecular weight of water vapor
x	fraction evaporated, ω/Ω_o
y	V_ℓ/V
Y	see Eq. 13
z	longitudinal distance from inlet plane
Z	see Eq. D-8
α	θ_o/T (see Eq. A-13)
β	See Table III
ε	diffuser loss coefficient (see Eq. D-15)
η_c	compressor efficiency
η_t	turbine efficiency
θ_o	mixture stagnation temperature (see Eq. A-13)

k	thermal conductivity of gas phase
μ	viscosity of gas phase
ρ	mass density of gas phase
ρ_l	mass density of water in droplet
ρ_{vl}	spatial mass density of saturated water vapor at droplet surface
$\rho_{v\infty}$	spatial mass density of water vapor far from droplet surface
τ_w	shear stress at pipe wall
ω	specific humidity of gas phase, lb. of water per lb. of air.
Ω_0	initial water-air ratio, w_{l0}/w_a

Subscripts

1	at inlet of evaporation section
2	at exit of evaporation section
3	at exit of diffuser
a	air
l	water
v	water vapor

3. INTRODUCTION

3.1 Object

The purpose of this paper is to present both an introduction and a progress report on a novel aerothermodynamic device which performs the function of a compressor but which requires only an extremely simple mechanical structure having no moving parts. Basically, the Aerothermopressor is a duct within which atomized water evaporates into a high-speed stream of high-temperature gas, thereby inducing a rise in isentropic stagnation pressure of the gas stream. One of the most attractive applications of the Aerothermopressor is as an auxiliary for improving the performance of a gas turbine plant.

The plan of the paper is (1) to develop the basic ideas and the theory of the Aerothermopressor, (2) to illustrate its application to the gas turbine plant, (3) to discuss the factors entering into the design of an Aerothermopressor and the considerations for handling them, (4) to present the theoretical and experimental results thus far obtained, and (5) to evaluate the future prospects of the Aerothermopressor and name the crucial problems which it faces.

3.2 Basic Concept and Preliminary Theory of Aerothermopressor

A glance at the history of typical inventions shows that almost without exception the theory of a device follows the conception of its mechanical arrangement. The Aerothermopressor seems to be one of those rare instances wherein a theoretical analysis revealed the practical possibilities; in fact, the mode of operation of the Aerothermopressor is so far removed from that intuitive sense which usually underlies invention, that

one can hardly imagine its having been rationally conceived prior to the theoretical advances in gas dynamics of the past decade.

Preliminary Analysis. The formula which motivated the developments reported here, presented by Shapiro and Hawthorne (ref. 1) in 1947, indicates how the isentropic stagnation pressure of a gas stream (Fig. 1) is affected by the various external influences which may alter the state of the stream:

$$\frac{dp_0}{p_0} = -\frac{kM^2}{2}\left[\frac{dT_0}{T_0} + 4f\frac{dz}{D} + 2(1-y)\frac{dw}{w} - \frac{1}{1+\frac{k-1}{2}M^2}\frac{dW}{W}\right] \qquad \text{(Eq.1)}$$

This equation, which is derived from the continuity, momentum, and energy equations for a perfect gas, is the result of a one-dimensional analysis of a simple model in which the external influences considered include changes in the stagnation temperature, pipe-wall friction, and the stepwise injection and evaporation of liquid with a concomitant change in molecular weight of the gas phase. The quantities appearing in this one-dimensional analysis may be thought of as representing certain average properties of the actual duct flow. The local stagnation pressure p_0 is the pressure which the stream would reach if it were isentropically decelerated to rest in steady flow; similarly, the local stagnation temperature T_0 is the absolute temperature which the stream would reach if it were adiabatically decelerated to rest in steady flow. The symbol k

denotes the ratio of specific heats; M, the local Mach Number; f, the pipe-wall skin-friction coefficient; D, the local hydraulic diameter of the duct; z, longitudinal distance along the duct; w, the local mass rate of flow of the gas phase; W, the local molecular weight of the gas phase; and y, the ratio of forward component of liquid injection velocity to gas velocity. In each infinitesimal interval dz, the mass dw of liquid is assumed to be injected into the gas per unit time, and to be completely evaporated and mixed at the end of the interval.

What Eq. 1 shows clearly is that the stagnation pressure tends to be reduced by wall friction, by the aerodynamic drag associated with the injection of liquid (assuming $y = V_l/V < 1$), and by a reduction in molecular weight. Changes in cross-sectional area do not in themselves alter the local rate of change of stagnation pressure. Most significant for our purpose, however, is the observation that a reduction in stagnation temperature (i.e., cooling of the gas flow) tends to <u>increase</u> the stagnation pressure. Moreover, Eq. 1 indicates that the effects noted are the result of a dynamic process, as evidenced by the proportionality of the stagnation pressure change to the square of the Mach Number, and that they may not be produced by thermodynamic changes in a static system. To obtain significant changes in p_0, therefore, it is evident, even from this preliminary analysis, that operation at high subsonic speeds or supersonic speeds may be necessary.

The only possibility for increasing the stagnation pressure is through a process in which the decrease in stagnation temperature can be accomplished in such a way that the adverse effects seen in Eq. 1 are outweighed.

Two practical possibilities come to mind: the first involves the use of ordinary heat exchangers, and the second involves the evaporation of a volatile liquid into the air stream.

Futility of Heat Exchangers. For an ordinary heat exchanger in which the air flows through a tube having cooled walls, Eq. 1 is simplified to the form

$$\frac{dp_0}{p_0} = -\frac{kM^2}{2}\left[\frac{dT_0}{T_0} + 4f\frac{dz}{D}\right] \qquad \text{(Eq. 2)}$$

Detailed analysis of this equation (ref. 1), employing Reynolds' analogy between friction and heat transfer, shows that the stagnation pressure loss produced by wall friction always exceeds the stagnation pressure rise attainable by cooling. Consequently heat exchangers can not accomplish the desired result.

Evaporative Cooling. In order to determine whether evaporative cooling offers any prospects whatsoever, the analysis will for this purpose be simplified in a favorable way by assuming that the frictional term of Eq. 1 is negligible compared with the other terms, and, conservatively, that the liquid is injected with negligible forward velocity. Then Eq. 1 may be written

$$\frac{dp_0}{p_0} = -\frac{kM^2}{2}\left[\frac{dT_0}{T_0} + 2\frac{dw}{w} - \frac{1}{1+\frac{k-1}{2}M^2}\frac{dW}{W}\right] \qquad \text{(Eq. 3)}$$

The energy equation may be written approximately, ignoring the kinetic energy increase of the injected fluid, by equating the decrease of stagnation enthalpy of the gas stream to the enthalpy rise of the evaporated liquid:

$$-wc_p dT_o \cong (h_v - h_\ell)dw \qquad \text{(Eq. 4)}$$

where c_p is the specific heat at constant pressure of the gas phase, h_v is the enthalpy of the injected liquid <u>after</u> it has been evaporated and brought to thermal equilibrium with the gas, and h_ℓ is the enthalpy of the injected liquid.

For the change in molecular weight, we find, from the definition of molecular weight for a gas mixture, the formula

$$\frac{dW}{W} = \left(1 - \frac{W}{W_v}\right)\frac{dw}{w} \qquad \text{(Eq. 5)}$$

where W_v is the molecular weight of the evaporated liquid.

Substituting Eqs. 4 and 5 into Eq. 3, we obtain

$$\frac{dp_o}{p_o} = -\frac{kM^2}{2}\left[2 - \frac{h_v - h_\ell}{c_p T_o} - \frac{1 - W/W_v}{1 + \frac{k-1}{2}M^2}\right]\frac{dw}{w} \qquad \text{(Eq. 6)}$$

From this relation it may be seen that the criterion for a rise in stagnation pressure is that

$$\frac{h_v - h_\ell}{c_p T\left(1+\frac{k-1}{2}M^2\right)} - \frac{W/W_v - 1}{\left(1+\frac{k-1}{2}M^2\right)} > 2 \qquad \text{(Eq. 7)}$$

Now, other things being the same, liquids with large latent heats are most likely to meet the criterion of Eq. 7, inasmuch as $(h_v - h_\ell)$ is of the order of magnitude of the latent heat. Hence water seems to be the desirable choice for the Aerothermopressor because, apart from obvious economic reasons, it has a larger latent heat than almost any other fluid. To gain some concept of orders of magnitude, Table I sets out approximate values of the left-hand side of Eq. 7 for evaporation of liquid water into air.

TABLE I

T_o(deg.R)	M=0	M=1	M=2	M=3	M=4
500	7.4	7.4	7.1	6.8	6.8
1000	4.4	4.3	4.0	3.7	3.6
2000	2.9	2.7	2.4	2.1	2.1

Comparing the figures in Table I with the criterion of Eq. 7, it may be concluded that there is indeed a possibility for increasing the stagnation pressure by evaporating water into a high-speed stream of air, and that this possibility exists over a wide range

of stagnation temperature and Mach Number.

In interpreting Table I it is well to recall (a) that water can be evaporated into the air only so long as the latter is not saturated with water vapor, and (b) that the amount of evaporation which can be effected per unit length of duct depends on the driving temperature difference essential for heat transfer between the gas and the liquid. These considerations, when combined with the values of Table I and the form of Eq. 1 (including the wall-friction term), demonstrate that the maximum rise in stagnation pressure will be obtained when the stagnation temperature is neither excessively high nor excessively low, and with Mach Numbers which are neither excessively large nor excessively small.

3.3 Application of Aerothermopressor to Gas Turbine Plant

Of the various applications of the Aerothermopressor which have been considered, its use in improving both the performance and the characteristics of a gas turbine plant seems to be one of the most promising as well as one of reasonably immediate application.

Cycle Arrangements. The most obvious place for the Aerothermopressor is at the exhaust of the power turbine in the simple gas turbine cycle, (Fig. 2a), where the Aerothermopressor is supplied (at no expense, as it were) with a stream of hot air at sufficiently high temperature to make significant increases in stagnation pressure possible. If the Aerothermopressor produces a rise in stagnation pressure and also discharges to the atmosphere, it follows that the stagnation pressure at the turbine exit will be reduced below atmospheric, thus making the Aerothermopressor analogous to the condenser in a steam power plant.

A second cycle arrangement is shown in Fig. 2b. Here more fuel is burned per unit of air flow than in the cycle of Fig. 2a, the compensating advantages being that the pressure at the turbine inlet is increased while at the same time the mass rate of flow through the turbine is augmented. Nothing stands in the way of installing a second Aerothermopressor at the turbine exhaust, as suggested by the dashed lines of Fig. 2b, thus compounding the improvements in performance.

Effects on Performance. In Figs. 3b and 3c are shown the results of cycle calculations for the simple cycle of Figs. 2a and 3a, illustrating the advantages mentioned above.

It may be seen that the reduction of back pressure betters the performance and the characteristics of the gas turbine plant in a number of ways: (a) the specific fuel consumption is reduced; (b) the specific air consumption is decreased, i.e., the power capacity of a given size of machine is increased; (c) the optimum compressor ratio is reduced in inverse proportion to the square root of the pressure ratio across the Aerothermopressor; and (d) the net work ratio is increased, thus making the plant performance less sensitive to such design variables as turbine inlet temperature and compressor and turbine efficiencies, and consequently permitting acceptable performance with less stringent specifications on these variables than would otherwise be possible.

With a high turbine inlet temperature and with high values of turbine and compressor efficiencies (Fig. 3b), the percentage improvements in fuel economy and in power capacity are approximately equal to the percentage rise in stagnation pressure across the Aerothermopressor. For example,

with a compressor pressure ratio of 4, a stagnation pressure ratio across the Aerothermopressor of 1.2 produces a reduction in specific fuel consumption and specific air consumption of 20%.

With a low turbine inlet temperature and low component efficiencies (Fig. 3c), the improvements in performance are even more marked, and may well change the situation from one of marginal net power output to one of reasonably acceptable performance.

Comparison of Aerothermopressor with Regenerator. In the embodiment of Figs. 2a and 3a, the Aerothermopressor must compete with the regenerator, the latter being the conventional scheme for utilizing the energy in the high-temperature exhaust gas. At this writing it does not seem that the Aerothermopressor can match the improvement in fuel economy accessible to the regenerator. On the other hand, the Aerothermopressor brings about a reduction in specific air consumption (i.e., a rise in power capacity) of magnitude equal to the reduction in specific fuel consumption, whereas the regenerator, by virtue of its frictional pressure drop, produces a slight loss in power capacity. What may be even more important in many practical applications is that an effective regenerator robs the gas turbine plant of the compactness and lightness which often is the outstanding claim of the gas turbine over rival prime movers. As will be seen, the Aerothermopressor is sufficiently small and light as not to be at a disadvantage in this respect, except perhaps for automotive applications. A final compensating advantage of the Aerothermopressor is that it is structurally simple and not subject to the serious problems of

fouling and corrosion which blight the status of the regenerator.

3.4 Effect of Size on Aerothermopressor Performance

So important is the scale effect in the Aerothermopressor that it seems desirable to conclude this introduction with an explanation of this phenomenon before proceeding to more detailed considerations.

For given gas properties at the beginning of the evaporation section and a given initial droplet cloud, the necessary length of the evaporation section is roughly established by the residence time required for the droplets substantially to be evaporated. If the gas and water flows are quadrupled, for example, the cross-sectional area of the duct will also be quadrupled, but such gas properties as velocity, pressure, temperature, etc., will at corresponding sections be nearly the same as before. Accordingly, the required residence time and the required length will also be unchanged, but the length-diameter ratio of the duct will be only half as large as in the first instance. Since the stagnation pressure loss associated with pipe friction is roughly proportional to the length-diameter ratio (Eq. 1), the net rise in stagnation pressure will be greater for the case with the larger air flow. This influence of air flow on the relative prominence of frictional effects is furthermore magnified because the net rise in stagnation pressure of Eq. 1 turns out to be a comparatively small difference between comparatively large quantities.

What all this amounts to is that below a certain scale of air flow the Aerothermopressor is doomed to failure; there is a critical size for which the Aerothermopressor will be on the verge of producing a rise in stagnation pressure; and above this critical size (which, according to our present knowledge, is in the diameter range of 2 to 3 inches)the attainable

stagnation pressure rise mounts rapidly as the scale of air flow is increased.

4. THEORY OF AEROTHERMOPRESSOR

4.1 Thermodynamic Limit of Performance

One of the first questions that comes to mind in evaluating a new device like the Aerothermopressor is, what is the maximum performance of which it is theoretically capable? This may be answered on purely thermodynamic grounds by considering a steady-flow process in which the streams of inlet air and inlet water are brought together in a hypothetical apparatus having no thermodynamic irreversibilities, and producing an exit stream of air saturated with water vapor. As in the actual Aerothermopressor, it is assumed that the reversible apparatus does not exchange heat or work with the surroundings.

The analysis, for given initial properties of air and water requires that (i) the stagnation enthalpy increase for the water equal the corresponding decrease for the air, (ii) the entropy rise of the water equal the corresponding decrease for the air, and (iii) the exit stream be saturated. Pertinent results of the calculations* are shown in Table II for a variety of inlet conditions.

*The analysis and calculations were made by Mr. Alve Erickson, Instructor in Mechanical Engineering, Massachusetts Institute of Technology.

TABLE II

THERMODYNAMIC LIMITS OF PERFORMANCE

Inlet Conditions					Outlet Conditions (Air Saturated)		
Air		Water		Water/Air Ratio			
T_a deg.F	p_a psia	T_w deg.F.	p_w psia		T_f deg.F	p_f psia	$\frac{p_f}{p_a}$
740	10.0	60	14.7	0.128	166	32.0	3.2
"	14.7	"	"	0.125	180	45.0	3.1
1040	10.0	"	"	0.185	214	67.0	6.7
"	12.0	"	"	0.183	222	78.6	6.6
"	14.7	"	"	0.181	230	92.3	6.3
1340	10.0	"	"	0.241	267	142.5	14.3
"	14.7	"	"	0.234	284	190.1	12.9
1040	14.7	60	14.7	0.181	230	92.3	6.3
"	"	100	"	0.187	230	89.8	6.1
1040	14.7	60	14.7	0.181	230	92.3	6.3
"	"	"	3000	0.182	231	93.6	6.4

The overall stagnation-pressure ratio of the gas stream (shown in the last column) is seen to depend primarily on the inlet stagnation temperature of the air. Variations in the inlet air pressure, inlet water pressure, and inlet water temperature exert relatively small influence on the overall stagnation-pressure ratio.

So attractive are the figures in the last column of Table II that a word of caution is necessary lest they be given too much weight. More detailed investigation discloses that it does not seem possible in a real Aerothermopressor even to approach the reversible mixing of air and water upon which Table II is predicted. The main sources of irreversibility in the Aerothermopressor are (i) wall friction, (ii) aerodynamic drag on the accelerating droplets, (iii) heat transfer from the air to the droplets across a finite temperature difference, and (iv) mass transfer of water vapor from the droplets to the air stream across a finite difference in partial pressure. As later discussions of the detailed mechanisms of the Aerothermopressor will show, there seems to be no means by which a device having the general character of the Aerothermopressor can simultaneously reduce all these irreversibilities to small proportions.

A corollary of these remarks is that the last column of Table II, while giving absolute thermodynamic limits, does not give a realistic view of what the actual ceiling to Aerothermopressor performance might be. Thus we are presently in the irritating status of not really knowing what is the best performance which might be reasonably expected of the Aerothermopressor, and it appears that detailed calculations like

those of Section 4.7 may be necessary for its prediction.

Still a further corollary is that the effects of inlet air and water temperature and of inlet pressure shown in Table II are probably not representative of their effects in an actual Aerothermopressor. Inasmuch as irreversibilities play such a strong role in the Aerothermopressor, the influence of the aforementioned properties might be realized most forcefully through their effects on the irreversibilities, and this of course is an aspect totally absent from the analysis underlying Table II.

4.2 One-Dimensional Analysis of Aerothermopressor

Because wall friction dictates a small length-diameter ratio for the Aerothermopressor, the continuously distributed injection and evaporation suggested by Fig. 1 does not represent a good design. In order to approximate maximum droplet residence times, it seems desirable for most of the water to be injected near the beginning of the evaporation section, as suggested in Fig. 2a. For a real Aerothermopressor, therefore, Eqs. 6 and 7 do not adequately represent what occurs, even though they are surely indicative of the true state of affairs inasmuch as the analysis on which they are based does in fact take account (albeit according to a somewhat distorted model) of the principle physical phenomena.

Definition of One-Dimensional Model. In order to obtain a better insight into the details of the Aerothermopressor process, however, and also to provide a more precise theory for numerical calculations, it is necessary to develop an analysis which is in better accord with the true events. In the model we now adopt, the flow is treated as one-dimensional (i.e., no

radial variations in any properties of either the gas stream or the droplet cloud), and the droplets are assumed to be of uniform size. Since atomization occurs very quickly, it is further assumed that at the inlet plane of the evaporation section, spherical droplets of equal size are uniformly distributed over the cross-section and have the velocity and temperature with which they left the injection nozzles.

At any section of cross-sectional area A, the gas flows at the mass rate w and has a certain velocity V, pressure p, temperature T, and composition ω. Simultaneously, the droplet cloud has a certain droplet diameter d and its own mass rate of flow w_ℓ, velocity V_ℓ, and temperature T_ℓ. A distance dz further downstream, the aforementioned properties of both the gas stream and droplet cloud have been altered in consequence of the combined effects of wall friction, change in cross-sectional area, droplet drag, heat transfer, and evaporation; the latter three phenomena result respectively from the differences between the two phases in velocity, temperature, and partial pressure of the water vapor.

Influence Coefficients. For the infinitesimal interval dz (Fig.4a), the analysis is based upon a simultaneous solution of the following equations written in differential form: (i) the governing equations representing conservation of mass, the momentum theorem, and the first law of thermodynamics, (ii) the equation of state of a perfect gas mixture having variable specific heat and obeying the Gibbs-Dalton law of partial pressures and enthalpies, and (iii) the definitions of Mach Number, gas-phase

stagnation temperature and pressure, and mixture stagnation temperature and pressure. Details of the analysis are given in Appendix A, and the results are summarized by the system of influence coefficients presented in Table III. The influence coefficients are simply the coefficients in the algebraic relations connecting the variables of the left-hand column with the variables of the top row. For example,

$$\frac{dM^2}{M^2} = -\frac{2\left(1+\frac{k-1}{2}M^2\right)}{1-M^2}\frac{dA}{A} + \frac{(1+kM^2)\left(1+\frac{k-1}{2}M^2\right)}{1-M^2}\frac{dQ - \frac{w_\ell}{w}dh_\ell}{c_p T_o} + \cdots$$

and so on.

Behavior of Stream Properties Under the Influence of Area Change, Heat Transfer, Evaporation, Wall Friction, and Droplet Acceleration. Apart from their utility for numerical calculations, the influence coefficients of Table III reveal clearly how the stream behaves under the action of area change, friction, etc. A discussion of these influence coefficients at this point will help later to explain the complex and varied behavior patterns exhibited by the Aerothermopressor as well as point the way to rules for design.

Detailed investigation of orders of magnitude shows that of the variables at the top of Table III, those which predominate in the actual Aerothermopressor process are the terms involving area change (dA/A), evaporation (dw/w), wall friction ($4f\,dz/D$), and droplet acceleration ($w_\ell\, dV_\ell / w\, V$). How these effects tend to change the stream properties is summarized in Table IV. Although the table is self-explanatory, some additional remarks will emphasize the most important results.

TABLE III – INFLUENCE COEFFICIENTS

	$\frac{dA}{A}$	$\frac{dQ-\frac{w_\ell}{w}dh_\ell}{c_pT_o}$	$\frac{dw}{w}$	$4f\frac{d_\ell}{D}$	$\frac{w_\ell}{w}\frac{dV_\ell}{V}$	$\frac{dW}{W}$	$\frac{dk}{k}$
$\frac{dM^2}{M^2}$	$-\frac{2\left(1+\frac{k-1}{2}M^2\right)}{1-M^2}$	$\frac{\left(1+kM^2\right)\left(1+\frac{k-1}{2}M^2\right)}{1-M^2}$	$-\frac{\left(1+kM^2\right)\left(1+\frac{k-1}{2}M^2\right)}{1-M^2}\left[\frac{h_v-h_\ell+\frac{V^2}{2}(1-y^2)}{c_pT_o}\right]+\frac{2\left(1+\frac{k-1}{2}M^2\right)}{1-M^2}\left[1+(1-y)kM^2\right]$	$\frac{kM^2\left(1+\frac{k-1}{2}M^2\right)}{1-M^2}$	$\left(\frac{kM^2}{1-M^2}\right)x'$ $\left[2\left(1+\frac{k-1}{2}M^2\right)-\frac{k-1}{k}\left(1+kM^2\right)y\right]$	$-\frac{1+kM^2}{1-M^2}$	-1
$\frac{dV}{V}$	$-\frac{1}{1-M^2}$	$\frac{1+\frac{k-1}{2}M^2}{1-M^2}$	$-\frac{1+\frac{k-1}{2}M^2}{1-M^2}\left[\frac{h_v-h_\ell+\frac{V^2}{2}(1-y^2)}{c_pT_o}\right]+\frac{1+(1-y)kM^2}{1-M^2}$	$\frac{kM^2}{2(1-M^2)}$	$\frac{kM^2-(k-1)M^2y}{1-M^2}$	$-\frac{1}{1-M^2}$	0
$\frac{dp}{p}$	$\frac{kM^2}{1-M^2}$	$-\frac{kM^2\left(1+\frac{k-1}{2}M^2\right)}{1-M^2}$	$\frac{kM^2\left(1+\frac{k-1}{2}M^2\right)}{1-M^2}\left[\frac{h_v-h_\ell+\frac{V^2}{2}(1-y^2)}{c_pT_o}-2+\frac{1+(k-1)M^2}{1+\frac{k-1}{2}M^2}y\right]$	$\frac{kM^2\left[1+(k-1)M^2\right]}{2(1-M)^2}$	$-\frac{kM^2}{1-M^2}\left[1+(k-1)M^2(1-y)\right]$	$\frac{kM^2}{1-M^2}$	0
$\frac{dT}{T}$	$\frac{(k-1)M^2}{1-M^2}$	$\frac{\left(1-kM^2\right)\left(1+\frac{k-1}{2}M^2\right)}{1-M^2}$	$-\frac{\left(1-kM^2\right)\left(1+\frac{k-1}{2}M^2\right)\left[\frac{h_v-h_\ell+\frac{V^2}{2}(1-y^2)}{c_pT_o}\right]+(k-1)M^2\left[1+kM^2(1-y)\right]}{1-M^2}$	$-\frac{k(k-1)M^4}{2(1-M)^2}$	$-\frac{(k-1)M^2}{1-M^2}\left[y+kM^2(1-y)\right]$	$\frac{(k-1)M^2}{1-M^2}$	0
$\frac{dT_o}{T_o}$	0	1	$-\frac{h_v-h_\ell+\frac{V^2}{2}(1-y^2)}{c_pT_o}$	0	$-\frac{(k-1)M^2y}{1+\frac{k-1}{2}M^2}$	$\frac{\frac{k-1}{2}M^2}{1+\frac{k-1}{2}M^2}$	$\frac{M^2/2}{1+\frac{k-1}{2}M^2}$
$\frac{d\theta_o}{\theta_o}$	0	$\frac{1+\frac{k-1}{2}M^2}{\alpha}$	$-\frac{1+\frac{k-1}{2}M^2}{\alpha}\left[\frac{h_v-h_\ell+\frac{V^2}{2}(1-y^2)}{c_pT_o}\right]-\frac{\frac{k-1}{2}M^2\left(1+\frac{w_\ell}{w}y^2\right)}{\alpha}$	0	0	$\frac{\frac{k-1}{2}M^2\left(1+\frac{w_\ell}{w}y^2\right)}{\alpha}$	$\frac{\frac{M^2}{2}\left(1+\frac{w_\ell}{w}y^2\right)}{\alpha}$
$\frac{dp_o}{p_o}$	0	$-\frac{k}{2}M^2$	$\frac{k}{2}M^2\left[\frac{h_v-h_\ell+\frac{V^2}{2}(1-y^2)}{c_pT_o}-2(1-y)\right]$	$-\frac{k}{2}M^2$	$-\frac{kM^2}{2}\left[2-\frac{(k-1)M^2y}{1+\frac{k-1}{2}M^2}\right]$	$\frac{\frac{k}{2}M^2}{1+\frac{k-1}{2}M^2}$	$\left(\frac{k}{k-1}\frac{M^2}{2}\right)\Big/\left(1+\frac{k-1}{2}M^2\right)$ $-\frac{k}{(k-1)^2}\ell n\left(1+\frac{k-1}{2}M^2\right)$
$\frac{dP_o}{P_o}$	0	$-\frac{k}{2}M^2$	$\frac{+\frac{k}{2}M^2\left(1+\frac{k-1}{2}M^2\right)\left(1+\frac{w_\ell}{w}y^2\right)}{\alpha}\left[\frac{h_v-h_\ell+\frac{V^2}{2}(1-y^2)}{c_pT_o}\right]$ $-\frac{kM^2}{2\alpha}\left(1+\frac{w_\ell}{w}\right)y^2-kM^2(1-y)$	$-\frac{k}{2}M^2$	$-kM^2(1-y)$	$\frac{kM^2}{2}\left(1+\frac{w_\ell}{w}y^2\right)$ α	$\frac{k}{(k-1)^2}\left[\frac{\alpha-1}{\alpha}-\ell n\,\alpha\right]$

Definitions:

$y = V_\ell/V$

$\alpha = \theta_o/T = 1+\left(1+\frac{w_\ell}{w}y^2\right)\frac{k-1}{2}M^2$

$T_o/T = 1+\frac{k-1}{2}M^2$

$\beta = \frac{h_v-h_\ell}{c_pT_o}+\frac{\frac{k-1}{2}M^2}{1+\frac{k-1}{2}M^2}(1-y^2)$

$P_o/p = \left(T_o/T\right)^{\frac{k}{k-1}}$

$P_o/p = \left(\theta_o/T\right)^{\frac{k}{k-1}}$

Note: The table summarizes the algebraic relations between the variables of the left-hand column and the variables of the top row, and is to be interpreted in the manner,

$$\frac{dM^2}{M^2} = -\frac{2\left(1+\frac{k-1}{2}M^2\right)}{1-M^2}\frac{dA}{A}+\frac{\left(1+kM^2\right)\left(1+\frac{k-1}{2}M^2\right)}{1-M^2}\frac{dQ-\frac{w_\ell}{w}dh_\ell}{c_pT_o}+\ldots\text{etc.}$$

TABLE IV - BEHAVIOR OF STREAM PROPERTIES UNDER INFLUENCE OF AREA CHANGE, EVAPORATION, WALL FRICTION, AND DROPLET DRAG

		Area increase produces(a)	Evaporation produces(b)	Wall friction produces(c)	Liquid acceleration produces(d)
Mach Number, M	subsonic	decrease	decrease(h)	increase	increase(e)
	supersonic	increase	increase(h)	decrease	decrease(e)
Gas Velocity, V	subsonic	decrease	decrease(h)	increase	increase(e)
	supersonic	increase	increase(h)	decrease	decrease(e)
Pressure, p	subsonic	increase	increase(h)	decrease	decrease(e)
	supersonic	decrease	decrease(h)	increase	increase(e)
Temperature, T	subsonic	increase	decrease(h)	decrease	decrease(e)
	supersonic	decrease	increase(h)	increase	increase(e)
Gas Stagnation Temperature, T_o	subsonic	nil	decrease	nil	decrease(f)
	supersonic	nil	decrease	nil	decrease(f)
Mixture Stagnation Temperature, θ_o	subsonic	nil	decrease	nil	nil(g)
	supersonic	nil	decrease	nil	nil(g)
Gas Stagnation Pressure, p_o	subsonic	nil	increase(h)	decrease	decrease(e)
	supersonic	nil	increase(h)	decrease	decrease(e)
Mixture Stagnation Pressure, P_o	subsonic	nil	increase(h)	decrease	decrease(g)
	supersonic	nil	increase(h)	decrease	decrease(g)

Notes:
(a) Opposite effects for area decrease.
(b) Opposite effects for condensation.
(c) Opposite effects are impossible.
(d) When $y < 1$, $dV_\ell > 0$; when $y > 1$, $dV_\ell < 0$
(e) Dependent upon magnitude of y for liquid deceleration.
(f) Opposite effect for liquid deceleration.
(g) Same effect for liquid deceleration.
(h) Based on β only, and generally correct for β in excess of two; otherwise effects are indeterminate.

Area Change. This has no direct effect on any of the local rates of change of the stagnation properties. Its greatest importance is that it gives the designer some control over the Mach Number and the temperature of the stream.

Heat Transfer and Changes in Liquid Temperature. The term in dQ represents external heat exchange between the two-phase stream and the duct wall; while the term in dh_ℓ represents the excess of all the heat received by the droplet cloud over the enthalpy rise of the evaporated liquid. Net energy extraction from the gas stream either through a negative value of dQ or through a positive value of dh_ℓ tends to produce a gain in stagnation pressure, a reduction in stagnation temperature, and a change in Mach Number away from unity (M decreases at subsonic speeds, but increases at supersonic speeds).

Evaporation. The terms involving dw/w represent several phenomena: (i) the energy exchange associated with the enthalpy increase of the evaporated liquid, (ii) the energy exchange associated with changes in kinetic energy of the evaporated liquid as its velocity changes from that of the liquid to that of the gas, and (iii) the momentum exchange associated with the acceleration of the evaporated liquid. For most intervals of the Aerothermopressor process the first two effects (embodied in the term β) are by far the most important, and therefore Table IV shows the effects due to the β term alone. With this assumption, the criterion for a rise in p_0 is that $\beta > 2(1-\gamma)$, which indicates that the stream is more apt to rise in stagnation pressure after the droplet cloud has been accelerated than in the period immediately following injection.

Wall Friction. Of all the independent variables in Table III, the wall friction term $4f\,dz/D$ is the only one which cannot assume negative values---that is, the term dz is by definition always positive, and the friction coefficient, according to the second law of thermodynamics, may never be negative. Consequently, both stagnation pressures are reduced with any increase in length, thus pointing to the prime requirement of accomplishing the evaporation in the minimum possible distance.

Changes in Liquid Velocity. The term in dV_ℓ must be interpreted with the necessary condition that the liquid is accelerated only while it is traveling more slowly than the gas ($y<1$), and is decelerated only while traveling more rapidly ($y>1$). It represents two physical phenomena: (i) The drag (or thrust, as the case may be) of the liquid droplets on the gas stream, and (ii) the work done by the gas on the liquid when the latter is accelerated. By virtue of its manner of definition, the mixture stagnation temperature θ_0 is unaffected directly by changes in liquid velocity, whereas the gas stagnation temperature T_0 reflects the work effect, liquid acceleration reducing T_0 and deceleration increasing T_0 . Liquid drag always decreases the gas stagnation pressure p_0 ; liquid thrust (negative dV_ℓ) usually, but not always, increases p_0 , (the exception being when y is quite large compared with unity). Of particular interest is the fact that the mixture stagnation pressure P_0 is altered by changes in liquid velocity only when y is different from unity. Strangely enough, both liquid drag and liquid thrust decrease P_0 . This is so because changes in P_0 are the result of the irreversibilities

in the acceleration or deceleration process, and the irreversibility reduces P_o whether the aerodynamic force is occasioned by the droplets moving faster than the gas or vice versa. When the acceleration or deceleration is brought about so slowly that the droplets follow closely the speed of the gas stream (y tending toward unity), the acceleration or deceleration tends to occur reversibly, and the loss in P_o approaches zero.

Molecular Weight. As indicated by Eq. 5, the term dW/W is controlled by the evaporation term dw/w and by the composition of the gas phase together with the molecular weights of air and water vapor. The evaporation of water (molecular weight 18) into air (molecular weight 29) reduces the molecular weight of the gas phase. With dW/W negative, Table III shows that the change in molecular weight induced by evaporation tends to decrease the stagnation temperatures and pressures and to drive the Mach Number toward unity.

Specific Heat. Since k for water vapor is about 1.3 as compared with about 1.4 for air, evaporation yields negative values of dk/k. This in turn tends to increase the Mach Number, decrease the stagnation temperatures, and increase the stagnation pressures.

Subsonic vs. Supersonic Speeds. Examination of Tables III and IV shows that, almost without exception, the effects of heat transfer, wall friction, etc. on the Mach Number, gas velocity, pressure, and temperature are of opposite signs at subsonic and supersonic speeds. This is a well-known phenomenon of gas dynamics, but it is of particular interest and importance here because the multiplicity of phenomena occurring simultaneously in the Aerothermopressor may, by any of several combinations, bring about either choking or continuous transition through the speed of sound (ref.3),

More will be said about this later.

Regarding the four stagnation properties, on the other hand, the effects observed at supersonic speeds are the same as those at subsonic speeds.

4.3 Description of Aerothermopressor Behavior

With the help of the concepts developed in the preceding section, it is now possible to explain the many types of flow patterns exhibited by the Aerothermopressor.

For simplicity, we begin with an Aerothermopressor having a long constant-area evaporation section and with a subsonic Mach Number at the plane of water injection (Fig. 5). In the entry plane the gas flows at high velocity and temperature, and the liquid is injected at low velocity and temperature. The most important phenomena are those of droplet drag, evaporation, and wall friction. Although these three effects of course occur simultaneously, each is predominant over some portion of the process. An appreciation of this fact is essential for a qualitative understanding of the Aerothermopressor operation.

Regime I - Droplet Drag Predominant. During the droplet acceleration period which accompanies and follows atomization, wall friction is comparatively negligible because the large velocity difference produces huge accelerations and excellent conditions for heat transfer to the droplet cloud. Although the effects of heat transfer and evaporation are enormous, they are nevertheless outweighed by the effects of droplet drag. We may therefore speak of Regime I as the zone in which drag is so predominant that it controls the qualitative behavior of the stream. According to

Table IV, therefore, the Mach Number increases, the static pressure decreases, the stagnation pressures decrease, the gas velocity increases, and the static and stagnation temperatures decrease.

At first the velocity and temperature differences between the gas and liquid are so great that they produce enormous rates of evaporation, droplet velocity increase, gas temperature decrease, and liquid temperature increase. These high rates, however, diminish the driving velocity and temperature differentials, with the consequence that the aforementioned rates decrease as the process proceeds.

In the case of the liquid temperature, an increase is reflected in a greatly magnified evaporation rate, which in turn tends to cool the droplet (the vapor pressure varies approximately as the fifteenth power of the absolute temperature in the applicable range). Therefore the droplets rapidly tend to approach the wet bulb temperature of the gas stream, in which state the heat received from the gas is equal to the enthalpy rise of the evaporated material. The local wet bulb temperature does not vary much, and so the droplets remain at nearly constant temperature (in the neighborhood of 150°F) for virtually the entire process.

Regime II-Droplet Evaporation Predominant. As the velocity difference between gas and liquid decreases (y ten ng toward unity), the effects of droplet drag decay much more rapidly than the effects of evaporation, the latter being substantial even for zero velocity difference. A point is reached, therefore, where the evaporative phenomena counterbalance the drag phenomena, and there ensues a zone in which evaporation predominates and controls the behavior of the stream.

Table IV shows that in Regime II the Mach Number decreases, the static and stagnation pressures increase, the gas velocity decreases, and the stagnation and static temperatures decrease.

An unexpected result is induced by the gas deceleration in Regime II. At some point in the vicinity of the transition from Regime I to Regime II, the gas velocity is diminished to the previously-increased droplet velocity. While the gas further decelerates because of evaporation, the liquid tends to retain its momentum, and thus the liquid soon finds itself traveling more rapidly than the gas and consequently being decelerated. For most of Regime II the liquid velocity is slightly greater than the gas velocity, with the velocity spread being constantly narrowed. Correspondingly, the momentum and energy returned to the gas stream induces changes in gas stream properties opposite to those experienced in Regime I. For example, the negative drag in Regime II assists in the recovery of the stagnation pressure lost in Regime I. It should be noted that these effects are proportional to the mass of liquid involved, which steadily decreases as evaporation proceeds. Hence less is returned to the stream in Regime II than taken from it in Regime I.

Regime III-Wall Friction Predominant. In the course of Regime II, the evaporation rate becomes ever smaller as the surface area of the droplets decreasss and as the velocity and temperature differences promoting heat transfer are eaten away. Ultimately a stage is reached where pipe friction, which hitherto has lurked in the background as a weak contender, takes over by default.

In Regime III, where wall friction is controlling, Table IV indicates that the Mach Number and gas velocity once again rise, and the static and stagnation pressures fall.

Little need be said about Regime III except that it has no place in a well-designed Aerothermopressor. Nothing is to be gained, and much can be lost, by allowing the evaporation section to be so long that evaporative cooling is outweighed by pipe friction. The stream should be allowed to enter a decelerating diffuser some distance before the transition from Regime II to Regime III.

Transition Through Speed of Sound. As observed in Fig. 5 and Table IV, the predominance of drag in Regime I drives the Mach Number toward unity, while the predominance of evaporative cooling in Regime II drives the Mach Number away from unity. This permits a continuous transition through Mach Number unity at the cross-over point where droplet drag and evaporative cooling nullify each other (ref.3); what happens is analogous to the passage through the speed of sound in an isentropic Laval nozzle, wherein the tendencies of the contracting section to force the Mach Number toward unity and of the diverging section to force it away from unity are exactly nullified at the geometric throat.

The longitudinal Mach Number distributions are shown in Fig. 6a for a subsonic entry. For a low initial Mach Number, M rises from a to b (drag controlling), then decreases (evaporation controlling). An increase of initial Mach Number from a to c increases from b to d the Mach Number at which evaporation begins to control over drag. There is a unique initial Mach Number (depending of course on such parameters as initial stagnation temperature, water-air ratio, etc.), called the critical

Mach Number, for which the cross-over point occurs exactly at Mach Number unity. This condition yields curve e-f, downstream of which the Mach Number may either ascend into the supersonic region or descend into the subsonic region, for either event satisfies the requirement of Table IV that, in the region where evaporation controls, the Mach Number proceed away from unity. Whether the flow follows the subsonic curve f-g or the supersonic curve f-h depends on the back pressure of the system, just as in the case of the Laval nozzle. Thus, contrary to widely-held belief, it is possible for a flow to pass from subsonic velocity to supersonic velocity in a duct of constant area.

Mathematically, the transition through point f may be interpreted in terms of the algebraic relation for dM^2/M^2 represented by the first line of influence coefficients of Table III. For our present purpose we may write this as

$$\frac{dM^2}{dz} = \frac{G(z)}{1-M^2} \qquad \text{(Eq. 8a)}$$

where

$$G = M^2\left(1+\frac{k-1}{2}M^2\right)\left[-2\frac{d(\log A)}{dz}+\frac{(1+kM^2)}{c_p T_0}\left(\frac{dQ}{dz}-\frac{w_z}{w}\frac{dh_0}{dz}\right)+\cdots\right] \qquad \text{(Eq.8b)}$$

in which, for a given case, G is a function of z alone inasmuch as all the stream properties, M, T, ρ, etc., and their derivatives, $dM/dz, dT/dz$, etc....are functions of z alone.

From what has been said before, the sign of G depends on whether

drag or evaporation is controlling. The sign of dM^2/M^2, however, depends not only on the sign of G, but also upon whether the flow is subsonic or supersonic, as summarized in Table V.

Table V - Sign of dM^2/dz

	M < 1	M = 1	M > 1
G > 0 (drag controls)	+	∞	-
G = 0	0	indeterminate	0
G < 0 (evaporation controls)	-	∞	+

For subsonic flow, the table clearly shows a maximum in the curves $M(z)$ at the point where $G=0$ (i.e. evaporation and drag evenly balanced), a rising Mach Number in Regime I, and a falling Mach Number in Regime II. What is of additional interest is that dM^2/dz is of the indeterminate form $0/0$ when G passes through zero as M becomes unity; it is this mathematical singularity which permits passage through Mach Number unity. The slope of the Mach Number curve at point f may be found by applying L'Hospital's Rule to Eq. 8a, from which it is found (ref. 3) that

$$\left(\frac{dM^2}{dz}\right)_f = \pm\sqrt{-\left(\frac{dG}{dz}\right)_f} \qquad \text{(Eq.9)}$$

Thus, when $M=1$ and $G=0$, the flow may be continued only if G is decreasing, and in that case there are two solutions having slopes of equal magnitude but opposite sign, one proceeding to supersonic speed and the other to subsonic.

The critical curve e-f-g and e-f-h is a singular curve in the family of solutions of Eq. 8a, and the point f is known as a saddle point singularity.

Choking. Referring again to Fig. 6a, an increase of initial Mach Number from e to j causes the Mach Number to reach unity while drag is still controlling(i.e., with G still positive). Under these conditions it is impossible for the solution to be continued (ref. 3), and we say that the flow is choked. In practice, the flow represented by the curve j-k is possible only if the duct area is increased at k or earlier. If the duct continues at constant area, a steady flow with initial Mach Number j may not be realized, and the highest initial Mach Number which is possible is that at e, hence the term critical Mach Number.

Shock Waves. When the flow becomes supersonic on the branch f-h of Fig. 6a, still another feature in the form of normal shocks may add to the variety of possible flow patterns. These take the flow from supersonic speed to subsonic speed, after which the Mach Number decreases according to Table V. Thus, depending on the back pressure, such Mach Number distributions as e-f-n-l-m or e-f-n-p-q may be observed.

Supersonic Entry. All the discussion relating to Figs. 5 and 6arefer to a subsonic initial Mach Number. For a supersonic Mach Number at the plane of injection the situation is analogous: there will be the same three predominating Regimes already described, but the directions of change will in many instances be different. A descriptive picture of the flow may, however, be constructed from Tables IV and V, and Fig. 6b shows some of the Mach Number distributions which may arise.

4.4 Self-frustrating Tendency of Constant-area Aerothermopressor

Perceptive readers may have already noticed in Fig. 6a a neurotic inclination of the constant-area Aerothermopressor toward either self-emasculation or suicide.

Referring to Eq. 1, or to the last two lines of influence coefficients of Table III, it is seen that the fractional gain in stagnation pressure is mathematically represented by the product of M^2 and an expression representing the net difference between the adverse effects of drag and wall friction and the favorable effects of evaporative cooling, an expression which for brevity we now call E (precisely, $E \equiv dp_o/p_o M^2$). The term E is positive when evaporative cooling is predominant, i.e., when the stagnation pressure is rising. Now E is influenced rather strongly by the local Mach Number because the rate of evaporation is controlled by heat transfer, and the latter in turn depends on the difference between the static temperatures of the gas and the liquid. Thus, other things being equal, E is a maximum at Mach Number zero, and decreases with increasing Mach Number until it becomes negative, at which condition the stagnation pressure decreases.

The product M^2E, which is a measure of the fractional change in stagnation pressure, therefore starts at zero for zero Mach Number, then increases as M increases, and, after passing through a maximum, decreases until it finally becomes negative at a sufficiently high Mach Number (see Fig. 7a).

Subsonic Impotence. In all the subsonic curves of Fig. 6a, the predominance of evaporative cooling causes the Mach Number to decrease in Regime II. By tending to restrain the gas temperature from decreasing, this Mach Number reduction in turn is favorable for maintaining high rates of evaporation, and thus the tendency toward decrease in Mach Number is further enhanced. The net result is that of evaporative cooling is strongly ascendant over drag and wall friction. Though this may seem desirable, it is of little avail, since the potency of the process is vitiated by the low Mach Number which the high value of E produces, and the gains realizable from evaporative cooling are to a degree forfeited.

In brief, the process is self-defeating because at the very moment when evaporative cooling stands at the center of the stage ready to produce large gains in stagnation pressure, it finds itself with equal fervor reducing the Mach Number to the point where what should be a shout is only a whisper!

Supersonic Suicide. Suppose now that the flow has achieved the supersonic curve e-f-h-n of Fig. 6a. Having arrived in Regime II, evaporative cooling pushes the flow to higher and higher Mach Numbers, both effects inducing a rapid drop in the gas temperature. As a consequence, the evaporation rate is seriously reduced. Ultimately, the rate of evaporation is reduced to such a negligible amount that the stream would scarcely change state any further except for the effects of wall friction which are now predominant. To be sure, the decelerating influence of wall friction permits a slight revival in the rate of evaporation, but this only produces a battle of attrition in which evaporation

occurs only insofar as the changes brought about by wall friction permit it to, and no net gain is possible.

The suicidal tendency is now revealed: At supersonic speeds, the predominance of evaporative cooling increases the Mach Number, paving the way for wall friction to become predominant and thus negating the benefits of further evaporation.

Importance of Mach Number Control. What may the designer, acting in the role of psychiatrist, do to assure a more healthy behavior of the Aerothermopressor, with the aim of extracting the maximum possible rise in stagnation pressure? He may in fact do a great deal, by controlling the Mach Number distribution either through the medium of changes in cross-sectional area of the evaporation section or through the introduction of additional water at downstream stations. The former possibility is discussed below.

In subsonic flow, a decrease in area is at first required to prevent the Mach Number from falling too rapidly. At supersonic speeds the area must also be diminished in order to prevent the Mach Number from becoming too high. In either case, however, as the process proceeds, a point is reached at which it is desirable to have a falling Mach Number in order to maintain the evaporation rate, and this ultimately dictates an increase in area at some subsonic speed. Thus the evaporation section merges continuously with the diffuser, and there is no real line of demarcation between the two.

From this discussion emerges the significance of area control as a means for achieving maximum performance. More is said on this important

subject in Sections 4.5 and 4.6.

Mach Number control by additional water injection depends on the fact that immediately after injection the drag of the additional water tends to predominate, and this provides a means whereby the Mach Number may be pushed towards unity.

4.5 Approximate Method for Selecting Best Area Variation in Evaporation Section

The discussion in the preceding section may be given an approximate analytical form which provides a design method for selecting a variation in cross-sectional area which is at least in the neighborhood of that for optimum performance.

Detailed calculations of the type shown in Section 4.7 indicate that the total distance occupied by Regime I is only a few inches, and that only a small fraction of the evaporation occurs during this period. In Regime II, where most of the evaporation occurs, the droplets have a speed very near that of the gas stream (i.e., $y \cong 1$), and the liquid temperature is nearly constant at a value differing little from the local wet-bulb temperature. By assuming that $y = 1$, and that the liquid temperature is constant and equal to an average value of the wet-bulb temperature, Eq. B-9 expressing the fractional rise in stagnation pressure per unit of humidity increase, $(1/P_0)(dP_0/d\omega)$ may be derived, as shown in Appendix B.

Design Procedure for Regime II. As explained in Appendix B, the choice of the parameters $T_{01}, \Omega_0, d_0, Nu$, and f/D permits the construction of the curves such as shown in Fig. 7a. For each value of ω , the curves show clearly the insignificant gains achievable at low Mach Numbers, and the rapidly deteriorating performance at excessively high

Mach Numbers.

To appreciate Fig. 7a, we first ask, what is the criterion for best performance? The answer is simply that the net stagnation pressure rise of the entire process be a maximum. Now this does not necessarily require that the most stagnation pressure rise be realized for each increment evaporated, for a sacrifice at an early stage may augment the potentialities at a later stage. Consequently, the maximization of the overall stagnation pressure rise is no simple matter, transcending by far in difficulty the conventional variational problem of the calculus. Dealing with this in its full complexity necessarily hinges on the numerical integrations discussed in Section 4.7. With the present simplified design procedure, there is no better choice than to make the plausible assumption that a design which maximizes the stagnation pressure rise for each interval of evaporation will in fact also approximate the design which gives maximum over-all rise in stagnation pressure.

The foregoing statement is equivalent to saying that the dashed line, labelled "design curve" in Fig. 7a, passing through the maximum points of the curves of constant ω , yields at least a first approximation to the best Aerothermopressor design in Regime II. Transferring each point of the "design curve" to Fig. 7b, we obtain the solid line representing the optimum variation of M with ω . The solid curve of Fig. 7c is determined by plotting the value of $dP_0/P_0 d\omega$ at each point of the "design curve" against the corresponding value of ω ; this curve represents the maximum fractional rise in stagnation pressure per unit of evaporation.

By integrating the area under the curve of Fig. 7c, the change in stagnation pressure associated with a given amount of evaporation may then be computed. From the equation of continuity it is then possible to calculate the cross-sectional area for each value of ω . Then, using Eq. B-8, the longitudinal coordinate of each point may be determined by numerical integration, thus establishing the shape of this portion of the Aerothermopressor.

The method described is found to lead to the result that the Mach Number must be decreased as the evaporation proceeds. This generally dictates a reduction in cross-sectional area in the early part of Regime II, followed by an increase in the later part.

Effects of Initial Parameters on Best Design. Figs. 7b and 7c illustrate with dashed lines the comparative positions of the "design curves" which result from Fig. 7a for different values of the initial parameters more favorable to effective operation. Such more effective operation comes from higher values of T_{o_1} and Nu , and from lower values of d_o and f/D .

Under these circumstances the curves of constant ω in Fig. 7a are displaced upwards and to the right. This in turn moves the corresponding "design curves" of Figs. 7b and 7c upwards. Thus, with more favorable initial parameters, the level of operating Mach Numbers is higher, and greater increases in stagnation pressure per unit of evaporation may be achieved.

Evaluation of Simplified Design Procedure. The principal defect of the method outlined above is that it is incapable of revealing the correct

Nusselt Number to be used at each stage. To determine Nu requires an evaluation of the velocity difference between the phases, and this can be found only from a consideration of the entire past history of the process. The $dP_o/P_o d\omega$ analysis gives recognition only to the present state of affairs, and does not look to the past or to the future. During the course of the process, the value of Nu changes continuously, and a series of charts like that of Fig. 7a, each with a different value of Nu, would be really necessary for establishing the best design (assuming that Nu were known at each point). This limitation is more important than it might at first seem to be, because the comparatively small difference between the total beneficial effects of evaporative cooling and the total detrimental actions of drag makes a change in Nu from, say 2 to 4, most significant in reorientating the optimum variation of M with ω.

What all this means is that the $dP_o/P_o d\omega$ method cannot give the Aerothermopressor the advantages which might accrue from control of the Nusselt Number. For example, by choosing what might appear to be a comparatively unfavorable Mach Number distribution at one stage, the ensuing acceleration or deceleration of the stream might be used to establish large velocity differences and correspondingly large Nusselt Numbers, with the consequence that increased gains in stagnation pressure realized at a later stage might more than compensate for the mediocre performance accepted at the earlier stage.

Thus the $dP_o/P_o d\omega$ analysis advises the Aerothermopressor to "live for the present only, with no thought for the future", and consequently cannot by itself give the final answer to the question of how

the Aerothermopressor should be designed. On the other hand, it certainly represents a starting point for a more adequate approach such as that outlined in Section 4.7, and it is hoped that ultimately a study of specific results generated by the rather involved procedure of Section 4.7 will in turn suggest some simple rules of thumb with which the results of the comparatively simple $dP_o/P_o d\omega$ method may be modified to be more closely in accord with the best design.

4.6 Some Design Considerations

Disarmingly simple as it is in structural arrangement, the Aerothermopressor is host to a bewildering variety of physical events. These phenomena, constituting fundamentally mass conservation, momentum effects, and energy effects for both the droplet cloud and the gas stream, are strongly inter-related. Consequently the designer, in attempting to give due weight to each factor influencing performance, is faced in the Aerothermopressor with a large number of conflicting tendencies. The best design is, as usual, a compromise among these. What is baffling is that at present there seems to be no simple way for evaluating the relative importance of each effect and thus of arriving at clear-cut design rules. No doubt a combination of sufficient experimental data with worked-out numerical cases such as those of Section 4.7 will someday help in this regard.

Having made these rather discouraging remarks, we may immediately add that much is indeed known in a qualitative way about the influences of the most important design variables. This knowledge is important not only because it reveals pitfalls, but also because it usually

suggests how experimental information can be used in improving a given design. Therefore we shall discuss below the major elements of the Aerothermopressor, state the decisions facing the designer in each, and present the major considerations by which the design choices may be made.

Design Specifications. In a specific situation, we are confronted by design values of air flow (w_a), initial stagnation temperature (T_{oi}), and initial stagnation pressure (p_{oi}), although the magnitudes of the two latter quantities are in some degree dependent on the performance of the Aerothermopressor itself. In addition, there may be a range of these three parameters specified in the area of off-design operation.

Control of Aerothermopressor. Once a particular unit has been built, at least three procedures are possible for adjusting to off-design conditions or for compensating for imperfections in design:

(i) By far the easiest scheme is to control the rate of water injection at inlet, thereby governing the water-air ratio. Presumably it would be routine procedure for the operator to adjust the water flow to the point of maximum stagnation-pressure rise. At best, however, this method can take care of off-design conditions or lapses in design only approximately.

(ii) "Trimming" of the lengthwise Mach Number variation may be accomplished by means of variable-area devices such as a central plug or a series of concentric sleeves located along the axis of the Aerothermopressor. This would considerably detract from the mechanical simplicity which the Aerothermopressor otherwise possesses.

(iii) "Trimming" of the lengthwise Mach Number variation may be achieved also by the injection of auxiliary water at several stations along the evaporation section. Even though the effectiveness of the auxiliary water may be slightly impaired through a loss in residence time, the effectiveness of the main injected water might be augmented sufficiently to effect a net gain.

Aerothermopressor Components. For purposes of isolating and dealing separately with the principle phenomena, it is convenient to think of the Aerothermopressor as comprising the following elements: (i) the air nozzle which accelerates the hot air from the low-speed upstream section into the high-speed section; (ii) the water injection system; (iii) the "acceleration" section, in which occur atomization and the major portion of the droplet acceleration; (iv) the evaporation section, in which evaporation is generally controlling and where most of the evaporation occurs; and (v) the diffuser, which ultimately decelerates the stream to low speeds and terminates the process.

Each of these components will now be considered separately.

Air Nozzle. Two questions arise here: (i) how high should be the Mach Number M_1 at the nozzle exit (which is also the plane of water injection), and (ii) what shape should the nozzle have?

For the specified values of w , p_{01} , and T_{01} , the diameter at the nozzle exit determines the Mach Number M_1. If M_1 is excessively large, the stagnation-pressure loss associated with the droplet acceleration may be prohibitive; however, if it is too small, the droplet diameter will be comparatively large, and the required length of the evaporation section will be excessive, leading to intolerable frictional

losses. The best value of M_1 in each case must, therefore, be determined either by experiment or by calculations of the type illustrated in Section 4.7.

The influence of the Mach Number level on the length required for evaporation may be seen from the following approximate considerations: For air atomisation, the droplet diameter d_0 varies inversely with the air velocity V (ref. 4). Since the distance travelled by each droplet during its acceleration period is a very small fraction of the total distance L required for evaporation, L may be approximated by supposing that the droplet moves with the same velocity as the air. From considerations of heat transfer,

$$-\frac{\rho_l(h_v-h_l)\pi d^2}{2}\frac{dd}{dt} = h_T\pi d^2(T-T_l)$$

For very low Reynolds Numbers, $h_T d/k = 2$. Substituting this value of h_T, and integrating the equation, we find that the time for complete evaporation follows the law $t \sim d^2$. In addition, the length L is proportional to the product of V and t. Therefore,

$$L \sim Vt \sim (1/d)(d^2) \sim d \sim 1/V$$

and the required length is seen to be inversely proportional to the velocity. For a given length, a greater fraction of total evaporation occurs at high air speeds than at low, even though high air speed means

a comparatively small residence time.

Regarding the shape of the air nozzle, the main considerations here are that (i) it should be longitudinally as short as possible so that any massive part of the water injection system may easily be placed in a low-velocity region, and (ii) it should avoid adverse pressure gradients on the walls large enough to induce boundary-layer separation.

Water Injection System. The requirements of the water injection system are that (i) the droplet cloud produced should have the smallest possible volume-surface mean drop size, (ii) the drop size spectrum be such that the mass fraction of the drops lying above the volume-surface mean size is not too large, (iii) the droplet cloud should be uniformly distributed over the cross section, and (iv) the parasitic stagnation-pressure loss associated with the aerodynamic drag of the injection system should be a minimum.

Without precluding the possibility of other arrangements which may prove more favorable, most of the effort thus far has been given to a "porcupine" type of injector, comprising small tubes in parallel, with the water injected at low speed into the high-speed air approximately at the exit of the air nozzle. Little more can be said now about the injection system except that the lack of precise information concerning the drop size produced is perhaps the weakest link connecting theory and experiment.

The best water-air ratio results from a compromise between two opposing effects. That is, as the water flow is increased, the acceleration drag is increased (unfavorable), but the amount of evaporation occurring

in a given distance is also increased (favorable). Fortunately this is a matter which in each case can be very easily settled on an operating Aerothermopressor.

Acceleration Section. Within the very few inches of length constituting the acceleration section, the droplet cloud is formed and accelerated approximately to the gas speed, and of the order of 1/4 the total evaporation occurs. Because of the exceedingly short length (ref. 5) and the extra complexity of the processes in this region, it may prove unfeasible to attempt any Mach Number control by means of area variations in this zone.

A considerable loss of stagnation pressure occurs in the acceleration section. The loss of stagnation pressure associated only with the acceleration of the droplet masses (disregarding heat transfer and evaporation) is illustrated by the following values (ref. 5) for a water-air ratio of 0.2 (the loss is approximately linear with water-air ratio):

M_1	p_{02}/p_{01}	P_{02}/P_{01}
0.3	0.978	0.988
0.4	0.957	0.977
0.5	0.927	0.961
0.615 (choked)	0.846	0.933

These losses are of the same order as the net gain in the Aerothermopressor, thus emphasizing strongly the necessity of careful design at

every point in order to achieve acceptable performance.

For the limiting case of vary low Mach Number, a formula for the irrecoverable loss of stagnation pressure due to droplet acceleration may be derived. From momentum considerations, the pressure change ($p_B - p_A$) due to the acceleration of the drops from zero speed to the gas speed V without area change is given by

$$p_A - p_B = \frac{w_e V}{A} = \frac{w_e}{w_a} \rho_a V^2 \qquad \text{(Eq. 9)}$$

and is equal to the loss in gas stagnation pressure during the acceleration. If the mixture is then reversibly decelerated to zero speed, the pressure p_C attained is calculated by considering the two-phase mixture to be homogeneous with the appropriate density:

$$p_C = p_B + \left(1 + \frac{w_e}{w_a}\right) \frac{\rho_a V^2}{2} \qquad \text{(Eq. 10)}$$

Accordingly the net loss in stagnation pressure is given by

$$\left(p_A + \tfrac{1}{2}\rho_a V^2\right) - p_C = \frac{w_e}{w_a} \frac{\rho_a V^2}{2} = \frac{w_e}{w_a} \frac{kpM^2}{2} \qquad \text{(Eq. 11)}$$

That is, the minimum conceivable net loss in stagnation pressure is one dynamic head multiplied by the water-air ratio, and is exactly one-half the loss in gas stagnation pressure during the acceleration.

The best water injection velocity is governed by the opposing considerations that (i) a low water injection velocity results in small drops but large acceleration loss, whereas (ii) a high water injection velocity gives large drops but small acceleration loss.

The required number of injection points depends on the angle of spread of the droplet spray. From the data obtained thus far, it appears that the best number probably lies within the range of 1/2 to 2 injection points per square inch of cross-section.

Evaporation Section. The primary considerations for the design of the evaporation section have already been discussed in Sections 4.4 and 4.5.

Diffuser. No precise line of demarcation in terms of the Aerothermopressor process can be made between evaporation section and diffuser, inasmuch as significant evaporation and droplet deceleration effects occur within the diffuser. A substantial portion of the evaporation may occur in that portion of the evaporation section which has geometrically diverging cross-section. Moreover, the gas decelerates and the pressure rises in virtually the entire length of the evaporation section.

Granting these facts, a stage is ultimately reached in the Aerothermopressor process where the main objective is to decelerate the stream and recover pressure efficiently. This part of the apparatus is arbitrarily called the diffuser. The best conventional diffuser is a cone of approximately 6° included angle. A consideration of the concurrent phenomena of evaporation and droplet deceleration occurring in the Aerothermopressor diffuser, however, can be interpreted to suggest a somewhat longer diffuser in order better to exploit these additional phenomena. The diffuser of smaller angle makes the revived evaporation in the diffuser more

effective because it causes the evaporation to occur at relatively higher Mach Numbers; and it adds to the efficiency of droplet deceleration by causing the droplets to remain more nearly at the gas speed (ref. 6).

Optimum Mach Number Distribution for Entire Aerothermopressor. Guided by a combination of the qualitative considerations presented in this Section, together with approximate design method for Regime II given in Section 4.5 and the results obtained by the more complete theoretical method discussed later in Section 4.7, the nature of the optimum Mach Number distribution for the entire Aerothermopressor may be rationally anticipated. The discussion is illustrated schematically in Fig. 7d.

From a consideration of the importance of maintaining a large temperature difference for heat transfer, we may confidently expect that the position of maximum Mach Number (point b) should occur near the beginning of the process where the humidity is low and the stagnation temperature high.

Now, referring to the approximate method for Regime II, large values of the relative Reynolds Number can be established only in the part of the process where the Mach Number is high and where large accelerations and decelerations are possible. Thus, in the neighborhood immediately downstream of point b, the curve of M vs. ω will be that of Fig. 7b for a Nusselt Number of about 4. Near the end of the evaporation region the Mach Number is necessarily smaller, the speed of sound is lower, and large accelerations or decelerations are no longer possible. Together with the fact that the droplet diameter is also smaller, all this implies that the relative Reynolds Number is quite small. Therefore,

near the end of the evaporation section (point c), the curve of M vs. ω should be like that of Fig. 7b for a Nusselt Number of about 2.

Assuming that point c represents the location where the rate of stagnation pressure rise has virtually vanished, the curve c-d will represent the diffuser. The latter, as explained previously, will most probably be a cone of half-angle somewhat less than 3°.

The best inlet Mach Number (point a) cannot be foreseen easily, as it depends on the best compromise between small droplet size and small acceleration drag. In some cases the inlet Mach Number might be the highest of the entire process, and then M would decrease continuously.

The value of ω at point b is determined by the advantage of making the Mach Number rise from a to b occur as quickly as possible, with the restraint, however, that too rapid an acceleration will maintain such large differences in velocity that large losses in P_o will be produced. It seems extremely important to choose the location and Mach Number of point b wisely, for the nature of the entire process calls for the maximum exploitation of the benefits of cooling in the very region where evaporation is most predominant, where the temperature differential is still large, and where there exists the possibility of operating locally at large Mach Numbers. Immediately downstream of point b is where the maximum gains are to be won, and if they are not won there, they are forever forfeited.

In summary then, the best Mach Number distribution for subsonic entry appears to call for a soaring rise of Mach Number in the acceleration zone, followed by a gradual decrease in Mach Number in Regime II (involving a gradual transition from the curve $Nu \cong 4$ to that for $Nu \cong 2$),

and concluded by a fairly rapid decrease of Mach Number in the diffuser.

4.7 Numerical Calculations of Aerothermopressor Process

Because of its complexity, its many diverse design considerations, and the fact that only by great care can a poor design be avoided, a successful future for the Aerothermopressor may depend as much on the development of a rational theory as on experimental development. The latter goes slowly, and may be of greatest significance in helping to form a theoretical design method which adequately represents Aerothermopressor performance. Then we may look to the theory for such matters as determining the optimum cross-sectional area variation, extrapolating performance to unknown ranges of supply pressures and temperatures, and predicting off-design performance.

Theoretical Model for Analysis. The analysis considered is purely one-dimensional: in any cross-sectional plane (i) the gas velocity, temperature, and pressure are uniform, and (ii) the droplet velocity, temperature, size, and spatial density are uniform. In addition it is assumed that the droplets are atomized immediately upon injection, and that no subsequent atomization or agglomeration occurs.

Variables of the Analysis. At the entry plane of the Aerothermopressor (section 1), the initial conditions may be characterized by seven quantities, of which the first six are intensive and the last extensive:

(i) p_{01} , inlet gas stagnation pressure

(ii) T_{01} , inlet gas stagnation temperature

(iii) M_1 , inlet Mach Number

(iv) Ω_0 , inlet water-air ratio

(v) T_{l1} , inlet liquid temperature

(vi) V_{l1} , inlet liquid velocity

(vii) A_1 , inlet cross-sectional area

Note that p_{01} , T_{01} , M_1 , and A_1 together determine the air flow rate w_a , so that w_a could be used in place of A_1 . Furthermore, for a given style of water injector, we may anticipate that the listed variables will determine the initial droplet diameter d_0 .

The duct itself may have a shape which might be characterized by relating the area ratio to the distance z from the inlet plane. For example, we might write

$$\frac{A}{A_1} = 1 + \alpha_1 \frac{z}{\sqrt{A_1}} + \alpha_2 \frac{z^2}{A_1} + \cdots \qquad \text{(Eq. 12)}$$

where α_1 , α_2 , etc., are dimensionless numbers defining the duct shape.

At any section z downstream of the inlet plane, having a local cross-sectional area A , the state of the stream may be characterized by six intensive quantities:

(i) p , gas pressure

(ii) T , gas temperature

(iii) M , Mach Number

(iv) ω , specific humidity

(v) T_l , liquid temperature

(vi) V_l , liquid velocity

Governing Equations. Thus, for specified values of the seven initial variables and a specified duct shape, six physically independent equations are necessary for establishing the six required properties at each station z. These six equations are fundamentally (i) the equations of continuity, momentum, and energy for the gas stream, and (ii) the equations of mass transfer, heat transfer, and drag for the droplet cloud.

The three governing equations for the gas stream are derived in Appendix A, and their simultaneous solution has already been summarized by means of the influence coefficient equations of Table III. In these equations the terms du/u and dW/W are dependent on mass transfer (evaporation) from the droplets; the term dk/k is dependent upon changes in temperature and humidity of the gas stream; the term in dh_2 is dependent on the mass transfer and heat transfer for the droplets; and the term in dV_2 is dependent on the drag forces between the droplet and gas. Therefore, a complete analytical formulation of the problem requires that the equations of Table III be augmented by the three equations of mass transfer, heat transfer, and drag for the droplets. The derivation of the latter equations is presented in Appendix C.

Numerical Solution of Equations. The system of ordinary, simultaneous, non-linear, differential equations referred to above seems to be well beyond the possibility of analytical integration, and numerical solution is therefore necessary. After a brief experience with working out solutions by hand computation, it became evident that real progress

could be made only by a much more rapid calculation procedure. The problem was accordingly programmed for the Whirlwind I computer, a high-speed, electronic, digital machine at the Massachusetts Institute of Technology.

Although extended discussion of the means of solution is inappropriate here, it may be mentioned in passing that some of the difficulties encountered during the development of this numerical treatment involved (i) adequately large high-speed memory, (ii) tolerably small truncation error without excessively large computational time, (iii) tendency of the numerical solution toward serious instability, and (iv) establishment of the singular solution passing continuously through Mach Number unity. More details are given by Gavril (ref. 8).

At the present time the fourth-order Runge-Kutta method of numerical integration is used, but the general scheme of calculation may be more easily illustrated by considering the first-order (Euler) method of numerical integration. In the latter the basic idea is to calculate the increment at a point using only the first term of the Taylor Series expansion about the point, for example, $\Delta M^2 \cong (dM/d\chi)\Delta\chi$. Suppose that the initial values of the problem are given, and that the fraction evaporated, $\chi = \omega/\Omega_o$, which is taken as running variable, is divided into many small intervals $\Delta\chi$. The finite difference equations are then solved for each interval, and the properties computed for the end of the interval are then available for use in the next interval.

To illustrate, imagine that the calculations have been carried to a certain value of χ , where the values of ω , d , V_ℓ , T_ℓ , ρ , T , V , M , z , and A are all known. Then, for an increment in humidity $\Delta\chi$: the values of Δd and $\Delta\omega$ are calculated from Eq.C-1;

ΔT_ℓ is computed from Eq. C-5b with Eqs. C-3, C-3a, C-4, C-6, and C-7; Δt is found from Eq. C-5a with Eqs. C-6 and C-7; ΔV_ℓ is obtained from Eq. C-8 with Eqs. C-9; and, finally, the distance Δz , in which the foregoing changes in droplet properties occur, is determined by Eq.C-10. Assuming that the duct shape is known ΔA may be found for the corresponding Δz . All the increments in the top row of Table III are now known for the step under consideration, and the corresponding changes in gas properties, ΔM^2 , Δp , ΔV, etc., may be reckoned from the equationsof Table III. Having carried out these calculations, the droplet and gas properties are completely determined at the end of the humidity interval, and all is in readiness for repeating the procedure within the next humidity interval.

It should be noted here that the solution is propagated by the fact that at any section x , where all the stream properties are known, it is possible to calculate the first derivative of each property by means of the equationsof Appendix C and Table III. The increment in each property can therefore be determined by any of the conventional numerical procedures. One of the crucial aspects of such a calculation is that each successive value depends on previous values.

Present Status of Numerical Calculations. At the present writing a considerable number of integrations has been carried out for the constant-area Aerothermopressor and a smaller number for the variable-area case. Currently, work is proceeding on a promising scheme for systematically optimizing the parameters and the area variation controlling performance, but this has not yet progressed to the point where results may be reported. Many of the results thus far obtained have been presented

by Gavril (ref. 8). A few are presented here for illustration, and in Section 5 we shall present additional computed results for comparison with the experimental results.

Constant-Area, Subsonic Aerothermopressor Process. Fig. 8 shows the results of numerical calculations for the case of a constant-area unit with an initial Mach Number of 0.7, a water-air ratio of 0.20, initial stagnation conditions of 1500°R and 14.7 psia, a friction parameter f/D of 0.004 ft^{-1} (corresponding to $f = 0.004$ with a duct of 12" diameter), and an initial droplet diameter of 13.8 microns (as computed from the Nukiyama and Tanasawa formula, ref. 4). All the varied phenomena previously described as occurring in Regimes I, II and III are seen here quantitatively. Noteworthy points include: (i) Regime I is of the order of only 0.1 ft. in length, although the actual delay in atomization will increase this somewhat; (ii) the liquid overtakes the gas in about 0.4 ft; (iii) about 10% of the water is evaporated in Regime I and about 30% at the end of the droplet acceleration period; (iv) the 7% loss in stagnation pressure incurred in Regime I is not recovered until about 50% of the water injected is evaporated, thus placing the burden of winning a net gain on the remaining part of the process; (v) the net rise in stagnation pressure is about 6%; (vi) the required length of evaporation section is of the order of 4 feet; and the droplet residence time is of the order of 0.01 seconds.

Constant-Area, Supersonic Aerothermopressor Process. Fig. 9 is for the same case as Fig. 8 except that the initial Mach Number is 1.5 and the corresponding initial droplet diameter is 7.34 microns (based on the

the risky extrapolation of the Nukiyama and Tanasawa drop-size formula to supersonic speeds). Here again the distinct phenomena of Regime I, II and III are clearly evident, although they are generally of opposite character to the subsonic case. The lengths of Regime I and of the evaporation zone are roughly the same as those in Fig. 8. The liquid temperature, however, is about 70°F as compared with about 140°F for the subsonic case, due primarily to the lower pressure level. From a consideration of the Mach Number and temperature variations, it appears that the net stagnation pressure rise of some 6% could be considerably augmented by decreasing the cross-sectional area of the duct at about 1 foot from the inlet in such a way that the Mach Number would be reduced.

Effect of Varying Initial Parameters for Subsonic, Constant-Area Operation. With regard to certain initial parameters, namely, f/D_1, d_o, and T_{01}, it can be said with assurance that a given change will be either undesirable or desirable. Specifically, the performance will improve as f/D_1 and d_o decrease and as T_{01} increases (except at very high values of the latter). This will generally be true irrespective of the values of such other parameters as Ω_o, M_1, p_{01}, V_{21}/V_1, and area variation, although the effect on performance associated with alterations in any of the variables f/D_1, d_o, and T_{01} will, of course, depend greatly on the values of all the parameters.

Considering on the other hand the parameters Ω_o, M_1, p_{01}, and V_{21}/V_1, we can only state vaguely that whether or not increases in

these will improve or detract from the net stagnation pressure rise depends on the specific values of these variables as well as those of f/D_1 , d_o , T_{01} , and of the area variation. The reason for this indeterminancy, as explained before, is that an increase (or decrease) of any of the variables Ω_o , M_1 , p_{01} , and V_{z1}/V_1 has both favorable and unfavorable aspects; in some circumstances the favorable aspects will hold the upper hand, in others the unfavorable aspects will predominate.

These remarks show that the effects of Ω_o , M_1 , p_o , and V_{z1}/V_1 can hardly be deduced from a few comparisons, and that hasty conclusions drawn from a few cases might be dangerous. What is more, a really meaningful study of the effects of Ω_o , M_1 , p_{01} , and V_{z1}/V_1 requires a selection of the optimum area variation for each set of initial variables for otherwise a favorable case might unfairly be compared with an unfavorable one. This really implies that determination of the optimum area variation and optimum values of the initial parameters must be made simultaneously. The studies already made may be far from these desiderata, so no attempt will be made here to evaluate systematically the influence of Ω_o , M_1 , p_{01} , and V_{z1}/V_1 .

Regarding f/D_1 , d_o , and T_{01} , it is well to repeat that the magnitudes of the effects on performance are in fact strongly dependent on all the other initial variables and on the area variation, although the direction of the effects is not in doubt. Recognizing in advance that the results of one comparison may not be meaningful in other circumstances, we nevertheless shall present certain specific results for the sake of

illustrating the influence of the variables f/D_1, Ω_0, and d_0.

Effect of Size. With values of the other variables remaining the same, Fig. 10 shows the effect of variations in rate of air flow on subsonic, constant-area operation. The parameter f/D_1 shown in Fig. 10 varies approximately inversely with the square root of the air flow. For a value of f in the neighborhood of 0.004, the three values of f/D_1 correspond to duct diameters of approximately ∞, 12", and 2"

The curves of temperature, velocity, and distance vs. fraction evaporated are nearly independent of f/D_1. The curves of p, p_0, and M, however, show a strong dependency. As f/D_1 increases, Regime III sets in earlier (Regime III is absent when $f/D_1 = 0$), and the maximum stagnation pressure is decreased. A net rise in p_0 seems impossible if f/D_1 exceeds a certain value. There seems to be little difference between the cases $f/D_1 = 0$ and $f/D_1 = 0.004$, yet the former would be very superior if the optimum area variation were employed for each case.

Effect of Droplet Size. Assuming that the initial droplet size may be varied independently of M_1 through the injector design, or that the droplet size produced differs from that of the Nukiyama and Tanasawa formula (ref. 4), Fig. 11 shows how a case of small-scale, subsonic, constant-area operation would be altered if the droplet size were either one-half or twice as large as the Nukiyama and Tanasawa value (d_{0j}).

The influence of d_0 is seen to be enormous, and would be even greater if each case had the optimum area variation. For 80% fraction evaporated,

the distances required are 1 ft, 5 ft, and 20 ft (approximately a square law, see Section 4.6) for the three droplet sizes. With $d_0 = 2d_{0j}$ evaporation never becomes predominant over wall friction, while with $d_0 = d_{0j}/2$, a net stagnation pressure rise appears possible even with a 2" diameter duct.

These results illustrate two conclusions of paramount significance: (i) nothing is more crucial to effective performance than an atomization system producing very small drops, and (ii) the weakest link between theory and experiment is a lack of knowledge of the actual drop size spectrum produced in the Aerothermopressor.

Effect of Water-Air Ratio. Again with a reminder concerning the inadvisability of drawing general conclusions, we show in Fig. 12 the effect of water-air ratio on a specific case of subsonic, constant-area performance.

Noting that here the amount of water required to saturate the air stream is in the neighborhood of $\Omega_0 \cong 0.2$, it is seen that the values of 0.1 and 0.3 correspond, respectively, to a considerable water deficiency and a considerable water excess. As Ω_0 increases, both the drag and evaporation phenomena are strengthened; Regimes II and III each set in at earlier values of x, but at about the same distance $\bar{x}$. Evaporation barely achieves some predominance for $\Omega_0 = 0.1$ and is most forceful for $\Omega_0 = 0.3$. A deficiency of water seems to be more detrimental than an excess, a result confirmed by experiment. The best performance seems to be obtained for a value of Ω_0 greater than that required for saturation, although it is of considerable practical consequence that the net stagnation pressure rise as well as the position of maximum p_0 are relatively insensitive to Ω_0.

Passage Through Speed of Sound. Fig. .13a illustrates constant-area operation at various subsonic initial Mach Numbers, and shows the extreme sensitivity of the flow to the initial Mach Number when it is in the neighborhood of the critical. To pass through the speed of sound, the calculations give $M_1 = 0.74289.....$, whereas $M_1 = 0.74$ gives purely subsonic operation with a peak Mach Number of 0.93 while $M_1 = 0.75$ leads to choking at $\chi \cong 0.1$. On the supersonic branch of the critical curve the rapid rise of Mach Number soon brings on Regime III, and frictional choking ensues in the vicinity of $\chi = 0.57$

Fig. .13b illustrates the corresponding curves of gas stagnation pressure. The corresponding static pressure variations are shown in Fig. 27, where they are compared with experimental data.

Shocks. Once supersonic speeds have been reached, there exists the possibility of normal discontinuities (shocks) in the gas phase. These may occur at various positions, depending on the back pressure level. In the calculations it was assumed that the gas stream passed through an adiabatic, normal shock as though the droplet cloud were not present, and the properties of the droplet cloud on the downstream side of the shock were assumed the same as those on the upstream side.

Figs. .13a and .13b show operation on the supersonic critical with a shock at $\chi = 0.35$, the performance downstream of the shock being typically subsonic. Following a slight drop in stagnation pressure across the shock itself, there is a rapid rate of rise brought on by the deceleration of the droplets and a high evaporation rate resulting from comparatively large differences in velocity and temperature.

Control of Cross-Sectional Area. How considerable are the gains to be won by proper control of the cross-sectional area is illustrated in Fig. 14. On this chart the base run for purposes of comparison is the constant-area supersonic critical curve with $T_{01} = 1500^\circ R$, $p_{01} = 14.7$ psia, $f/D_1 = 0.004$ ft^{-1}, $\Omega_o = 0.25$, and $d_o = d_{oj} = 134\mu$, for which the critical Mach Number is $M_1 = 0.727.....$ The striking feature of this constant-area case is its earlier mentioned suicidal character: after passing through Mach Number unity, the Mach Number is pushed to such high values by evaporative cooling that the temperature potential for heat transfer is severely depressed and, after about 48% fraction evaporated, wall friction gains control, and the stagnation pressure declines rapidly before it is ever able to ascend even to its initial value.

By inserting a normal shock at $\chi = 0.30$ $(M = 1.26)$, the gas temperature is not allowed to fall too rapidly, and there is a notable gain in performance, the net stagnation pressure rise being more than 10%.

With operation at constant area on the subsonic critical curve, the maximum rise in stagnation pressure is seen to be in the neighborhood of 7 or 8%.

In the light of the discussions of Sections 4.4 and 4.5 and of other considerations too lengthy for discussion here, the Mach Number distribution shown in Fig. 14 was described. In this figure the solid lines represent operation on the subsonic and supersonic critical curves for a unit of about 12"-diameter. The variable area case (dashed line) is compounded of (i) constant-area operation on the supersonic critical up to $\chi = 0.30$, (ii) variable area operation from $\chi = 0.30$ to $\chi = 0.54$ with the Mach Number distribution illustrated, and (iii) operation in a conical

diffuser of 6°-included angle for $\chi > 0.54$. It may be seen that the maximum area reduction is 25% of the initial area, and that the diffuser begins shortly after the position of minimum area. What is of greatest practical importance is that, in the variable-area case shown, a stagnation pressure rise of more than 18% is indicated.

The foregoing example is only an isolated instance presented merely to show the importance of Mach Number control, and is illustrative of the improvements to be gained whether this control is brought about by area control or by lengthwise water injection. In this example, the Mach Number variation was chosen arbitrarily and would be the optimum only through coincidence. As mentioned earlier, more systematic ways of determining the optimum are under development. Only fragmentary results of this more systematic study are available, the most important practical conclusion thus far being that with $T_{01} = 1500^\circ R$ and an air flow of about 20 lb/sec, a stagnation pressure rise of more than 20% seems to be attainable provided that the drop size is that of the Nukiyama-Tanasawa formula (ref. 4).

4.8 Approximate Discontinuity Analysis

For real insight into the details of the Aerothermopressor process, or for knowledgeable optimization of the area variation, we have no better procedure at the moment than the extended numerical integrations described in Section 4.7. But for the approximate computation of the order of magnitude of attainable performance, a comparatively simple algebraic method may be constructed.

Rather than dealing accurately with the history of the process, the approximate analysis proceeds on the assumption that in the evaporation section the curve of pressure vs. area may be represented as a

straight line. The core of the analysis is then the integral equations of continuity, momentum, and energy connecting the inlet and exit states of the evaporation section. At low Mach Numbers an especially simple form of the analysis becomes usable.

Details of the analysis are recorded in Appendix D, and a typical set of computed results is shown in Fig. 15. More extended analyses of the discontinuity type together with a wealth of numerical results are presented in ref. 8.

In Fig. 15 the solid curves represent the low Mach Number analysis. For comparison, the dashed curve shows how, for the case of no friction in the evaporation section and diffuser, the results are modified when the more accurate iterative calculation procedure of Appendix D is used. With the inlet parameters shown, an abscissa of 1.0 of course corresponds to constant area; 1.24 corresponds to equal Mach Number at inlet and exit; and 1.51 corresponds to equal pressures at inlet and exit.

A glance at the results of Section 4.7 shows that the linear pressure-area relationship is a crude approximation. Nevertheless it is believed that as far as gross orders of magnitude are concerned, the curves of Fig. 15 are significant in respect to the attainable stagnation pressure rise and in displaying the effects of area change, wall friction, and diffuser loss. Among the conclusions that may be drawn are the following:

(i) With a diffuser loss coefficient of 0.1, a diameter of 1 foot, a length of 6 feet, and $f = 0.004$, a stagnation pressure rise approaching 20% is possible.

(ii) A net rise in stagnation pressure is not possible if fL/D exceeds approximately 0.075 (for $f = 0.005$, this limits L/D to 15).

(iii) Area decrease is definitely beneficial, and the optimum amount of area contraction increases as the frictional effects are minimised.

5. EXPERIMENTS WITH A SMALL-SCALE, CONSTANT-AREA AEROTHERMOPRESSOR

5.1 Objective of Small-Scale Experiment

The experiments described below were carried out on a scale of air flow so small that there was no expectation of a net rise in stagnation pressure. Instead the goals were as follows:

(i) To explore quickly and economically the diverse phenomena and regimes of operation in the Aerothermopressor.

(ii) To obtain experimental data for testing the validity of the theoretical calculations.

(iii) To estimate by extrapolation what would be the prospects of effective operation on a large scale, with the purpose of assessing the advisability of an expensive, medium-scale experiment.

(iv) To acquire information necessary for the intelligent design of such a medium-scale unit.

All these aims were achieved. The methods and results are described in full detail by Wadleigh (ref. 9), and a summary of this work is presented here.

5.2 Details of Apparatus

Flow System. Powered by a steam-jet ejector at the downstream end, the entire system (Fig. 16) operated at sub-atmospheric pressure. Air from the atmosphere was drawn into a gas-fired combustion chamber; from

the latter the heated air passed through two mixing elbows and a straightening length to the upstream stagnation section; thence through a converging, accelerating nozzle into the evaporation duct; and, after being cooled by water evaporation, into a conical diffuser of 6° included angle; finally, the air flowed through a large quench tank to the jet pump via a control valve by means of which the back pressure on the Aerothermopressor was adjusted.

Test Duct. As the objective was to obtain basic data rather than maximum performance, the evaporation duct was of constant area, 2.13 inches in diameter and 73 inches long. The test section was fitted with twenty static pressure taps on the wall, and with eight access ports for introduction of measuring probes.

Water Injection System. Atomization of the so-called "gas atomization" type was achieved by introducing water at low speed into the high-velocity air stream at the beginning of the 2.13-inch evaporation duct. Since the type of water injection system which would best yield the desirable features of small droplets together with uniform spatial distribution could hardly be predicted in advance, preliminary experiments were carried out with some twenty different injection schemes (ref. 9), involving combinations of axial-flow water jets, radial-flow water jets originating in the pipe wall, and water-sheet formation nozzles. The merit of each injection system was judged by comparing the net change in stagnation pressure from upstream stagnation section to downstream quench tank, with all other variables at the inlet plane of the evaporation duct held constant. Very substantial differences in performance were found. The best injection system, and that used for all further

work, was an axial injection system in which the water was introduced at the inlet plane of the 2.13 -inch duct by means of seven tubes of dimensions 0.125"-OD, 0.110"-ID , with one tube on the axis and the others disposed symmetrically on a circle of 1.25 -inches diameter.

Measurements. The following measurements were made:

(i) Stagnation pressure and stagnation temperature in the upstream stagnation section were measured directly by an impact tube and a multi-shielded thermocouple.

(ii) Stagnation pressure at the diffuser exit was measured by an impact tube.

(iii) Air flow rate was inferred from the upstream stagnation properties and the pressure drop across the inlet bell mouth, assuming for the latter a discharge coefficient of unity.

(iv) Water flow was measured by a rotameter and a sharp-edged orifice.

(v) Entrance air Mach Number (at the plane of water injection) was calculated from the isentropic law connecting it with the upstream stagnation pressure and the pressure drop across the inlet bell mouth.

(vi) Longitudinal static pressure distributions along the length of the test section were determined by connecting the wall static taps to a multiple manometer board.

(vii) The amount of water evaporated at the sections where access ports were available was determined by traversing these sections with a special sampling probe designed for withdrawing a sample of the gas phase only and by measuring the humidity of the air-vapor sample by means of a Foxboro "Dewcel" indicator. Details of the humidity-measuring system and

of the novel sampling probe are given in ref. 9.

Control of Variables. In the apparatus described, the significant parameters which could be controlled were (i) the upstream stagnation pressure, p_{01} (ii) the upstream stagnation temperature, T_{01} ; (iii) the water-air ratio, Ω_o and (iv) either the initial Mach Number, M_1 , or, in the case of choked flow where M_1 was uniquely determined by p_{01} , T_{01} , and Ω_o , the position of a normal shock in the test section.

These were varied in a systematic manner during the course of the tests.

5.3 Experimental Results

We present here selected results which illustrate the theoretical considerations of Section 4 and which also show the influences of the controllable parameters. Here again the reader is cautioned that the effects of these parameters in a small-scale, constant-area apparatus are generally not the same as in a large-scale unit having an optimum area variation.

Comparison of Flows With and Without Evaporation. Figure 17 illustrates in an unmistakable way the powerful influence of that evaporative cooling which is the heart of the Aerothermopressor process.

The three runs with $T_{01} = 1500°R$ constitute essentially adiabatic flows. With no water injection ($\Omega_o = 0$) the process is the one-dimensional Fanno-line process (ref. 2, chapter 6) and exhibits a constantly falling static pressure typical of subsonic flow, with the

rate of pressure decrease increasing because the Mach Number is increased by friction. As water is introduced, with Ω_0 first equal to 0.1 and then 0.2, a larger drop in pressure than before occurs near the inlet because of droplet drag; after the first few inches, the droplet drag is small, and the pressure drop is primarily that of pipe friction. However, the rate of frictional pressure drop is greater at the larger values of Ω_0 because the droplet drag increases the Mach Numbers at which friction occurs throughout the duct. For the case $T_{01} = 530°R$ and $\Omega_0 = 0.2$, in fact, the flow at the duct exit is nearly choked, i.e. the Mach Number is nearly unity.

The case of $\Omega_0 = 0$ at $T_{01} = 1500°R$ is again essentially adiabatic and is directly comparable with the case of $\Omega_0 = 0$ at $T_{01} = 530°R$. The small difference in the rates of pressure drop for these two Fanno-line runs is present because of a difference in initial Mach Number and also because the pipe friction factor f is altered by the difference in length Reynolds Number between the two cases.

Turning to the curves for $T_{01} = 1500°R$ with water injection, we see pronounced differences owing to the evaporative cooling which is now present. Whereas for $T_{01} = 530°R$ (i.e., no evaporation) water injection <u>increases</u> the pressure drop, with $T_{01} = 1500°R$ (i.e., strong evaporation) water injection <u>decreases</u> the pressure drop. It seems safe to say also that the Mach Number rise here when evaporation occurs is less than when evaporation does not occur.

<u>Effect of Water-Air Ratio</u>. Certain aspects of the phenomena just discussed are brought out more clearly in Figure 18, for which the initial Mach Number of 0.65 is higher than that for the runs shown in Figure 16,

thus magnifying the pressure gradients. The fact that cooling at subsonic speeds does indeed tend to decrease the Mach Number was clearly evidenced by this series of runs, inasmuch as it was not even possible to operate at $M_1 = 0.65$ with no water injection, the initial Mach Number for choking when operating dry being less than 0.65 .

For each value of Ω_0 , the three characteristic Regimes discussed in Section 4.3 are observed:

(i) Regime I. For a distance of about two inches the pressure falls rapidly because of droplet drag. The magnitude of this initial pressure drop is roughly proportional to the rate of water flow, i.e. to Ω_0 .

(ii) Regime II. A rapidly rising pressure occurs in the next 20 inches or so, where evaporative cooling is predominant. The maximum rate of pressure rise increases as Ω_0 increases, chiefly because an increased Ω_0 means a greater amount of heat transfer surface in the droplet cloud. For such a small Ω_0 as 0.10 , the net rise is rather small,and reaches its peak at $x \cong 10$ inches; in this case there is scarcely enough surface to accomplish much cooling, and the droplet cloud vanishes comparatively rapidly because the driving temperature differential is not decreased very much by cooling of the gas. With values of Ω_0 between 0.2 and 0.4 the pressure rise exceeds the loss in Regime I, such that at $x \cong 25$ inches the pressure is higher than in the inlet plane. The maximum pressure in the duct and also at the diffuser exit is obtained with $\Omega_0 \cong 0.3$, this being the water-air ratio for which the balance between pressure rise due to cooling and pressure drop due to droplet acceleration and wall friction is an optimum. For low values of Ω_0 , the

distance ℓ to the point of maximum pressure increases as Ω_0 increases because the droplet cloud persists for greater distances. For high values of Ω_0, on the other hand, the distance decreases as Ω_0 increases because the gas stream tends towards saturation more quickly.

(iii) Regime III. After the rate of evaporation has been reduced sufficiently by the falling gas temperature and diminishing droplet diameter, wall friction gains control. The pressure begins to drop, and the rate of pressure fall grows as evaporation becomes weaker and weaker.

Passage Through Mach Number Unity. Figure 19 shows the pressure distributions obtained with constant values of T_{01}, p_{01}, and Ω_0, but with varying initial Mach Numbers, M_1.

The curves for $M_1 = 0.48$ and $M_1 = 0.65$ are for values of back pressure so high that the entire flow is subsonic. Qualitatively similar to those of Fig. 18, they demonstrate as well the dynamic character of the events in the sense that the pressure gradients grow as the Mach Number ascends.

All the remaining curves of Fig. 19 are for the critical initial Mach Number, $M_1 \cong 0.78$, for which evaporation becomes predominant over drag just at the point where the local Mach Number is unity. The lowermost curve in Fig. 19 is for the greatest possible length of supersonic flow in the test section, and, except for a shock near the exit, corresponds to the supersonic critical curve shown in Fig. 13. The branch curves rising precipitously from this lowermost curve represent normal shocks followed by subsonic flow.

Shock Configurations. Considering in more detail the lowermost curve in Fig. 19, it is seen that the pressure falls and the Mach Number rises to unity in Regime I, up to $x \cong 2$ inches; the pressure continues to fall and the Mach Number rises to substantial supersonic values in Regime II, up to $x \cong 28$ inches; then, because of wall friction, the pressure begins to rise and the Mach Number to fall in Regime III, up to $x \cong 55$ inches. However, the duct length is too great for supersonic flow to continue to the exit, for in the absence of shocks, the Mach Number would reach the choking value of unity before the exit. Therefore, a shock must stand somewhere in the duct. For very low back pressures (e.g., condition 2 in Fig. 19), the shock is at its furthermost possible position downstream, that is, at the position for which the subsonic flow following the shock becomes choked at the duct exit. In this case the shock lies in the range of x between 55 and 62 inches, and $M=1$ at the duct exit; the flow in the diverging diffuser (now operating as a nozzle) then accelerates to supersonic speeds, and is again decelerated to subsonic speeds by means of a shock in the "diffuser", the shock having a loss in stagnation pressure sufficiently high to match the prescribed low back pressure. The lowermost curve therefore exhibits an amazing range of gas dynamics phenomena, comprising two continuous accelerations through the speed of sound (albeit by different mechanisms), two normal compression shocks, three distinct regions of subsonic flow, and two distinct regions of supersonic flow.

As the back pressure is increased, say from condition 2 to condition 3, the shock in the "diffuser" moves upstream to lower supersonic Mach Numbers, but the flow in the duct is completely unaltered. When

the back pressure reaches condition 4, however, the "diffuser" shock disappears in the duct exit where M = 1, and this then represents the limit of operation with choked flow at the duct exit, and with the furthermost downstream position of the shock in the duct.

A further rise in back pressure over that for condition 4 therefore causes the shock in the duct to move upstream. As the back pressure is increased the shock continuously and successively moves from position 1 to positions, 5, 6, 7 and 8. For all the latter modes of operation the flow following the shock and at the duct exit is subsonic. Following the shock, the pressure at first rises because of subsonic cooling and deceleration of the liquid droplets, and subsequently falls because of subsonic friction.

Because of the now-familiar shock-boundary layer interaction, the shocks, rather than being discontinuities, occupy a distance of about 8 inches, corresponding to about 4 duct diameters.

Stable vs. Unstable Operation at the Critical Mach Number. Attempts to operate on the subsonic branch of the critical curve or with shocks further upstream than the position corresponding to curve 8 were unsuccessful. When the back pressure was raised slightly above that of condition 8 (corresponding to curve 8), the entire flow became highly unsteady, with large surges in pressure, flow rate, and shock position.

This strange behavior may be explained by reference to the schematic diagram of Fig. 20, which refers to a small-scale Aerothermopressor in which there is at all times a net loss in stagnation pressure from inlet to diffuser exit. Consider an experimental arrangement in which p_{01}, T_{01}, and Ω_0 are fixed and in which, at least for the present, steady

flow is assumed possible. Then, as M_1 increases from zero, the value of p_o at the diffuser exit will at first decrease because the net loss in p_0 is roughly proportional to M_1^2. This loss continues until M_1 reaches its critical value, after which M_1 may increase no further, and we may use the position of the shock as the controllable variable governing performance. From the theoretical consideration of Section 4, there will be a particular position of the shock (point a) in Fig. 20 for best performance. In Fig. 19, therefore, the curve of p_o versus shock position will first rise to point a, and will subsequently fall as the shock moves further downstream.

Now, operation at a point to the right of a, such as at b, is stable in the sense that a slight variation in the imposed back pressure will induce a change in Aerothermopressor operation of such nature as to make the delivered exit pressure adjust to the imposed back pressure. For example, suppose that steady operation prevails at b, and that the imposed back pressure is suddenly increased slightly. This will generate a small compression wave which will propagate upstream until it reaches the shock, and its interaction with the shock will force the latter slightly upstream. But the latter event increases the delivered back pressure and thus the Aerothermopressor adjusts stably to the imposed disturbance.

Operation at a point such as c on the portion of the curve between a and e, on the other hand, is unstable. If, after an assumed steady operation at c, the imposed back pressure is suddenly raised slightly, the generated compression wave will on reaching the shock again move

the latter upstream. But this reduces the delivered exit pressure, with the result that conditions are further from equilibrium than before, and the point of operation is driven toward e. There ensues an oscillatory mode of large amplitude, the character of which depends upon the transient characteristics of the air and water flow systems, that is, on the way in which p_{01} , T_{01} , and Ω_0 react to the changes in air flow pursuant to M_1 dropping below its critical value.

These phenomena are reminiscent of the behavior of converging-diverging diffusers for supersonic flow. It is well known that the operation of such a diffuser is stable when the shock is in the divergent portion (in which region a downstream displacement of the shock reduces the delivered stagnation pressure), but unstable when the shock is in the convergent section (in which region a downstream displacement of the shock increases the delivered stagnation pressure).

Definition of Performance Coefficient. Inasmuch as all the phenomena occurring within the Aerothermopressor are strongly dynamic in character, a measure of overall performance is required from which most of the sensitivity to Mach Number has been removed. Being mindful of the form of the influence coefficients for dp_0/p_0 shown in Table III, we form the over-all performance coefficient

$$\frac{p_{03} - p_{01}}{p_{01} M_1^2}$$

where p_{03} is the stagnation pressure at the diffuser exit.

Although the use of this dimensionless figure of performance does in fact illuminate the results, it seems in place once again to state that the value of this performance coefficient depends not only on p_{01} , T_{01} , Ω_o , M_1 , and length of evaporation section, but also on the actual duct diameter and on the area variation, because both friction and area change act to alter the local Mach Number.

Effect of Water-Air Ratio on Over-All Performance. The curves of Fig. 21 are typical of the variation in over-all performance when the water injection rate is varied and the initial stagnation conditions and Mach Number all held constant. For each set of initial parameters (M_1, T_{01}, p_{01}), there is an optimum value of Ω_o . Below this optimum Ω_o , the total amount of cooling is weak compared with wall friction; above this value, the added droplet drag cannot be offset by evaporative cooling because of the tendency of the stream to reach saturation too quickly. The performance is less sensitive to variations in Ω_o above the optimum value, however, than to variations below the optimum, i.e., excessive water is not as detrimental to performance as a deficiency. The curves are fortunately quite flat near their peaks, and so the precise adjustment of the water flow is not critical.

As might be expected from the theoretical considerations, an increase in T_{01} requires an increase in Ω_o . For example, with $p_{01} = 14.8$ psia, the table below shows the optimum values of Ω_o at several temperatures:

T_{01}:	1200°R	1500°R	1800°R
Ω_o:	0.16	0.24	0.31

Figure 21 shows also that the optimum water-air ratio is substantially independent of p_{01} .

No significant trend of optimum water-air ratio with initial Mach Number was observed.

Effect of Initial Stagnation Temperature on Over-all Performance. From Fig. 21 it may be seen that, with a given initial Mach Number, the best performance attainable with the appropriate value of Ω_0 is improved as the initial stagnation temperature is raised. The same result is obvious also from Fig. 22, which shows only the best performance at each Mach Number and temperature. An increase in the temperature difference available for cooling, as well as an increase in the saturation humidity, account in a simple manner for the better performance at high temperatures. On the same grounds it is easy to understand also why the optimum water-air ratio rises as the initial stagnation temperature increases, at least in the range of the latter under consideration.

Effect of Initial Mach Number on Over-All Performance. Naturally, the net loss in stagnation pressure in the small-scale Aerothermopressor increases as the Mach Number level is increased. However, this gives a false picture of how the performance of a large-scale unit might depend upon initial Mach Number. A better representation is given in Figure 22, where the over-all performance coefficient is plotted against initial Mach Number. The right-hand end of each curve represents the choking Mach Number for the specified values of T_{01} , p_{01} , and Ω_0 ; the corresponding value of the ordinate is for the shock position yielding

the maximum final stagnation pressure.

What Figure 22 shows is that the over-all performance improves as the initial Mach Number increases. If the wall friction were somewhat less than in the case here considered, curves such as those in Figure 22 would also have negative values of the ordinate at low Mach Numbers; however, they would differ in that they would have positive values at high Mach Numbers. Thus there is in general a certain initial Mach Number below which a rise in p_o cannot be achieved, and above which the net rise in stagnation pressure mounts rapidly as the initial Mach Number is increased. The explanation of this behavior is related to the effect of M_1 on droplet diameter; as M_1 increases, the droplet diameter decreases, and/a greater fraction of the water is evaporated in the given length of duct, as described previously in Section 4.6 and as shown later in Figure 26.

Effect of Initial Stagnation Pressure on Over-all Performance. Figures 21 and 22 also show a considerable worsening in performance as the inlet stagnation pressure is reduced. For fixed values of M_1, T_{01}, and Ω_0, the influence of decreasing p_{01} may be felt in several ways, namely; (i) through an increase in initial droplet diameter produced by decreased atomization forces; (ii) through a reduction in heat transfer coefficient and in drag effects produced by lessened relative Reynolds Numbers; (iii) through an increase in pipe friction factor produced by the decrease in pipe Reynolds Number; (iv) through the lowered wet-bulb temperature and the increased vapor-carrying capacity of the

stream before saturation is reached; and (v) through an increase in the mass transfer coefficient associated with an increase in the mass diffusivity.

As heat transfer rather than mass transfer is controlling in the evaporation process effects (iv)and (v) are probably of small consequence. Furthermore, it is hard to imagine effect (iii) as accounting for the results seen in Figs. 21 and 22.

Some additional relevant facts appear in Fig. 23, which shows the longitudinal pressure distributions at two pressure levels with comparable (but slightly different) values of M_1 and Ω_0. Taking note of the comparative values of M_1 and Ω_0, what is most striking is the enormous difference in the rates of pressure rise at the beginning of Regime II. In the theoretical calculations of ref. 8, the effect of p_{01} under conditions of unchanged d_0 was found to be extremely small, i.e., the net influence of item (ii) in the foregoing list was found to be unimportant. Accordingly the evidence points to item (i) as being controlling, i.e., that the effect of initial stagnation pressure is strongest through its influence on drop size.

Evaporation Profiles. For fixed initial conditions, Fig. 24 shows typical profiles of specific humidity at four different transverse cross-sections of the flow.

Near the inlet, at $z = 4.5$, the humidity profile reflects the deficiencies of the water injection system in achieving uniform distribution. However, even in the short distance of 4.5 inches, an astonishing amount of evaporation has occurred, thus testifying to the tremendous

heat transfer surface of a droplet cloud.

Further downstream, a rapid straightening of the humidity profile is observed, until at $z = 67.5"$ the profile is nearly flat. By virtue of the large droplet inertia, it does not seem likely that the turbulence of the stream does much to redistribute the droplets in a more uniform way. What the data suggest, rather, is that the turbulent migrations of the gas itself rapidly mixes those portions of the gas in contact with many droplets with those portions in contact with few. Or from a different point of view, each piece of gas courses turbulently through the different parts of the droplet cloud, and thus experiences the average water distribution. If this picture is true, uniformity of the spray distribution on a fine-grained scale may not be critically important, so long as uniformity on a large-grained scale is achieved. Weight is added to this picture of highly turbulent gas motion by the observation in Fig. 24 that the gas humidity at $r \cong 0.5$ inches decreases as the gas goes from z=13.5 in. to z = 40.5 inches; this can only be accounted for by the mixing of the very humid gas at $r \cong 0.5$ inches with the much less humid gas near the walls.

Ultimately, the humidity is higher near the walls than at the center. This seems to be the result of the velocity profile in the duct, which grants to droplets near the walls a longer residence time than to those at the center.

Longitudinal Rate of Evaporation. By integrating humidity profiles such as those of Fig. 24, we obtain the open-point curves of Fig. 25, showing how average humidity increases with longitudinal distance. There

is evident here the very rapid initial rate of evaporation followed by a decreasing rate which continues to fall as the stream tends toward saturation. At a given duct position, the specific humidity increases as the water injection rate is increased. The fraction evaporated, however, decreases as Ω_o increases because the increased water concentration causes the stream to approach saturation more rapidly.

For the case $\Omega_o = 0.150$,50% of the water is evaporated in the first 10 inches, and 95% is evaporated in a distance of 40 inches. For the case $\Omega_o = 0.252$, which is slightly greater than the saturation value of about 0.21, approximately 50% of the saturation amount is evaporated in the first 10 inches, and about 85% of the saturation amount in 40 inches.

In addition to the direct humidity measurements, it was possible to infer the local fraction evaporated from a knowledge of initial conditions, from the measured local static pressure, and from a one-dimensional analysis involving the equations of continuity, momentum, and energy between the inlet and the section in question (refs. 9 and 8). Three additional assumptions were necessary, to wit; (i) the droplet moves at the gas speed, (ii) the value for the pseudo friction factor used in the analysis may be taken at an average value for f of 0.004, and (iii) the droplet temperature is 130°F. With these assumptions the curves marked by the full points in Figure 25 were obtained. Because of assumption (i) above, the discontinuity analysis can be fairly accurate only at considerable distance from the inlet. Where the assumption $V_\ell/V = 1$ is a fairly good one, the validity of the calculated humidity will depend on the

choice of the value used for f. With conventional values of the friction factor, this discontinuity analysis leads to values of humidity which are too high. A comparison of the direct humidity data with those inferred from the pressure measurements indicates similar trends and orders of magnitude, with the quantitative agreement improving as x increases.

Total Water Evaporated. Figure 26 shows how the specific humidity near the end of the duct ($x = 67.5"$) varies with water-air ratio (Ω_o) and initial Mach Number (M_1).

For a fixed value of M_1, the exit specific humidity increases with Ω_o because the total amount of heat transfer surface in the droplet cloud is proportional to Ω_o. As Ω_o proceeds above 0.3, however, the exit specific humidity tends to level off owing to the stream having become nearly saturated at a specific humidity of about 0.21, such that the exit humidity can scarcely increase no matter how much water is fed in.

How important a role is played by drop size is shown strikingly in Fig. 26, where it may be seen that for fixed values of T_{o1}, p_{o1}, and Ω_o, the exit humidity increases as M_1 increases. This despite the fact that the residence time of the droplets is less at the higher Mach Numbers. As shown in Section 4.6, the length required for complete evaporation varies approximately in inverse proportion to the initial Mach Number; in a given length the total amount evaporated increases as M_1 increases.

Wall Friction Factor. In order to interpret the small-scale experimental data and to predict the performance of large-scale units, knowledge

of the effective friction factor f is desirable. The value of f may well be different from that for ordinary fully-developed pipe flows for several reasons: (i) the water cloud probably tends to make the velocity profile more uniform; (ii) evaporation alters the density and viscosity profiles; (iii) near the pipe inlet the boundary layer surely does not fill the pipe; (iv) in much of the evaporation section the static pressure is rising, which is opposite to the falling pressure characteristic of simple pipe flow; (v) impingement of water on the walls, crashing of droplets into the boundary layer, and tearing of water off the walls, all must have some influence on the skin-friction coefficient. These effects are separate and complex, and for the present it is necessary to simply lump them all into an "effective" friction factor.

Values of the effective friction factor under various circumstances were evaluated from three types of experiments:

(i) Dry runs at low and high temperatures.

(ii) Wet runs at low temperature and therefore with no evaporation.

(iii) Wet runs at high temperature, with considerable evaporation.

For type (i), the friction factor could be determined from the Fanno-line analysis (ref. 2, Chapt. 6). In addition, a friction factor for [illegible] types could be estimated from a "discontinuity" [illegible] conservation laws of mass, momentum, and [illegible] exit of the constant-area duct [illegible] pressure and humi[illegible] example, th[illegible] Deta[illegible] ar[illegible]

T_{01}, deg.R	1500	1500	520	520	1500	1500
p_{01}, psia	14.8	10.9	14.7	14.7	14.6	14.6
Ω_o	0	0	0	0.30	0.15	0.25
M_1	0.597	0.597	0.595	0.500	0.500	0.500
f(discontinuity) analysis	0.0034	0.0034	0.0032	0.0035	0.0040	0.0046
f (Fanno-line)	0.0038	0.0038	0.0035	- - -	- - -	- - -
$\rho_1 V_1 D_1/\mu_1$	175,000	128,000	605,000	502,000	154,000	154,000
$0.046(\rho_1 V_1 D_1/\mu_1)^{-0.2}$	0.0041	0.0044	0.0032	0.0033	0.0043	0.0043

The last two rows represent, respectively, the pipe Reynolds Number and the usual friction factor for fully-developed turbulent pipe flow at that Reynolds Number.

In the dry runs the discontinuity analysis (which involves certain assumptions leading to small errors in the computation of the wall force)

5.4 Comparison of Theory and Experiment

We turn now to a comparison of the experimental results of Section 5.3 with those computed using the theoretical method of Section 4.7.

Figure 27 shows, in addition to the observed curves of Figure 25 for $\Omega_0 = 0.[illegible]$, the corresponding theoretical curves computed with f = 0.005 and the Nukiyama and Tanasawa drop size of 19 microns as well as with slightly smaller drop sizes. The measured and theoretical curves are of the same general character, and the agreement is not disappointing when one considers the broad sweep of physical phenomena which the theory attempts to model.

In Fig. 28 are shown the theoretical curves corresponding to the observed critical curves of Fig. 19. The theoretical critical Mach Number of 0.74 compares favorably with the measured value of 0.78, and the theory gives a gratifyingly accurate picture of the different regimes of operation, including the interposition of shocks with subsequent subsonic operation.

These results speak well for the theory as a means of estimating perform-

[illegible]large-scale unit, and as a basis for determining the optimum area

with cooling, drag, etc. The extrapolation can be made only if the Mach Number distributions are the same in the two cases (it is found that humidity distribution is quite insensitive to changes in $4fL/D$). As the comparatively large wall friction in the small-scale constant-area unit tends to force the Mach Number toward unity (Table IV), an equivalent Mach Number distribution in a large-scale unit requires area changes to accomplish the same result. This means that the comparison to be made below is between the small-scale constant-area unit and a large-scale unit in which the area is constantly reduced in such a way as to give the same Mach Number at each value of z as in the small-scale unit.

Based on the foregoing reasoning, we may proceed as follows. Inasmuch as all the phenomena, except that of wall friction, are alike in the cases considered, we may (using Table III) express the performance coefficient as

$$\frac{p_{03} - p_{01}}{p_{01} M_1^2} = Y - 2fk\frac{L}{D} \qquad \text{(Eq. 13)}$$

where Y includes the effects of all terms other than that of wall friction, and is the same for all the cases considered. Now, assuming f equal to 0.0040, Y may be computed for the small-scale unit, and the following results, corresponding to the maximum points of Fig. 21, are obtained:

TABLE VI - EXTRAPOLATION OF SMALL-SCALE PERFORMANCE

T_{01}, deg.R	1200	1500	1800
M_1	0.777	0.780	0.783
p_{01}, psia	14.7	14.7	14.7
w_a, lb/sec	0.755	0.677	0.612
f	0.0040	0.0040	0.0040
k	1.35	1.35	1.35
D, inches	2.13	2.13	2.13
L/D	34.5	34.5	34.5
Ω_o	0.17	0.24	0.31
$\left[(p_{03}-p_{01})/p_{01}M_1^2 \right]_{max.}$	-0.23	-0.16	-0.13
Y	0.15	0.22	0.25
$\frac{p_{03}}{p_{01}}$ L/D = 20	0.95	1.00	1.02
$\frac{p_{03}}{p_{01}}$ L/D = 15	0.99	1.03	1.05
$\frac{p_{03}}{p_{01}}$ L/D = 10	1.02	1.07	1.08
$\frac{p_{03}}{p_{01}}$ L/D = 5	1.05	1.10	1.12
$\frac{p_{03}}{p_{01}}$ L/D = 0	1.09	1.13	1.15

The results under the dashed line in the table represent extrapolated performance for the large-scale unit.

To gain some estimate of size, we observe from the pressure and humidity data that a length of about five feet is required. A diameter of one foot would correspond to an air flow of about 25 lb/sec, or that of a gas turbine of about 1500 net horsepower. With $L/D = 5$, a stagnation pressure reduction at the turbine exit of about 10% is seen from the table above to be possible when $T_{01} = 1500°R$.

There seems little doubt that the large-scale performance estimated above may be achieved as a minimum. It seems equally likely that considerably better performance is attainable, the reasons being as follows:

(i) Only a strange coincidence could assure that the Mach Number distributions involved in the foregoing calculations are the optimum for each combination of p_{01}, T_{01}, Ω_0, M_1, and f/D_1. What is more, in large-scale units the optimum values of Ω_0, M_1, and length will surely differ from those in smaller units.

(ii) The friction factor should be less for large units than for small because of a more favorable pipe Reynolds Number.

(iii) Little attention was given to diffuser design in the small-scale unit, and gains may very likely be won by careful attention to this element of the apparatus.

(iv) Undesirable effects associated with water near the walls can be minimized in larger units.

Therefore, the extrapolations should be considered conservative, and the extrapolated performance of large-scale units shown in the table above as assured levels, with a considerable margin of improvement possible.

As explained before, the extrapolated performance refers to a large-scale unit having an area variation that will produce the same Mach Number distribution as in the small-scale unit. Considerable practical importance is therefore attached to the question of how much area variation is required to assure the attainment of extrapolated performance. This may be estimated from the influence coefficients in the first line of Table III. To obtain the same Mach Number variation in a variable-area unit without friction as in a constant-area unit with friction, it is only necessary to set equal the terms in dA/A and in $4f\,dz/D$ appearing in the equation for dM^2/M^2, remembering that the terms involving dw/w will be the same in both instances. Thus we obtain

$$\frac{dA}{A} = -\frac{kM^2}{2}\,4f\,\frac{dz}{D}$$

as the sought-for criterion. Lacking precise information as to the Mach Number distribution in the small-scale unit, we may only compute the over-all change in area in terms of some average value of M^2. Thus we may write

$$\frac{\Delta A}{A} \cong -\frac{k}{2}\,\overline{M^2}\cdot 4f\,\frac{L}{D}$$

Taking $k \cong 1.35$, $f = 0.004$, $L/D = 34.5$, and using a value of $\overline{M^2} \cong 0.7$, we obtain $\Delta A/\bar{A} \cong -0.26$. This means that the exit area must be approximately three-fourths of the inlet area in a unit so large that friction is negligible. Whether this is the best area reduction for a large-scale unit remains problematical. The actual manner of area variation required to obtain the Mach Number distribution of the small-scale unit cannot of course be found from this simplified calculation.

6. MEDIUM-SCALE AEROTHERMOPRESSOR EXPERIMENT

At the time of this writing, there is under preliminary test a medium-scale Aerothermopressor, 11 inches in diameter, with a maximum available air flow of 25 lb/sec. For these preliminary tests the evaporation section is of constant outside diameter and is thoroughly instrumented. Area variations will subsequently be provided by means of internal tapered plugs; this general approach is thought best suited to determining optimum area variation most quickly and economically.

In Section 4 it was shown that the greater portion of the evaporation section should be of diminishing area in order to establish a desirable Mach Number variation. In the small-scale constant-area unit, the comparatively large frictional effects accomplished the same Mach Number variation as that which would result from an area reduction of about one-fourth in the absence of friction. Therefore, the Mach Number distribution of the medium-scale constant-area unit is less favorable than that of the small-scale constant-area unit. Accordingly it may be expected that

the medium-scale constant-area unit will not have as good performance as the extrapolated performance shown in Table VI.

Despite the handicaps accompanying this medium-scale constant-area unit mentioned above, the preliminary tests have already yielded the gratifying result of a net rise in stagnation pressure of about 3% from the upstream stagnation section to the diffuser exit. What is important here is the positive proof of the Aerothermopressor principle, rather than the smallness of the net rise achieved under unfavorable circumstances. There is every reason to believe that substantial improvements lie ahead, ready to be gained by intelligent control of the cross-sectional area.

7. ASSOCIATED PROBLEMS

The research and development discussed in this report has brought to the fore a number of technical problems which are of special significance to the Aerothermopressor. These are named below, and the steps looking toward their solution outlined.

7.1 Determination of Drop Size

The weakest link between theory and experiment is currently a knowledge of the drop size produced during atomization. Two methods of measuring mean droplet size are under development, one depending on optical scattering of a light beam (ref. 10), the second depending on the pressure gradient near the hose of an impact tube (refs. 11, 12, 13).

7.2 Atomization

Nothing would better assure good performance of the Aerothermopressor than a means for producing extremely small droplets. Experiments are

being planned to determine the effect of gas speed and gas properties on droplet size, and to determine whether tricks of injector design can lead to smaller droplets.

7.3 Measurement of the Properties of a Droplet-Laden Stream

An understanding of what happens inside the Aerothermopressor requires the measurement of sufficient properties to establish the point properties of the gas and the droplet cloud. Various types of devices have been developed or are under development for this purpose:

(i) A probe for drawing a sample of the gas phase only has been successfully developed (ref. 9).

(ii) Probe designs for accurately measuring the stagnation pressure of the gas phase only have been devised and calibrated (ref. 13).

(iii) Techniques for sampling the liquid flow per unit area are under development (refs. 13,14).

(iv) A scheme for determining the droplet velocity has received some experimental attention and appears promising (ref. 13).

8. CONCLUSIONS

1. The wide variety of gas dynamics phenomena observable within the Aerothermopressor are explainable in terms of heat transfer, evaporation, droplet drag, wall friction, and cross-sectional area variation.

2. Experiment and theory both show that the Aerothermopressor can produce a net rise in stagnation pressure with mass flows of about 2 lb/sec or greater.

3. A Net rise in stagnation pressure has already been won in a

25 lb/sec unit, and in this size the theory suggests that rises of perhaps 20% are achievable. The latter figure would lead to improvements in both fuel economy and power capacity of a simple gas turbine plant of about 20%.

4. The theoretical analysis of the Aerothermopressor gives a generally correct picture of its performance.

5. With high subsonic Mach Numbers at the inlet, the required length of evaporation section is about 5 feet, and for an initial stagnation temperature of 1500°R, the optimum water-air ratio is in the neighborhood of 0.25.

9. ACKNOWLEDGMENTS

Most of the experimental work described here was carried out under the sponsorship of the Office of Naval Research and Bureau of Ships, and their financial assistance is gratefully acknowledged.

The experimental work has been done in the Gas Turbine Laboratory of M. I. T., with the assistance and cooperation of the Laboratory staff.

For the use of the 25 lb/sec air supply, thanks are given to the Fuels Research Laboratory of M.I.T.

All the numerical computations were carried out on Whirlwind I, an electronic, digital computer at the Massachusetts Institute of Technology. The availability of computer time was made possible by the Office of Naval Research.

Finally it should be stated, if it is not already obvious, that the considerations and results presented here were not given birth full-blown, but rather were evolved slowly through the stimulating exchange

of ideas between staff members and students, all working enthusiastically toward the specific goal of making a workable Aerothermopressor. For their contributions we wish to thank C. A. Templeton, J. R. Wish, R. A. Hawkins, L. V. Mowell, P. A. Gisvold, J. C. Matheson, P. Plender, E. Feher, M. Booth, H. K. Larson, R. E. Kosiba, F. H. Vose, J. W. Carpenter, F. W. L. Martin III, A. Erickson, J. Dussourd, J. M. McGrew, Jr., V. G. Pesek, J. Fenske G. E. Keeler, and J. B. Cheatham, Jr., H. Foust, and M. Tefft.

10. APPENDIX A - DERIVATION OF INFLUENCE COEFFICIENTS

The analysis is most conveniently carried out by casting the definitions and physical laws applicable to the infinitesimal control volume of Fig. 4 into the form of logarithmic differentials. The gas mixture is assumed to obey the perfect gas law and the Gibbs-Dalton law, but with variable specific heats.

Definition of Mach Number. For a perfect gas,

$$M^2 \equiv \frac{V^2}{c^2} = \frac{V^2 W}{k\bar{R}T} \tag{A-1}$$

$$\frac{dM^2}{M^2} = 2\frac{dV}{V} + \frac{dW}{W} - \frac{dk}{k} - \frac{dT}{T} \tag{A-2}$$

Perfect-gas Law.

$$p = \rho \bar{R} T / W \tag{A-3}$$

$$\frac{dp}{p} = \frac{d\rho}{\rho} + \frac{dT}{T} - \frac{dW}{W} \tag{A-4}$$

Conservation of Mass. With w the mass rate of flow of the gas phase, an A the net cross-sectional area for gas flow,

$$w = \rho A V \tag{A-5}$$

$$-\frac{dw_\ell}{w} = \frac{dw}{w} = \frac{d\rho}{\rho} + \frac{dA}{A} + \frac{dV}{V} \tag{A-6}$$

Momentum Theorem. Taking account of the pressure and shear forces acting on the control volume, and of the momentum fluxes entering and leaving, we have(Fig. 4b)

$$pdA - d(pA) - \tau_w \pi D\, dz = (w+dw)(V+dV) + (w_\ell - dw)(V_\ell + dV_\ell) - wV - w_\ell V_\ell$$

Introducing the definition of local skin-friction coefficient,

$$\tau_w \equiv f \cdot \tfrac{1}{2}\rho V^2$$

simplifying, and rearranging in dimensionless form with the help of the relation $\rho V^2 = k p M^2$, the momentum equation becomes

$$\frac{dp}{p} + kM^2\frac{dV}{V} + \frac{kM^2}{2}\left(4f\frac{dz}{D} + 2\frac{w_\ell}{w}\frac{dV_\ell}{V}\right) + kM^2(1-y)\frac{dw}{w} = 0 \tag{A-7}$$

Energy Equation. Considering the heat transfer dQ from the walls and the fluxes of enthalpy and kinetic energy (Fig. 4c), the first law of thermodynamics is written as

$$w dQ = d(w_a h_a) + d(w_v h_v) + d(w_\ell h_\ell) + d(wV^2/2) + d(w_\ell V_\ell^2/2)$$

For a mixture of perfect gases following the Gibbs-Dalton law,

$$\frac{w_a}{w} dh_a + \frac{w_v}{w} dh_v = c_p dT$$

Moreover, from continuity,

$$w = w_a + w_v$$

$$dw = dw_v = -dw_\ell$$

Combining these, simplifying, and rearranging, the energy equation becomes

$$\frac{dT}{T} + (k-1)M^2 \frac{dV}{V} + \left[\frac{h_v - h_\ell + \frac{V^2}{2}(1-\psi^2)}{c_p T}\right]\frac{dw}{w} - \frac{dQ - \frac{w_\ell}{w} dh_\ell}{c_p T} + \frac{w_\ell}{w}(k-1)M_{U}^2 \frac{dV_\ell}{V} = 0 \quad \text{(A-8)}$$

Formation of Influence Coefficients. Equations A-2, A-4, A-6, A-7, and A-8 constitute five simultaneous linear algebraic equations among twelve differential variables: dM^2/M^2, dp/p, $d\rho/\rho$, dT/T, dV/V, dW/W, dw/w, dk/k, dA/A, $4f\,dz/D$, $w_\ell dV_\ell/wV$, and $[dQ-(w_\ell/w)dh_\ell]/c_pT$. Therefore, seven of these may be chosen as independent, and the remaining five may be computed from the values of these seven independent variables. For the latter, the last seven are selected, inasmuch as these represent most directly the influence of the duct geometry and of the droplet acceleration and evaporation on the gas properties. Solving the equations simultaneously in the manner outlined, the influence coefficients appearing in the first four lines of Table III are obtained.

Gas Stagnation Temperature. The stagnation temperature of the gas phase alone is defined as the temperature which would be reached if the gas phase were steadily and adiabatically decelerated to zero speed without interacting with the liquid. Placing its exact variation within the scheme of the influence coefficients is complex because k varies during the deceleration. Since the effect of this variation in k is very small, and for the sake of obtaining results simple and instructive in form, a pseudo-stagnation temperature is defined as above, except that the gas is assumed to have constant k during the deceleration. Then (ref. 2),

$$T_0/T = 1 + \frac{k-1}{2}M^2 \tag{A-9}$$

$$\frac{dT_0}{T_0} = \frac{dT}{T} + \frac{\frac{k-1}{2}M^2}{1+\frac{k-1}{2}M^2}\frac{dM^2}{M^2} + \frac{\frac{kM^2}{2}}{1+\frac{k-1}{2}M^2}\frac{dk}{k} \tag{A-10}$$

from which the fifth line of Table III is found.

Gas Stagnation Pressure. The stagnation pressure of the gas phase alone is defined as the pressure which would be reached if the gas phase were steadily, reversibly, and adiabatically decelerated to zero speed without interacting with the liquid. As above, we define a pseudo-stagnation pressure based on the assumption of unchanged k during the deceleration. Then (ref.2),

$$p_o/p = \left(1+\frac{k-1}{2}M^2\right)^{\frac{k}{k-1}} \qquad \text{(A-11)}$$

$$\frac{dp_o}{p_o} = \frac{dp}{p} + \frac{kM^2/2}{1+\frac{k-1}{2}M^2}\frac{dM^2}{M^2} + \left[\frac{k^2M^2/2}{(k-1)\left(1+\frac{k-1}{2}M^2\right)} - \frac{k}{(k-1)^2}\log\left(1+\frac{k-1}{2}M^2\right)\right]\frac{dk}{k} \qquad \text{(A-12)}$$

from which the seventh line of Table III is found.

Mixture Stagnation Temperature. For certain purposes a consideration of the stagnation properties of the mixture of gas and droplets is more revealing than that of the gas phase alone. Here the question arises of how to define the mixture stagnation properties; that is, what are the interactions between the droplets and gas during the fictitious decelerations? After reflection on the various possibilities, what seem most useful are definitions which differ from the previous definitions only in that they take account of the kinetic energy of the droplets. Therefore, the mixture stagnation temperature is defined as the gas temperature which

would be reached if the mixture were steadily and adiabatically decelerated to zero speed with only mechanical (i.e., no heat transfer or evaporation) interactions between the gas and droplets. Then, again using the notion of a pseudo stagnation temperature for constant k during the deceleration,

$$c_p\theta_o \equiv c_pT + \frac{V^2}{2} + \frac{w_\ell}{w}\frac{V_\ell^2}{2} = c_pT_o + \frac{w_\ell}{w}\frac{V_\ell^2}{2}$$

which, after some manipulation becomes

$$\theta_o \equiv T\left[1+\left(1+\frac{w_\ell}{w}\frac{V_\ell^2}{V^2}\right)\frac{k-1}{2}M^2\right] = T_o\left[\frac{1+\left(1+\frac{w_\ell}{w}\frac{V_\ell^2}{V^2}\right)\frac{k-1}{2}M^2}{1+\frac{k-1}{2}M^2}\right] \equiv \alpha T \qquad \text{(A-13)}$$

or, in differential form,

$$\frac{d\theta_o}{\theta_o} = \frac{1}{\alpha}\left(1+\frac{k-1}{2}M^2\right)\frac{dT_o}{T_o} + (k-1)\frac{M^2y}{\alpha}\left(\frac{w_\ell}{w}\frac{dV_\ell}{V}\right) - \frac{k-1}{2}\frac{M^2y^2}{\alpha}\left(1+\frac{w_\ell}{w}\right)\frac{dw}{w}$$
$$+ \frac{k-1}{2}\frac{M^2y^2}{\alpha}\frac{w_\ell}{w}\frac{dW}{W} + \frac{M^2y^2}{2\alpha}\frac{w_\ell}{w}\frac{dk}{k} \qquad \text{(A-14)}$$

from which the sixth line of Table III is found.

Mixture Stagnation Pressure. Analogously with the mixture stagnation temperature, we define the mixture stagnation pressure as the gas pressure which would be reached if the mixture were steadily, reversibly, and adiabatically decelerated to zero speed with only mechanical interactions between the gas and droplets. For the deceleration to be reversible, the gas alone must first change speed until it is at the same speed as the droplets; then the two phases must decelerate together so slowly that the difference in velocity between the phases is at each point vanishingly small. Since the gas undergoes isentropic changes during the defined process, the pseudo-stagnation pressure P_o obtained by ignoring variations in k during the deceleration is found with the help of Eq. A-13 to be

$$\frac{P_o}{p} = \left(\frac{\theta_o}{T}\right)^{\frac{k}{k-1}} = \left[1 + \left(1 + \frac{w_\ell}{w}\frac{V_\ell^2}{V^2}\right)\frac{k-1}{2}M^2\right]^{\frac{k}{k-1}} \qquad (A-15)$$

$$\frac{dP_o}{P_o} = \frac{dp}{p} + \frac{k}{k-1}\left(\frac{d\theta_o}{\theta_o} - \frac{dT}{T}\right) - \frac{k}{(k-1)^2}\left(\log\frac{\theta_o}{T}\right)\frac{dk}{k} \qquad (A-16)$$

from which the last line of Table III is found.

11. APPENDIX B-ANALYSIS FOR APPROXIMATE OPTIMIZATION PROCEDURE IN REGIME II

With the aim of obtaining an explicit and simple design procedure, the following assumptions are made which are approximately valid in Regime II: (i) $y = 1$; (ii) T_ℓ is constant; and (iii) the influence of the

dk/k term on stagnation pressure is negligible. For the purpose to which the present analysis is later put, a consideration of the gas stagnation pressure p_0 leads down a blind alley (because the analysis would indicate speciously that p_0 could locally be made to rise most rapidly by extreme decelerations which would profit p_0 through the momentum of the droplets), and so we shall deal with the mixture stagnation pressure P_0 .

11.1 Approximate Equation for dP_0/P_0

Using the assumptions listed above, Table III yields for dP_0/P_0 the expression

$$\frac{dP_0}{P_0} = \frac{kM^2}{2}\left[\frac{\left(1+\frac{k-1}{2}M^2\right)\left(1+\frac{w_\ell}{w}\right)}{1+\left(1+\frac{w_\ell}{w}\right)\frac{k-1}{2}M^2}\,\frac{h_v - h_\ell}{c_p T_0} - \frac{1+\frac{w_\ell}{w}}{1+\left(1+\frac{w_\ell}{w}\right)\frac{k-1}{2}M^2}\right]\frac{dw}{w} \quad \text{(Eq. B-1)}$$

$$+ \frac{kM^2}{2}\left[-4f\frac{dz}{D} + \frac{1+\frac{w_\ell}{w}}{1+\left(1+\frac{w_\ell}{w}\right)\frac{k-1}{2}M^2}\,\frac{dW}{W}\right]$$

In what follows, we shall express dW and dz in terms of dw, and thus we shall obtain an expression showing the amount of stagnation pressure rise per unit of evaporation.

11.2 Introduction of Specific Humidity

Using the definitions of local specific humidity ($\omega \equiv w_v/w_a$) and of initial water-air ratio ($\Omega_0 \equiv w_{\ell 0}/w_a$), we may form the following equations relating the mass-flow terms of Eq. B-1 to the

specific humidity:

$$1+\frac{w_\ell}{w} = 1+\frac{w_{\ell_0}-w_v}{w_a+w_v} = \frac{w_a+w_{\ell_0}}{w_a+w_v} = \frac{1+\Omega_0}{1+\omega} \qquad \text{(Eq.B-2)}$$

$$\frac{dw}{w} = \frac{dw_v}{w_a+w_v} = \frac{d(w_v/w_a)}{1+(w_v/w_a)} = \frac{d\omega}{1+\omega} \qquad \text{(Eq. B-3)}$$

11.3 Change of Droplet Diameter

Assuming the existence of a droplet cloud of uniform size, and that neither further atomization or agglomeration occurs in Regime II, the number of droplets per unit time passing any section will be unchanged. The mass rate of water flow will therefore be proportional to be cube of the droplet diameter:

$$\left(\frac{d}{d_0}\right)^3 = \frac{w_{\ell_0}-w_v}{w_{\ell_0}} = \frac{\Omega_0-\omega}{\Omega_0} \qquad \text{(Eq. B-4)}$$

Differentiating, we get

$$dd = -\frac{d_0^3}{3d^2}\frac{dw_v}{w_{\ell_0}} = -\frac{d_0}{3}\left(\frac{\Omega_0-\omega}{\Omega_0}\right)^{-2/3}\frac{d\omega}{\Omega_0} \qquad \text{(Eq. B-5)}$$

11.4 Evaluation of dW/W

The molecular weight of the mixture of gases is related to the molecular weights of the component species by

$$W = \frac{w_v + w_a}{\frac{w_v}{W_v} + \frac{w_a}{W_a}} = W_a \frac{1+\omega}{1+\omega(W_a/W_v)} \qquad \text{(Eq.B-6)}$$

Hence Eq. 5 becomes, after rearrangement

$$\frac{dW}{W} = \frac{(W_v/W_a) - 1}{(W_v/W_a) + \omega} \frac{d\omega}{1+\omega} \qquad \text{(Eq.B-7)}$$

11.5 Heat Transfer to Droplet

Since, by assumption, the droplet temperature is unaltered, and the droplet and gas have the same speed, the amount of heat transferred between gas and droplet during the time interval dt may be equated to the enthalpy change of that portion of the droplet which evaporates. Thus

$$h_t \pi d^2 (T - T_\ell)\, dt = -\pi d^2 \rho_\ell \frac{dd}{2} (h_v - h_\ell)$$

The distance traveled by the droplet during the time dt is

$$dz = V dt = \frac{M}{\sqrt{1 + \frac{k-1}{2} M^2}} \sqrt{kRT_o}$$

Combining these relations, employing Eqs. B-4 and B-5, and expressing the heat-transfer coefficient by the Nusselt Number through the definition

$$Nu \equiv h_t d/k \quad ; \quad h_t = (Nu)k/d$$

we get

$$dz = \frac{1}{6(Nu)} \frac{h_v - h_\ell}{T - T_\ell} \frac{\rho_\ell d_o^2}{k} \frac{M}{\sqrt{1+\frac{k-1}{2}M^2}} \sqrt{kRT_o} \left(\frac{\Omega_o - \omega}{\Omega_o}\right)^{-1/3} \frac{d\omega}{\Omega_o} \qquad \text{(Eq.B-8)}$$

11.6 Working Formula for $dP_o/P_o d\omega$

Setting Eqs. B-2, B-3, B-7, and B-8 into Eq. B-1, simplifying and rearranging, we finally obtain

$$\frac{1}{P_o}\frac{dP_o}{d\omega} = \frac{kM^2}{2}\left\{\frac{1+\Omega_o}{(1+\omega)^2\left(1+\frac{1+\Omega_o}{1+\omega}\frac{k-1}{2}M^2\right)}\left[\left(1+\frac{k-1}{2}M^2\right)\frac{h_v-h_\ell}{c_pT_o} - \frac{1+\omega}{(W_v/W_a)+\omega}\right]\right.$$

$$\left. - \frac{2}{3}\frac{f/D}{(Nu)}\frac{(h_v-h_\ell)\sqrt{1+\frac{k-1}{2}M^2}}{T_o - T_\ell\left(1+\frac{k-1}{2}M^2\right)}\frac{\rho_\ell d_o^2}{k}\frac{M\sqrt{kRT}}{\Omega_o\left(1-\frac{\omega}{\Omega_o}\right)^{1/3}}\right\} \qquad \text{(Eq.B-9)}$$

11.7 Calculation of T_o

Considering the energy equation relating the properties at the Aerothermopressor inlet to those at any section where y = 1, we may write

$$W_a h_{o_a} + W_{\ell_o} h_{\ell_o} = W_a h_{oa} + W_\ell h_\ell + W_\ell \frac{V^2}{2} + W_v h_{ov} \qquad \text{(Eq.B-10)}$$

The enthalpy changes may be closely approximated by

$$h_{o_a} - h_{o_a} \cong c_{pa}(T_{o1} - T_o)$$

$$h_{ov} - h_\ell \cong \mathcal{L} + c_{pv}(T_o - T_{o1}) + c_{pv}(T_{o1} - T_\ell)$$

$$h_\ell - h_{\ell_o} \cong c_{p\ell}(T_\ell - T_{\ell_o})$$

and the term $V^2/2$ may be expressed as

$$\frac{V^2}{2} = \frac{M^2 k R T_o}{2\left(1 + \frac{k-1}{2} M^2\right)}$$

Introducing these into the energy equation, the local stagnation temperature may be solved for as

$$T_o \cong \frac{1 + \frac{k-1}{2} M^2}{1 + (1 + \omega - \Omega_o)\frac{k-1}{2} M^2} \left[T_{o1} - \frac{\omega \mathcal{L}}{c_p} - \Omega_o \frac{c_{p\ell}}{c_p}(T_\ell - T_{\ell_o}) - \omega \frac{c_{pv}}{c_p}(T_{o1} - T_\ell) \right] \quad \text{(Eq. B-11)}$$

11.8 Estimate of Nusselt Number

The value of Nu depends upon the relative Reynolds Number between droplet and gas stream (ref.7). If y were exactly unity, this Reynolds Number would be zero, and Nu would be 2.00. Although y may be so close to unity that it may be so assumed for the purpose of Eq. B-1, its deviation from unity may generate a sufficiently high Reynolds Number to give Nusselt

Numbers substantially greater than 2.00. To find the local value of Nu, therefore, would require integrating the entire set of governing equations of the Aerothermopressor after the manner of Section 4.7. But this is exactly what we wish to avoid in the present simplified design method. Fortunately, the numerical integrations of the type of Section 4.7 show that in Regime II, the value of Nu lies between 2 and 4, thus setting upper and lower limits on Nu which are not excessively apart.

11.9 Method of Constructing Curves of $dP_o/P_o d\omega$

Suppose that in a given case the conditions at the Aerothermopressor inlet, i.e., T_{o1} , Ω_o , and d_o , are known. In Regime II the value of T_ℓ may be set equal to the average wet-bulb temperature, which, for the range of pressures and temperatures encountered, is generally not far from 140°F. A particular value of Nu between 2 and 4 is also selected. In addition, we choose an appropriate average value of f/D, neglecting the variations of diameter, inasmuch as these amount only to some 10 or 20% in the range of interest.

Then, for each combination of M and ω , Eqs. B-9 and B-10 allow the value of $dP_o/P_o d\omega$ to be calculated. Thus it is possible to construct curves of $dP_o/P_o d\omega$ versus M, with ω as a parameter, as exemplified by the chart of Fig. 7a.

12. APPENDIX C - GOVERNING PHYSICAL EQUATIONS FOR DROPLETS

Consider a single droplet of diameter d, velocity V_ℓ , and temperature T_ℓ , journeying in a gas stream of velocity V , temperature T , pressure p , and specific humidity ω . As the mean distance between droplets is of the order of 10 droplet diameters or more, mutual interactions between the droplets are ignored, and the gaseous medium surrounding each droplet is imagined as infinite in extent.

12.1 Droplet Diameter vs. Stream Humidity

Since the droplets are uniform and incompressible, and of unchanged number per unit time, the mass rate of liquid flow at any section is proportional to the cube of the droplet diameter. Thus the local humidity, which is a measure of the loss in liquid mass flow, is given by

$$\chi \equiv \frac{\omega}{\Omega_o} = 1 - \left(\frac{d}{d_o}\right)^3$$

or, after differentiation, the change in droplet diameter is related to the change in humidity by

$$\frac{dd}{d_o} = -\frac{1}{3}\frac{d\chi}{(d/d_o)^2} = -\frac{1}{3}\frac{d\omega/\Omega_o}{(d/d_o)^2} \qquad \text{(Eq. C-1)}$$

12.2 Mass Transfer

The reduction in droplet diameter is the result of transfer of mass from the saturated water vapor at the surface of the droplet to the external gaseous medium. The resulting rate of change of mass is expressed in terms of the mass-transfer coefficient, the surface area, and the "driving force" which constitutes the difference in spatial mass concentration,

$$-\frac{d}{dt}\left(\frac{\pi}{6}d^3\rho_l\right) = h_D(\pi d^2)(\rho_{vl} - \rho_{v\infty})$$

which simplifies to

$$\frac{dd}{dt} = -\frac{2h_D}{\rho_l}(\rho_{vl} - \rho_{v\infty}) \qquad \text{(Eq. C-2)}$$

For the coefficient h_D, we have used the seemingly satisfactory (at least for solid spheres with small temperature differences and mass transfer rates) correlation of Ranz and Marshall (ref. 7):

$$Nu_D = 2 + 0.6\,(Sc)^{1/3}(Rey)^{1/2} \qquad \text{(Eq. C-3)}$$

where

$$Nu_D = h_D d/\mathcal{D} \; ; \; Sc = \mu/\rho\mathcal{D} \; ; \; Rey = (\rho d|V - V_l|)/\mu \qquad \text{(Eq. C-4)}$$

In evaluating the driving potential, ρ_{vl} is taken as the reciprocal of the specific volume of saturated water vapor at the temperature T_l ; $\rho_{v\infty}$ is computed from the perfect gas law of mixtures as

$$\rho_{v\infty} = \frac{p}{R_a T} \frac{\omega}{1+\omega W_a/W_v} \qquad \text{(Eq. C-4)}$$

12.3 Heat Transfer

From a consideration of the first law of thermodynamics, the rate of heat transfer to the droplet is equal to the sum of the rate of enthalpy change of both the evaporated and unevaporated water. Thus

$$h_T(\pi d^2)(T-T_l) = \left(\frac{\pi d^3}{6}\rho_l\right)\frac{d}{dt}(c_{pl}T_l) - \mathcal{L}\frac{d}{dt}\left(\frac{\pi d^3}{6}\rho_l\right)$$

which simplifies to

$$\frac{dT_l}{dt} = \frac{6h_T}{\rho_l d c_{pl}}(T-T_l) + \frac{3\mathcal{L}}{d c_{pl}}\frac{dd}{dt} \qquad \text{(Eq. C-5a)}$$

where $\mathcal{L}$ is the latent heat at the temperature T_l . Using Eqs. C-1 and C-2, this may be written in the alternate form

$$\frac{dT_l}{dX} = -\frac{1}{c_{pl}(1-X)}\left[\mathcal{L} - \frac{h_T}{h_D}\frac{(T-T_l)}{\rho_{vl}-\rho_{v\infty}}\right] \qquad \text{(Eq.C-5b)}$$

The heat-transfer coefficient h_T has also been taken from the correlation of Ranz and Marshall (ref. 7),

$$Nu_T = 2 + 0.6\,(Pr)^{1/3}(Rey)^{1/2} \qquad \text{(Eq. C-6)}$$

where

$$Nu_T \equiv h_T d/k \quad ; \quad Pr \equiv c_p \mu/k \qquad \text{(Eq. C-7)}$$

12.4 Droplet Acceleration

Employing the conventional definition of drag coefficient for blunt bodies like spheres, we may equate the net force on the particle to the product of mass and acceleration. Thus

$$C_D\left(\frac{\pi}{4}d^2\right)\frac{\rho}{2}(V-V_\ell)\left|V-V_\ell\right| = \rho_\ell \frac{\pi d^3}{6}\frac{dV_\ell}{dt}$$

from which

$$\frac{dV_\ell}{dt} = \frac{3}{4}(C_D Rey)\frac{\mu}{\rho_\ell d^2}(V-V_\ell) \qquad \text{(Eq. C-8)}$$

In the numerical calculations the well-established correlation between C_D and Rey for solid spheres has been approximated by

$$C_D = 24/Rey \quad \text{for} \quad 0 < Rey \leq 1$$
$$C_D = 24/Rey^{2/3} \quad \text{for} \quad 1 \leq Rey \leq 390 \qquad \text{(Eq.C-9)}$$
$$C_D = 0.45 \quad \text{for} \quad 390 \leq Rey < \infty$$

12.5 Displacement of Droplet

The distance dz along the duct traveled by the droplet cloud in the time dt is given by

$$dz/dt = V_l \qquad \text{(Eq. C-1}$$

13. APPENDIX D - APPROXIMATE DISCONTINUITY ANALYSIS

13.1 Governing Integral Equations

Let section 1 be the inlet plane and section 2 the exit plane of the Aerothermopressor, and let the entire water input be evaporated completely at section 2 (it is known from other considerations that excess water has little effect on performance). Then we may write the following conservation equations between sections 1 and 2.

Energy:

$$(h_{oa_2} - h_{oa_1}) + \Omega_o (h_{ov_2} - h_{ov_1}) + \Omega_o (h_{ov_1} - h_{l_1}) = 0$$

or $$(1+\Omega_o)\bar{c}_{p_{12}}(T_{o2} - T_{o1}) = -\Omega_o (h_{ov_1} - h_{l1})$$

$$\frac{T_{o2}}{T_{o1}} = \frac{T_2}{T_1} \frac{1 + \frac{k-1}{2} M_2^2}{1 + \frac{k-1}{2} M_1^2} = 1 - \frac{\Omega_o}{1+\Omega_o} \frac{h_{ov} - h_{l1}}{\bar{c}_{p_{12}} T_{o1}} \qquad \text{(Eq. D-1}$$

Continuity:

$$\frac{V_2}{V_1} = (1+\Omega_0)\frac{\rho_1}{\rho_2}\frac{A_1}{A_2} \qquad \text{(Eq. D-2)}$$

Definition of Mach Number:

$$M_1^2 = \frac{V_1^2 W_1}{k_1 \bar{R} T_1} \quad ; \quad M_2^2 = \frac{V_2^2 W_2}{k_2 \bar{R} T_2} \qquad \text{(Eq. D-3)}$$

Equation of State:

$$\frac{\rho_2}{\rho_1} = \frac{W_2}{W_1} \cdot \frac{T_1}{T_2} \cdot \frac{P_2}{P_1} \qquad \text{(Eq.D-4)}$$

Momentum Equation: Omitting wall friction for the present,

$$P_1 A_1 - P_2 A_2 + \int_1^2 p\,dA = -\int_1^2 A\,dp = \rho_1 A_1 V_1 \left[(1+\Omega_0)V_2 - V_1\right]$$

To compute the definite integral requires a detailed knowledge of the drop history, which we are here avoiding. As shown by Wadleigh (ref.9), the results are insensitive to the way in which A varies with p, and so we have arbitrarily chosen a linear variation:

$$\frac{dp}{dA} = \text{constant} = \frac{P_2 - P_1}{A_2 - A_1}$$

Evaluating the integral in the momentum equation, and simplifying, we get

$$\frac{p_2 - p_1}{k_1 p_1 M_1^2} = \frac{2}{1+\frac{A_2}{A_1}}\left[1 - (1+\Omega_0)\frac{V_2}{V_1}\right] \qquad \text{(Eq.D-5)}$$

Stagnation Pressure: The well-known isentropic relation gives

$$\frac{p_0}{p} = \left(1 + \frac{k-1}{2}M^2\right)^{\frac{k}{k-1}} \qquad \text{(Eq.D-6a)}$$

As shown in ref. 2, p. 95, the isentropic stagnation pressure may also be expressed approximately, at least in terms up to order M^4, as

$$\frac{p_0 - p}{p} = \frac{kM^2}{2}\left(1 + \frac{M^2}{4} + \cdots\right)$$

Retaining only the terms of order M^2, we may form

$$\frac{(p_{02} - p_{01})_\infty}{k_1 p_1 M_1^2} \cong \frac{p_2 - p_1}{k_1 p_1 M_1^2} + \frac{1}{2}\frac{p_2}{p_1}\frac{k_2 M_2^2}{k_1 M_1^2} - \frac{1}{2} \qquad \text{(Eq.D-6b)}$$

where the subscript infinity here refers to infinite duct size, for which the wall friction is indeed zero.

First-Order Solution. Explicit algebraic solution of the foregoing set of equations for $(p_{02} - p_{01}) / k_1 p_1 M_1^2$ seems impossible. For low Mach Numbers, however, such a solution may be approximated. Having in mind the assumption of low Mach Numbers, we may according to Eq. D-5 set $p_2/p_1 \cong 1$ in Eqs. D-4 and D-6; and we may further set $T_{02}/T_{01} \cong T_2/T_1$ in Eq. D-1. Algebraic combination of Eqs. D-2, D-3 and D-4 then yields

$$\frac{k_2 M_2^2}{k_1 M_1^2} \cong (1+\Omega_o)\left(\frac{A_1}{A_2}\right)\mathcal{Z} \qquad \text{(Eq.D-7)}$$

where

$$\mathcal{Z} \equiv (1+\Omega_o)\frac{A_1}{A_2}\frac{W_1}{W_2}\frac{T_2}{T_1} \qquad \text{(Eq.D-8)}$$

In addition, algebraic combination of Eqs. D-2, D-4 and D-5 produces

$$\frac{p_2 - p_1}{k_1 p_1 M_1^2} \cong \frac{2}{1+\frac{A_2}{A_1}}\left[1-(1+\Omega_o)\mathcal{Z}\right] \qquad \text{(Eq.D-9)}$$

The calculation procedure is now as follows, for given values of M_1, T_1, Ω_o, and A_2/A_1 :

(i) T_2 is calculated from the low Mach Number approximation for Eq. D-1.

(ii) $k_2 M_2^2 / k_1 M_1^2$ is calculated from Eq. D-7.

(iii) $(P_2 - P_1)/k_1 p_1 M_1^2$ is calculated from Eq. D-9.

(iv) $(P_{02} - P_{01})_\infty / k_1 P_1 M_1^2$ is calculated from Eq. D-6b.

Exact Discontinuity Solution. If more accurate results than those obtainable from the low Mach Number analysis are desired, trial-and-error solution of Eqs. D-1, D-2, D-3, D-4, D-5 and D-6a is necessary, the approximate solution serving as a useful starting point. First we derive several required formulas.

Eliminating V_2/V_1 from Eq. D-5 with the help of Eqs. D-2 and D-4, we obtain

$$\frac{P_2 - P_1}{k_1 p_1 M_1^2} = \frac{2}{1+\frac{A_2}{A_1}} \left\{ 1 - \frac{(1+\Omega_0)\Xi}{1 + \frac{2k_1 M_1^2}{1+\frac{A_2}{A_1}}\left[1-(1+\Omega_0)\Xi\right]} \right\} \qquad \text{(Eq. D-10)}$$

Solution of this for P_2/P_1 yields

$$\frac{P_2}{P_1} = 1 + \frac{2k_1 M_1^2}{1+\frac{A_2}{A_1}} \left\{ 1 - \frac{(1+\Omega_0)\Xi}{1 + \frac{2k_1 M_1^2}{1+\frac{A_2}{A_1}}\left[1-(1+\Omega_0)\Xi\right]} \right\} \qquad \text{(Eq. D-11)}$$

Then, employing Eqs. D-10, D-2 and D-4, the value of $k_2 M_2^2 / k_1 M_1^2$ may be found from Eq. D-3 as

$$\frac{k_2 M_2^2}{k_1 M_1^2} = \frac{(1+\Omega_0)\frac{A_1}{A_2}\Xi}{\left\{1 + \frac{2k_1 M_1^2}{1+\frac{A_2}{A_1}}\left[1-(1+\Omega_0)\Xi\right]\right\}^2} \qquad \text{(Eq. D-12)}$$

The exact expression for the stagnation pressure ratio may be found from Eq. D-6a as

$$\left(\frac{p_{02}}{p_{01}}\right)_{\infty} = \frac{p_2}{p_1} \frac{\left(1 + \frac{k_2-1}{2} M_2^2\right)^{k_2/(k_2-1)}}{\left(1 + \frac{k_1-1}{2} M_1^2\right)^{k_1/(k_1-1)}} \qquad \text{(Eq.D-13)}$$

in which the value of p_2/p_1 is that given by Eq. D-11.

Assuming that values of M_1, T_1, Ω_o and A_2/A_1 have been selected, the numerical calculations may be carried out in the following order:

(i) Guess M_2, using the low Mach Number analysis as a guide.

(ii) Compute the corresponding T_2 from Eq. D-1.

(iii) Evaluate $\bar{z}$ from Eq. D-8.

(iv) Check whether the guessed value of M_2 is correct by computing M_2 from Eq. D-12.

(v) Using the value of M_2 from Eq. D-12, repeat steps (i) to (iv) until satisfactory convergence is obtained. Only two trials are usually necessary.

(vi) Calculate $(p_2 - p_1)/p_1$ from Eq. D-10.

(vii) Solve Eq. D-13 for $(p_{02}/p_{01})_{\infty}$.

Effects of Wall Friction and Diffuser Loss. We may now take account of wall friction in a manner which is in the same vein as the approximations already made. Taking note of the influence coefficients of Table II,

the change in p_o associated with wall friction may be expressed as

$$\frac{(p_{o2}-p_{o1})_f}{p_{o1}} \cong -\frac{\overline{kM^2}}{2} 4f\frac{L}{D} \qquad \text{(Eq.D-14)}$$

where $\overline{kM^2}$ is the arithmetic mean of $k_1M_1^2$ and $k_2M_2^2$

Besides wall friction, there is a loss in the diffuser which may be expressed as a percent loss of stagnation pressure in terms of a loss-coefficient ϵ .

$$\epsilon \equiv -\frac{(\Delta p_o)_{diff}}{\frac{1}{2}k_2 p_2 M_2^2} \qquad \text{(Eq.D-15)}$$

Linearly superposing the losses due to wall friction and the diffuser on the previous results, we obtain

$$\frac{p_{o2}-p_{o1}}{k_1 p_1 M_1^2} \cong \frac{(p_{o2}-p_{o1})_\infty}{k_1 p_1 M_1^2} - \frac{1}{2}\frac{\overline{kM^2}}{k_1M_1^2}\frac{p_{o1}}{p_1} 4f\frac{L}{D} - \frac{\epsilon}{2}\frac{k_2M_2^2}{k_1M_1^2}\frac{p_2}{p_1} \qquad \text{(Eq.D-16)}$$

14. REFERENCES

1. "The Mechanics and Thermodynamics of Steady One-Dimensional Gas Flow", by Ascher H. Shapiro and W. R. Hawthorne, Jour. App. Mech., vol. 14, no. 4, pp. A-317-A-336 (1947).

2. "The Dynamics and Thermodynamics of Compressible Fluid Flow", by Ascher H. Shapiro, New York, The Ronald Press Co., 1954, vol. 1, p.83.

3. Ibid, pp 255-260.

4. "An Experiment on the Atomization of Liquid by Means of an Air Stream", by S. Nukyama and Y. Tanasawa, Trans. S.M.E. Japan, vol. 4, Reports 1-6 (1938).

5. "One-Dimensional Analysis of Steady-Flow Air-Water Mixtures in Pipes", by Merson Booth, thesis for Nav. Eng. Degree, M.I.T., (1953).

6. "Experimental and Theoretical Investigation of Subsonic Air Diffusers with Entrained Liquid Droplets", by E. G. Feher, thesis for S.M. Degree, M.I.T. (1953).

7. "Evaporation from Drops", by W. E. Ranz and W. R. Marshall, Jr., Chem. Eng. Prog. vol. 48, nos. 3 and 4 (1952).

8. A Theoretical Investigation of the Thermodynamic and Dynamic Effects of Water Injection into High-Velocity, High-Temperature Gas Streams", by Bruce D. Gavril, Thesis for Sc. D. Degree in Mechanical Engineering, M. I. T. (1954).

9. "An Experimental Investigation of a Small Scale Aerothermopressor-A Device for Increasing the Stagnation Pressure of a High-Temperature, High-Velocity Gas Stream by Evaporative Cooling", by Kenneth R. Wadleigh, thesis for Sc. D. Degree in Mechanical Engineering, M.I.T. (1953).

10. "The Photometric Measurement of Particle Size", by John B. Cheatham, Jr., thesis for Mech. Eng. Degree, M. I. T. (1954).

11. "Measurement of Droplet Size in an Aerosol by a Modified Impact Probe" by George E. Keeler, thesis for M. S. Degree in Mech. Eng., M. I. T. (1954).

12. "Investigation of Aerodynamic Droplet Measuring Probe", by Victor G. Pesek, thesis for S. B. Degree in Mech. Eng., M. I. T. (1954).

13. "Theoretical and Experimental Investigation of a Deceleration Probe", by Jules Dussourd, thesis for Sc. D. Degree in Mechanical Eng., M. I. T. (1954).

14. "A Sampling Technique for a Measurement of Water Air Ratio of a High Speed Spray-Laden Air Stream", R. E. Kosiba and F. H. E. Vose, thesis for Naval Eng. Deg., M. I. T. (1953).

CAPTIONS TO FIGURES

Fig. 1 Illustrates one-dimensional process on which Eq. 1 is based.

Fig. 2 Application of the Aerothermopressor to the simple gas turbine

(a) At exit of turbine

(b) Between burner and turbine

Fig. 3 Effect of Aerothermopressor on performance of gas turbine plant

(a) Cycle arrangement

(b) Fuel economy and power capacity for favorable cycle parameters

(c) Fuel economy and power capacity for unfavorable cycle parameters

Fig. 4 Illustrates one-dimensional analysis of Appendix A.

(a) Nomonclature and control volume.

(b) Forces and momentum fluxes for control volume

(c) Fluxes of enthalpy and kinetic energy for control volume

Fig. 5 Schematic representation of behavior of subsonic, constant-area Aerothermopressor

Fig. 6 Continuous passage through the speed of sound

(a) From subsonic to supersonic

(b) From supersonic to subsonic

Fig. 7 Approximate optimization method, based on analysis of Appendix B.

(a) Typical curves of fractional rate of change of mixture stagnation pressure with specific humidity as a function of Mach Number, with local specific humidity as a parameter, and for constant values of T_{o_1}, Ω_o, d_o, Nu, f/D.

(b) Optimum curve of Mach Number vs. humidity, corresponding to "design curve" of Fig. 7a. Dashed curve, shows comparative position of optimum curve for more favorable values of parameters.

(b) Optimum curve of $dP_o/P_o d\omega$ vs. humidity, corresponding to "design curve" of Fig. 7a. Dashed curve shows comparative position of optimum curve for more favorable values of parameters.

(d) Illustrates optimal Mach Number variation of entire Aerothermopressor.

Fig. 8 Typical theoretical calculations for subsonic, constant-area operation.

Fig. 9 Typical theoretical calculations for supersonic constant-area operation. Initial conditions: $M_1 = 1.5$; $T_{01} = 1500°R$; $p_{01} = 14.7$ psia; $f/D_1 = 0.004$ ft^{-1}; $\Omega_o = 0.15$; $T_{l1} = 530°R$; $V_{l1}/V_1 = 0$; $d_o = d_{oj} = 7.34\mu$.

Fig. 10 Theoretical effect of size on small-scale, constant-area, subsonic operation. Initial conditions:

$M_1 = 0.5$; $T_{01} = 1500°R$; $p_{01} = 14.7$ psia ; $\Omega_o = 0.2$;

$T_{l1} = 530°R$; $V_{l1}/V_1 = 0$; $d_o = d_{oj} = 19\ \mu$.

Fig. 11 Theoretical effect of initial drop size on small-scale, constant-area, subsonic operation. Initial conditions:

$M_1 = 0.5$; $T_{01} = 1500°R$; $p_{01} = 14.7$ psia, $f/D_1 = 0.0226$ ft^{-1};

$\Omega_o = 0.2$; $T_{l1} = 530°R$; $V_{l1}/V_1 = 0$; $d_{oj} = 19\ \mu$.

Fig. 12 Theoretical effect of initial water-air ratio on small-scale, constant-area subsonic operation. Initial conditions:

$M_1 = 0.5$; $T_{01} = 1500°R$; $p_{01} = 14.7$ psia ; $f/D_1 = 0.0226$ ft^{-1};

$T_{l1} = 530°R$; $V_{l1}/V_1 = 0$; $d_o = d_{oj} = 19\ \mu$.

Fig. 13 Theoretical curve of constant-area operation at various subsonic initial Mach Numbers, illustrating continuous passage at critical initial Mach Number through speed of sound, and normal shocks on on supersonic critical branch. Corresponding curves of static pressure are shown in Fig. 27.

Fig. 14 Illustrates theoretical improvement by control of cross-sectional area. Initial conditions:

$M_1 = 0.727$; $T_{01} = 1500°R$; $P_{01} = 14.7$ psia ; $f/D_1 = 0.004\ ft^{-1}$;

$T_{\ell 1} = 530°R$; $V_{\ell 1}/V_1 = 0$; $d_o = d_{oj} = 13.4\mu$; $\Omega_o = 0.25$.

Solid curves represent subsonic and supersonic critical operation. Dashed curves show variable-area operation with Mach Number distribution shown (beginning at x = 0.30), followed by 6°-included angle diffuser (beginning at x = 0.54). Dash-dot curves show constant-area operation on supersonic critical with shock at x = 0.30.

Fig. 15 Typical results of calculations based on "low-velocity" discontinuity analysis. Dashed curve shows results of "exact" discontinuity analysis.

Fig. 16 Arrangement of small-scale experimental unit.

Fig. 17 Small-scale experimental results, showing comparison between water injection without evaporation ($T_{01} = 530°R$), and with evaporation ($T_{01} = 1500°R$).

Fig. 18 Small-scale experimental results, showing effect of water-air ratio.

Fig. 19 Small-scale experimental results, showing effect of initial Mach Number, continuous passage through speed of sound, and shocks in supersonic regime.

Fig. 20 Illustrates schematically shock positions for stable and unstable operation.

Fig. 21 Small-scale experimental results, showing effects on over-all performance of water-air ratio, initial stagnation temperature, and initial stagnation pressure. Each point is for the initial Mach Number or shock position of best performance.

Fig. 22 Small-scale experimental results, showing effects on over-all performance of initial stagnation temperature and pressure. Each point is for the water-air ratio of best performance. The right-hand point of each curve represents the choking Mach Number, and refers to the shock location of best performance.

Fig. 23 Small-scale experimental results, showing effect of stagnation-pressure level on static pressure distribution.

Fig. 24 Small-scale experimental results, showing humidity profiles at several longitudinal cross sections.
$M_1 = 0.502$; $\Omega_0 = 0.150$; $T_{01} = 1500^\circ R$; $P_{01} = 14.6$ psia.

Fig. 25 Small-scale experimental results, showing fraction evaporated vs. longitudinal distance. Open points refer to direct humidity measurements. Closed points are inferred from static pressure data.

Fig. 26 Small-scale experimental results, showing exit humidity ($\bar{z} = 67.5$ inches) as function of water-air ratio and initial Mach Number.

Fig. 27 Comparison of small-scale experimental results (dashed curves) with theoretical calculations (solid curves) for completely subsonic operation.

Fig. 28 Comparison of small-scale experimental results (dashed curves) with theoretical calculations (solid curves) for subsonic-supersonic operation.

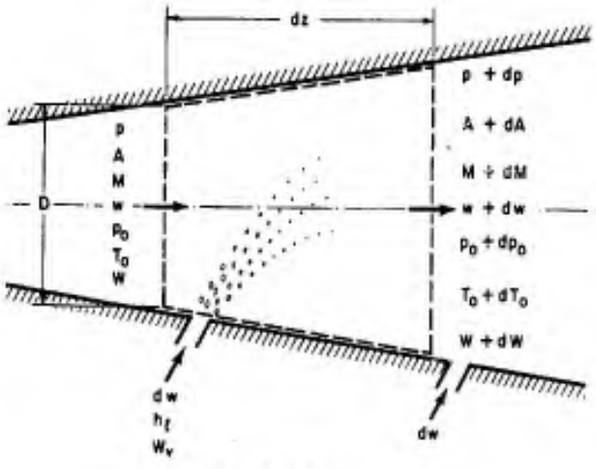

FIG. 1

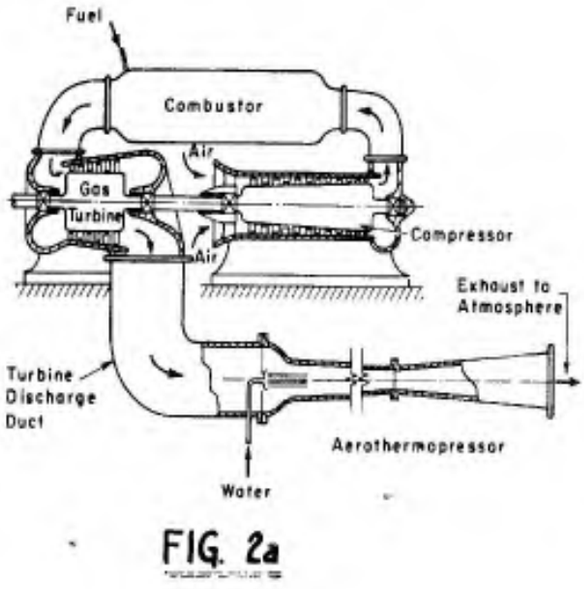

FIG. 2a

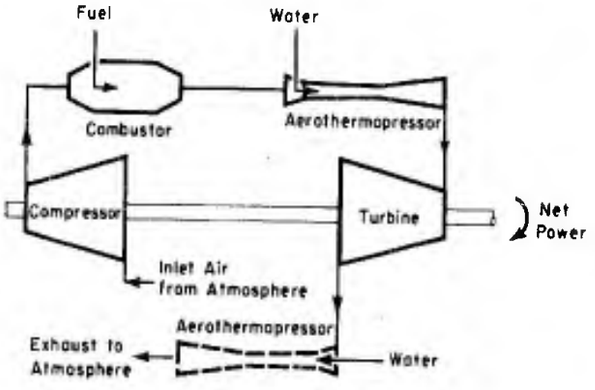

FIG. 2b

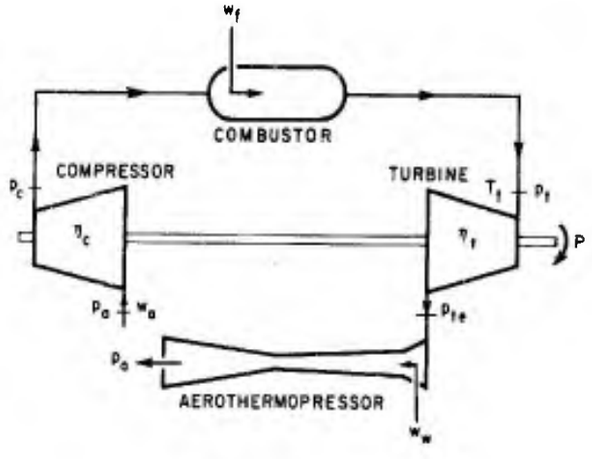

FIG. 3a

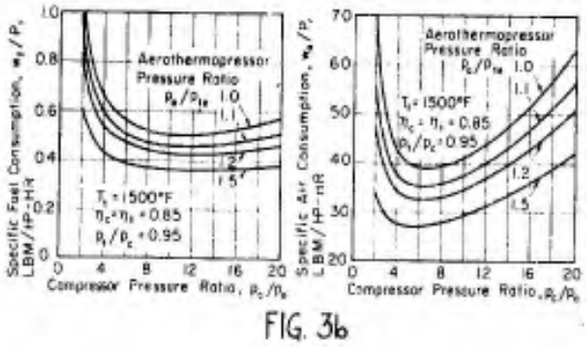

FIG. 3b

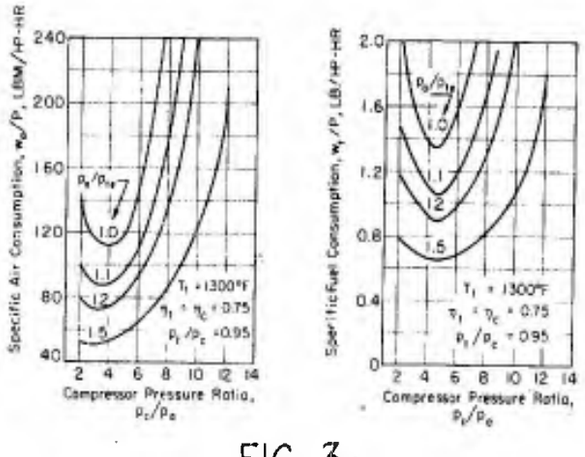

FIG. 3c

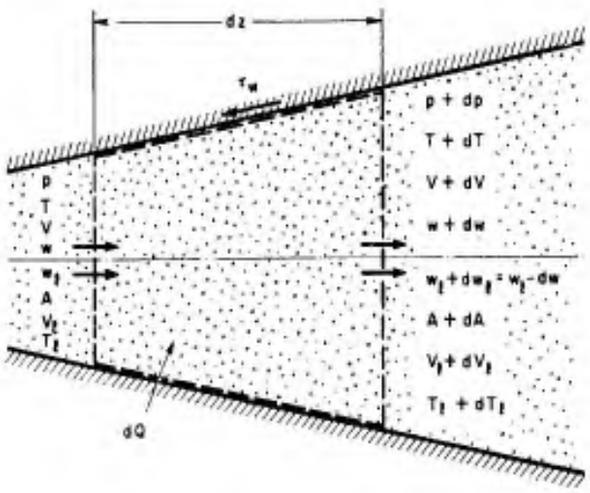

FIG. 4a

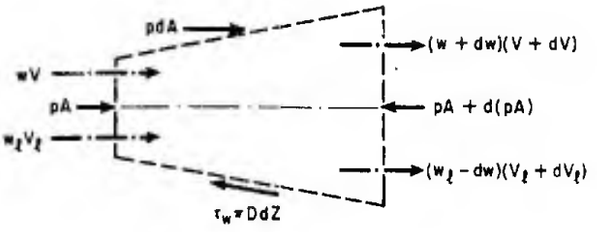

FIG. 4b

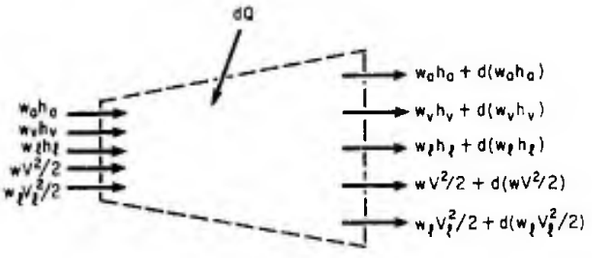

FIG. 4c

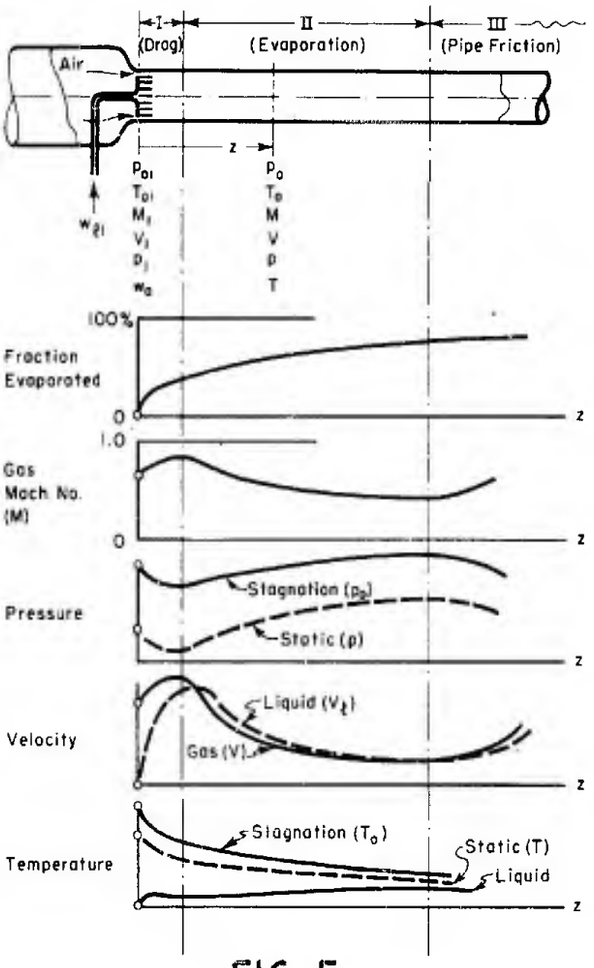

FIG. 5

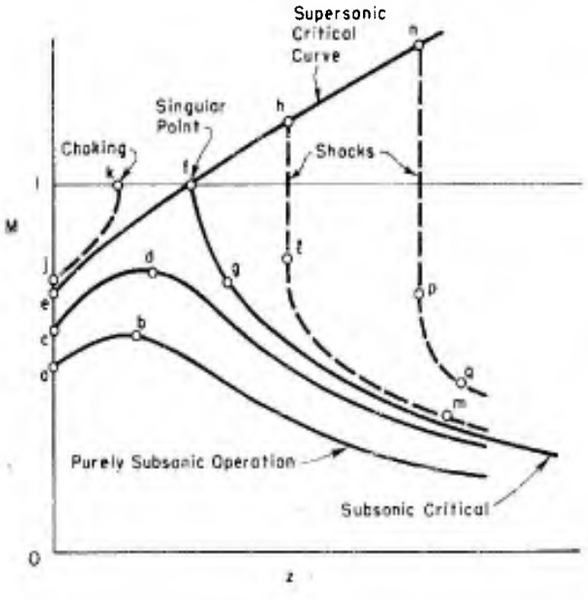

FIG. 6a

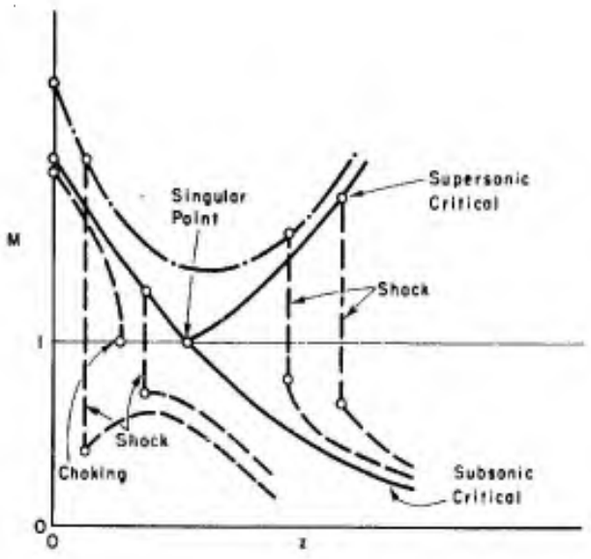

FIG. 6b

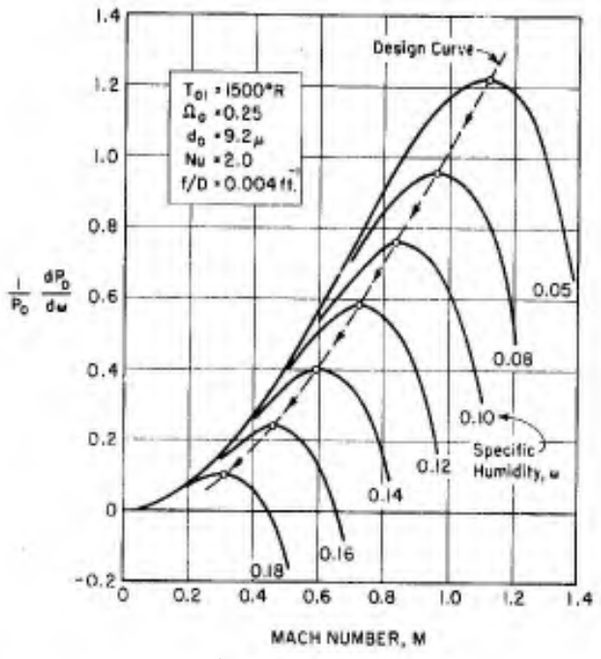

FIG. 7a

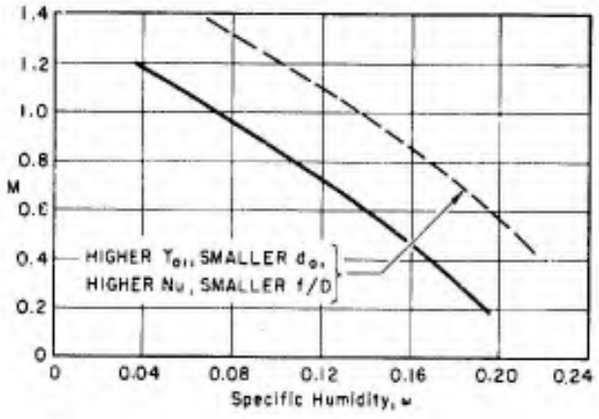

FIG. 7b

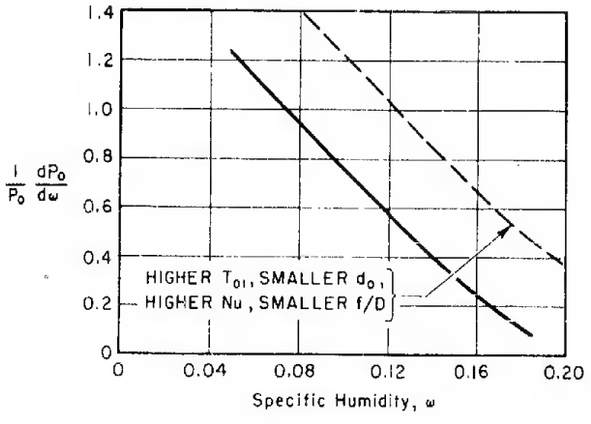

FIG. 7c

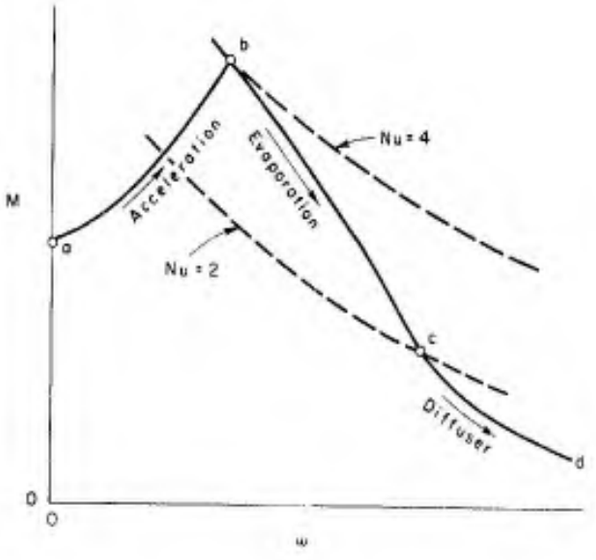

FIG. 7d

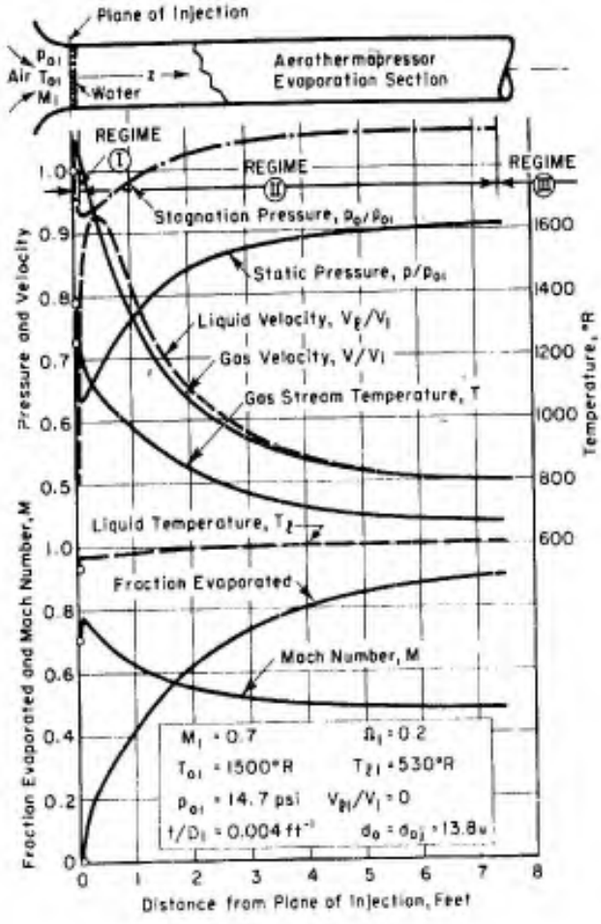

FIG. 8

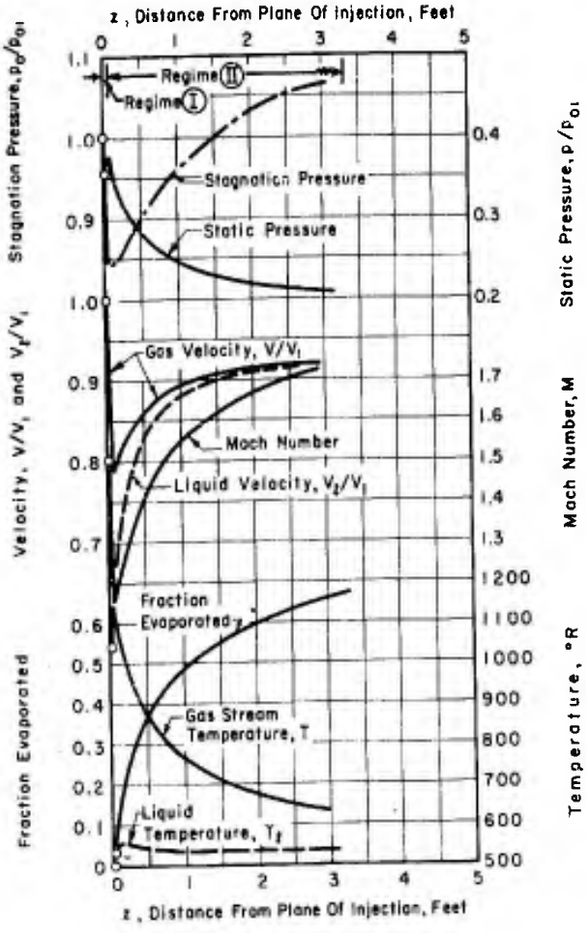

FIG. 9

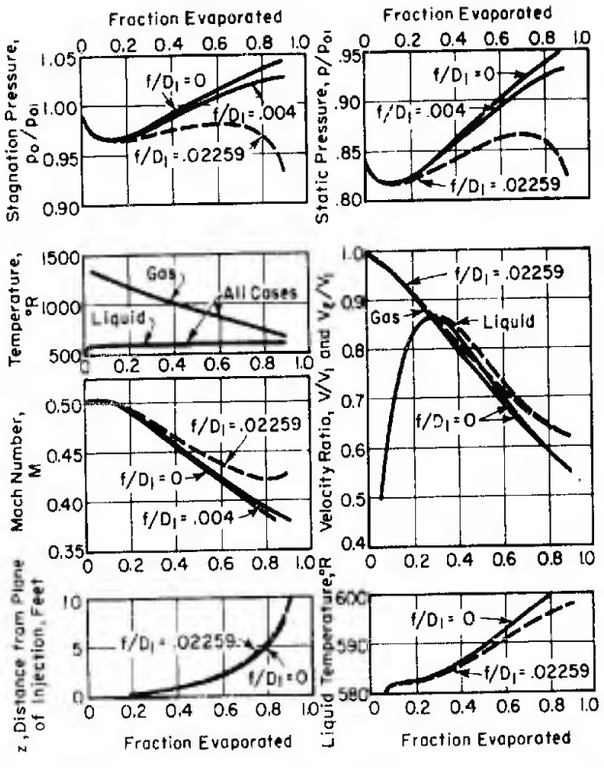

FIG. 10

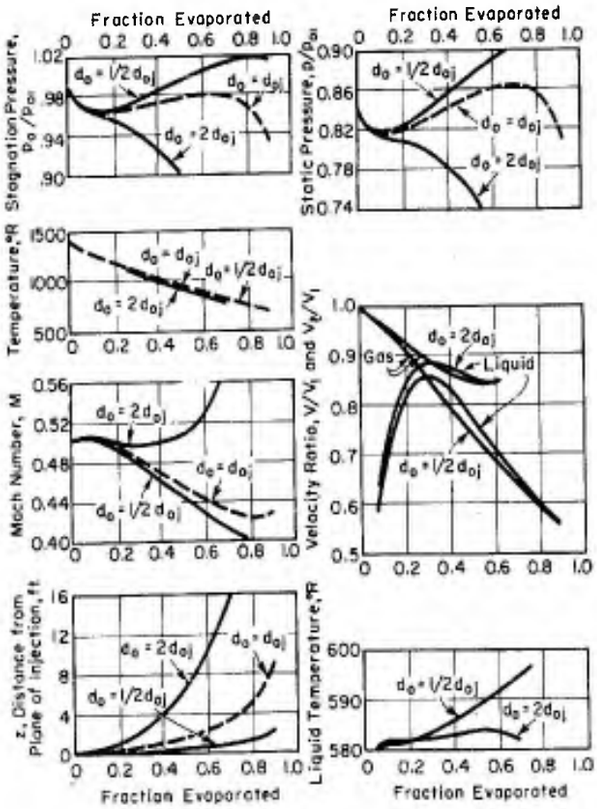

FIG. 11

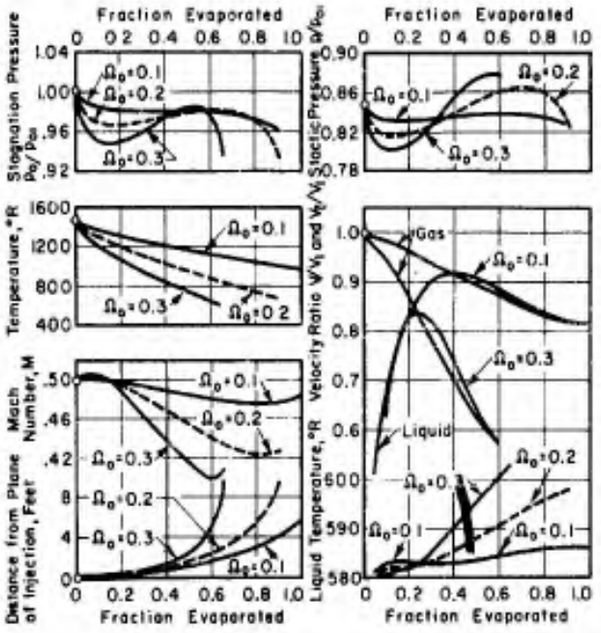

FIG. 12

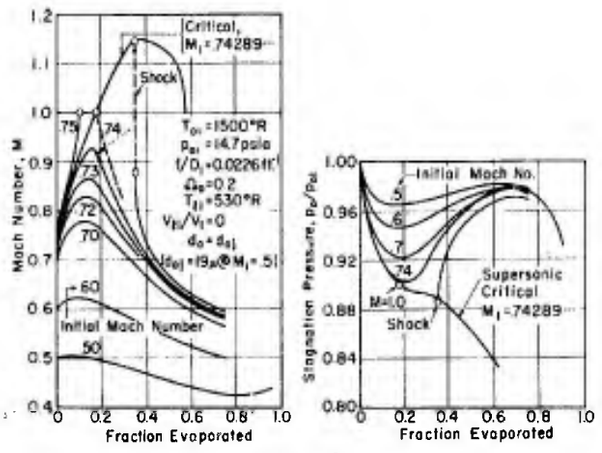

FIG. 13

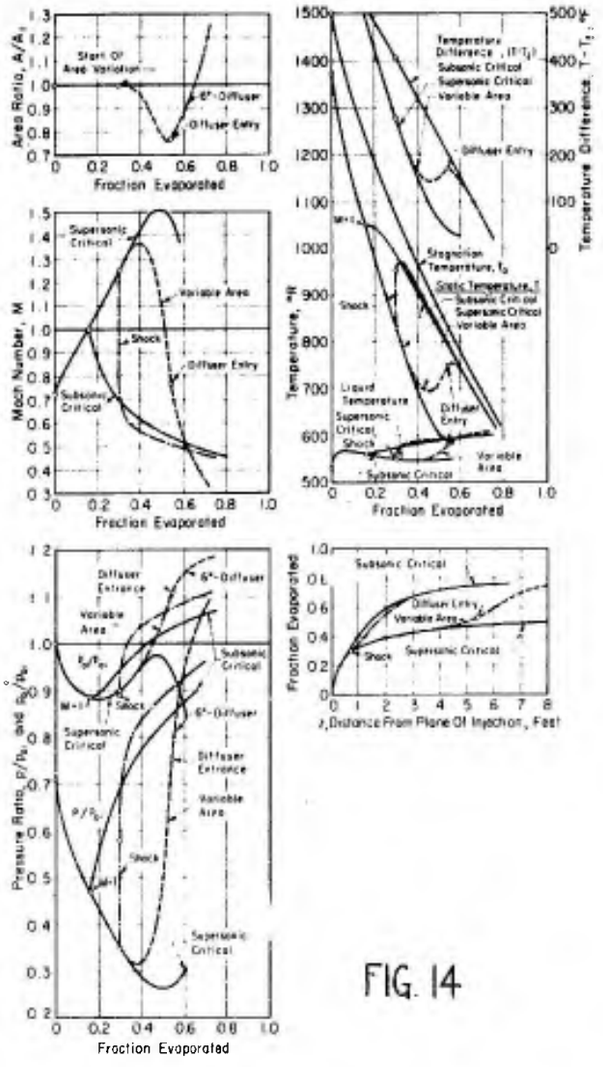

FIG. 14

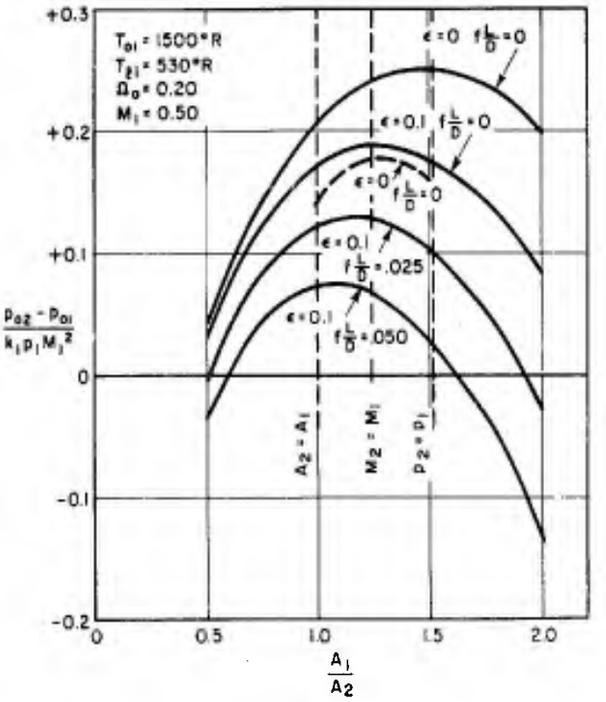

FIG. 15

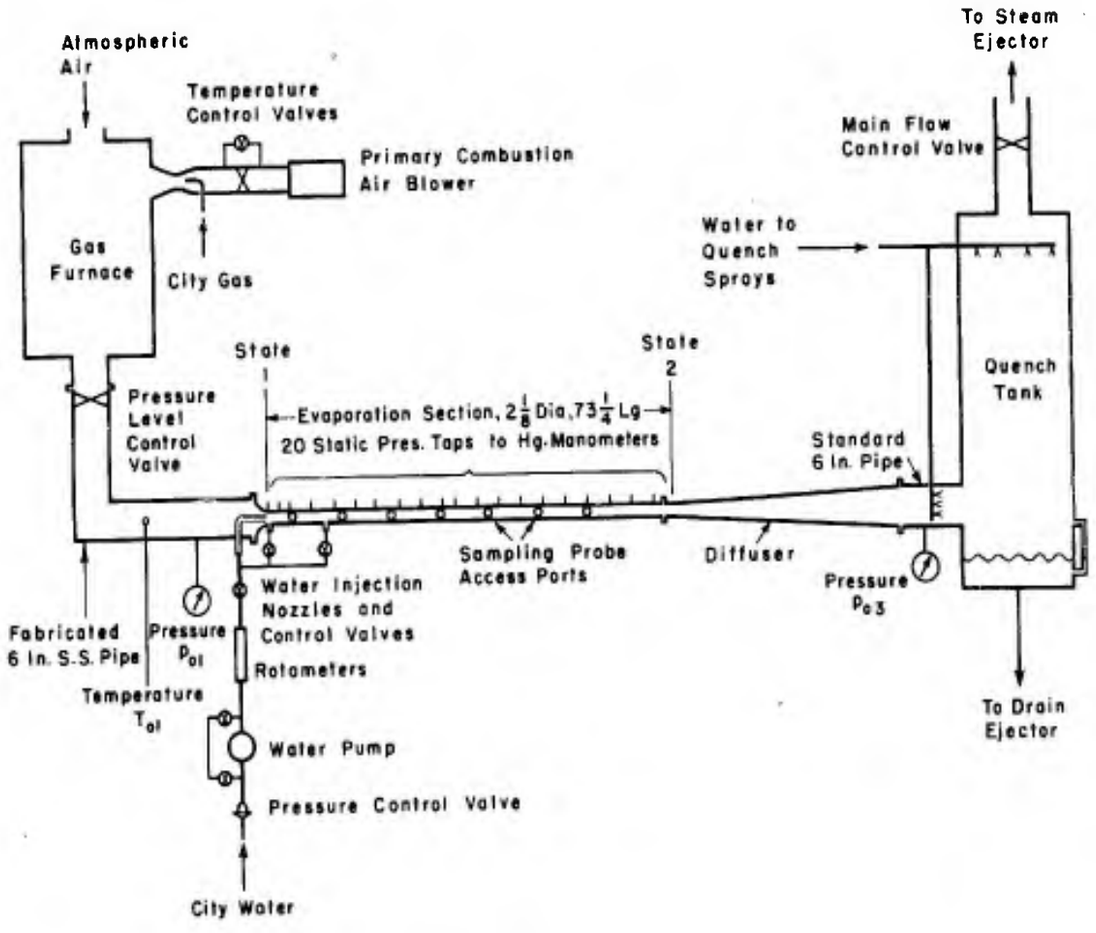

FIG. 16

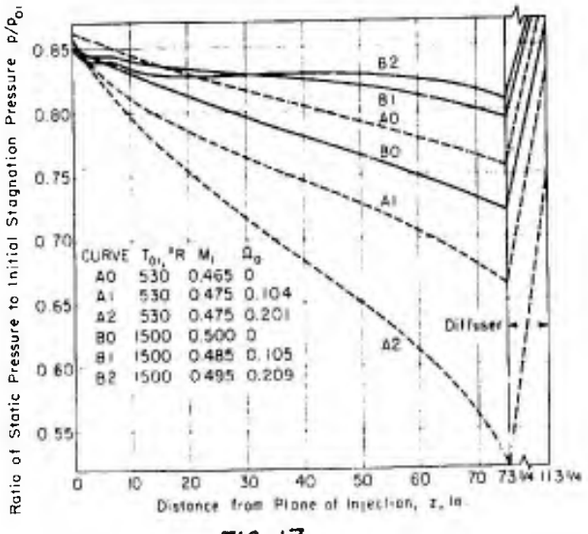

FIG. 17

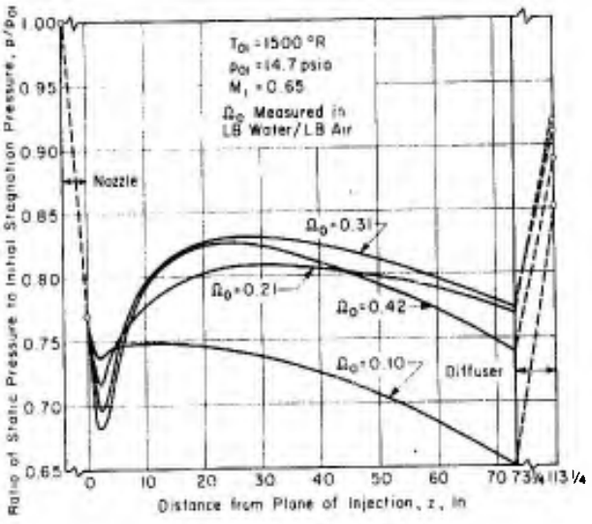

FIG. 18

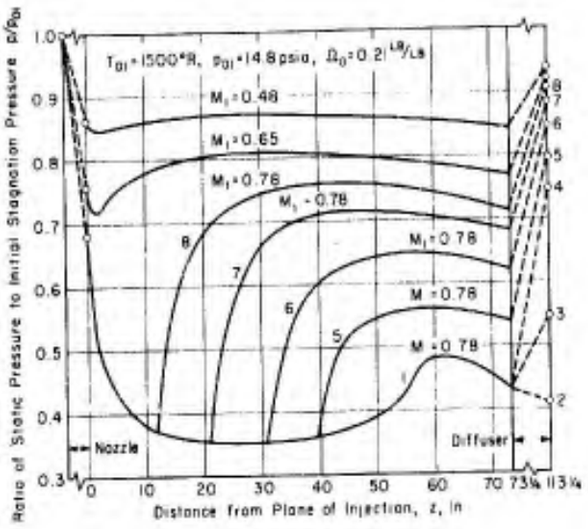

FIG. 19

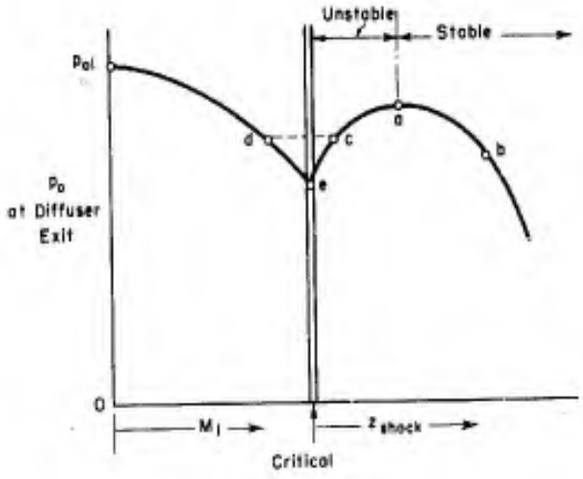

FIG. 20

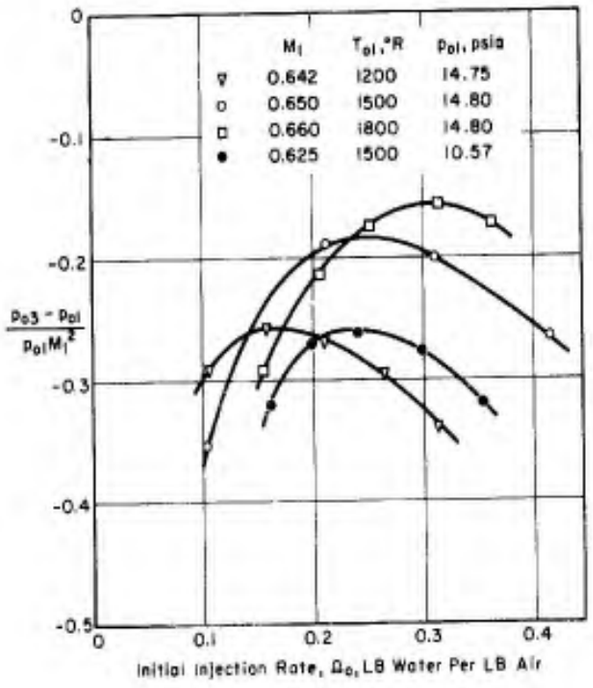

FIG. 21

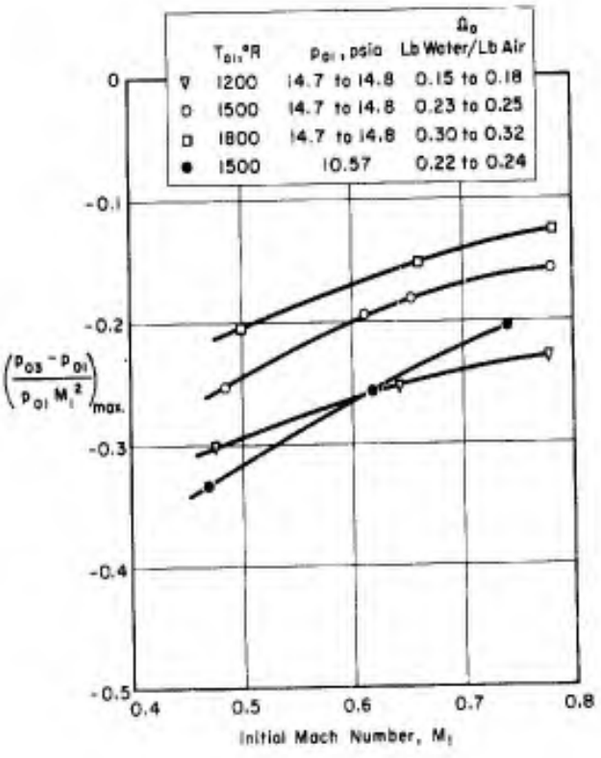

FIG. 22

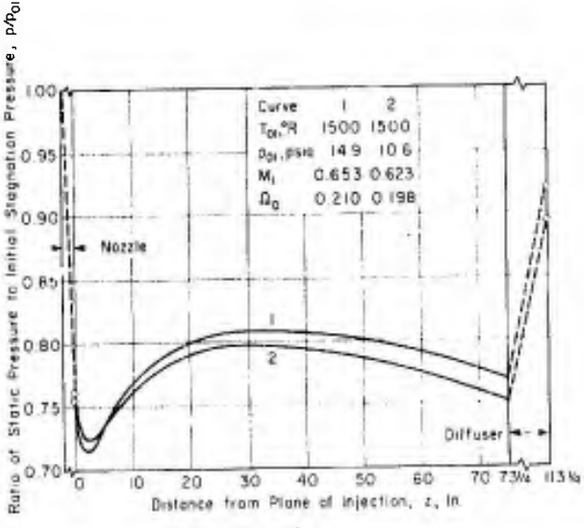

FIG. 23

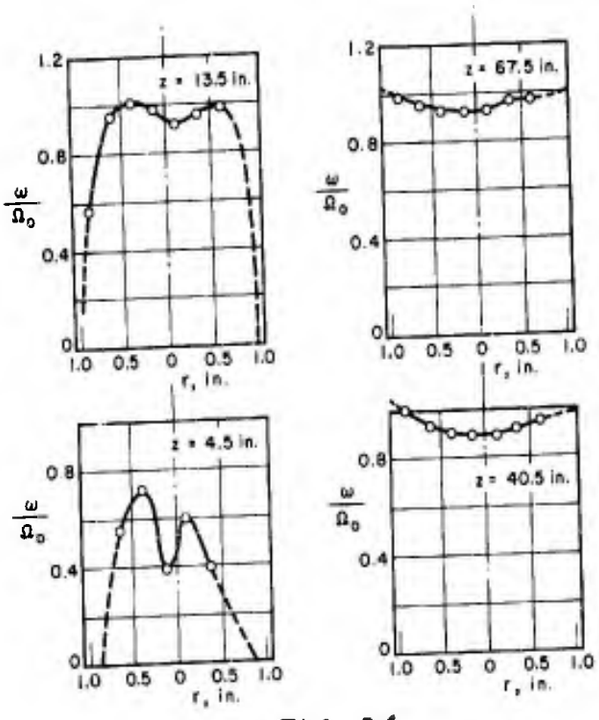

FIG. 24

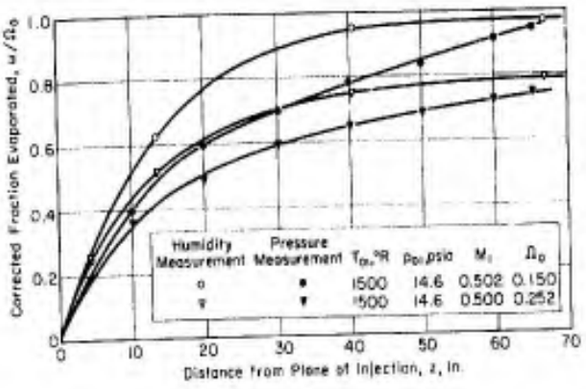

FIG. 25

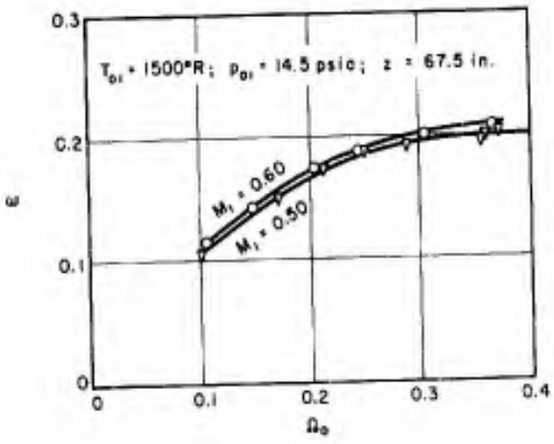

FIG. 26

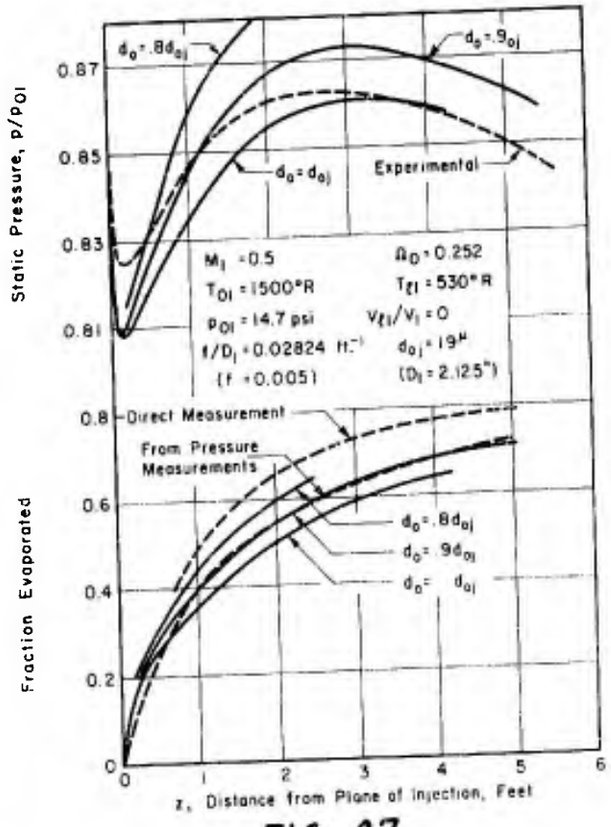

FIG. 27

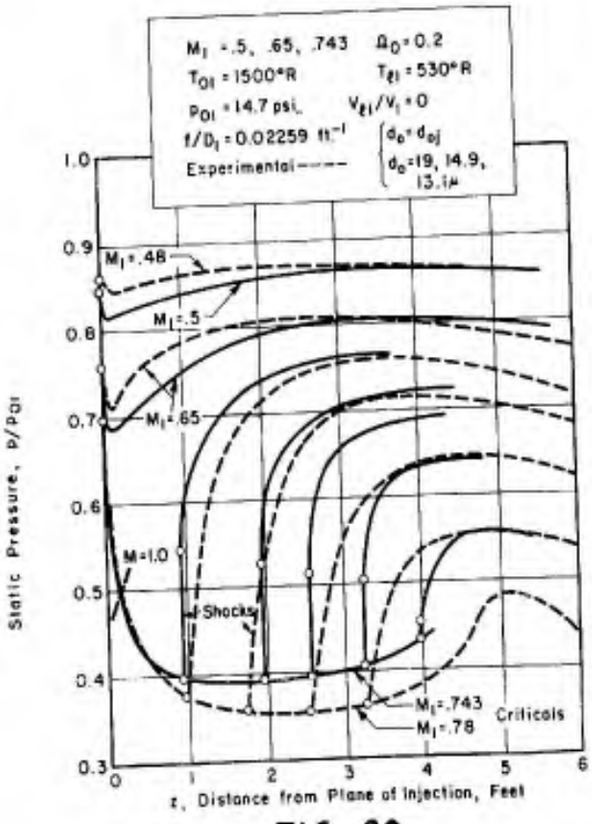

FIG. 28